Distribution Agreement

In presenting this thesis or dissertation as a partial fulfillment of the requirements for an advanced degree from Emory University, I hereby grant to Emory University and its agents the non-exclusive license to archive, make accessible, and display my thesis or dissertation in whole or in part in all forms of media, now or hereafter known, including display on the world wide web. I understand that I may select some access restrictions as part of the online submission of this thesis or dissertation. I retain all ownership rights to the copyright of the thesis or dissertation. I also retain the right to use in future works (such as articles or books) all or part of this thesis or dissertation.

Signature:

_____ _____

Jennifer Rha Date

The RNA-binding protein, ZC3H14, is critical for control of polyadenylation and translation, neuronal development, brain morphology, and working memory in mice

By

Jennifer Rha
Doctor of Philosophy

Graduate Division of Biological and Biomedical Sciences
Biochemistry, Cell, and Developmental Biology

_____
Anita H. Corbett, Ph.D.
Advisor

_____
Gary J. Bassell, Ph.D.
Committee Member

_____
Yue Feng, Ph.D.
Committee Member

_____
Paul S. Garcia, MD., Ph.D.
Committee Member

_____
Kenneth H. Moberg, Ph.D.
Committee Member

Accepted:

_____
Lisa A. Tedesco, Ph.D.
Dean of the James T. Laney School of Graduate Studies

_____
Date

The RNA-binding protein, ZC3H14, is critical for control of polyadenylation and translation, neuronal development, brain morphology, and working memory in mice

By

Jennifer Rha
B.A., The University of Pennsylvania, 2007

Advisor: Anita H. Corbett, Ph.D.

An abstract of
a dissertation submitted to the Faculty of the
James T. Laney School of Graduate Studies of Emory University
in partial fulfillment of the requirements for the degree of
Doctor of Philosophy
in Biochemistry, Cell, and Developmental Biology
2017

Abstract

The RNA-binding protein, ZC3H14, is critical for control of polyadenylation and translation, neuronal development, brain morphology, and working memory in mice

By Jennifer Rha

A number of mutations in genes that encode ubiquitously expressed RNA-binding proteins cause tissue specific disease, many of which are neurological, suggesting critical roles for this class of proteins in the brain. We recently identified mutations in a gene that encodes a ubiquitously expressed polyadenosine RNA-binding protein, ZC3H14 (Zinc finger CysCysCysHis domain-containing protein 14), that cause a nonsyndromic, autosomal recessive form of intellectual disability. This finding reveals the molecular basis for disease and provides evidence that ZC3H14 is essential for proper brain function. To investigate the role of ZC3H14 in the mammalian brain, we have generated a *Zc3h14* knockout mouse. We show here that *Zc3h14* is not essential in mice. Utilizing these mice, we provide the first *in vivo* functional characterization of ZC3H14, as a regulator of RNA poly(A) tail length. The $Zc3h14^{\Delta/\Delta}$ mice show defects in brain structure as well as working memory. Proteomic analysis comparing the hippocampi of $Zc3h14^{+/+}$ and $Zc3h14^{\Delta/\Delta}$ mice reveal dysregulation of several pathways that are important for proper brain function and shed light onto which pathways are most affected by the loss of ZC3H14. This newly generated mouse provides a model to study the function of ZC3H14 in the brain and thus elucidating how mutation in Zc3h14 could lead to intellectual disability.

The RNA-binding protein, ZC3H14, is critical for control of polyadenylation and translation, neuronal development, brain morphology, and working memory in mice

Jennifer Rha
B.A., The University of Pennsylvania, 2007

Advisor: Anita H. Corbett, Ph.D.

A dissertation submitted to the Faculty of the
James T. Laney School of Graduate Studies of Emory University
in partial fulfillment of the requirements for the degree of
Doctor of Philosophy
in Biochemistry, Cell, and Developmental Biology
2017

Acknowledgements

I first want to thank my advisor, Anita Corbett, for giving me this unique, challenging, and gratifying opportunity to pursue my desire to work on a new mouse model to study the function of the brain. She has always been incredibly supportive and encouraging throughout the entire process. She is an excellent role model as a scientist, emphasizing the importance and necessity for collaboration with others both within the field and outside. She taught me how to garner and keep the interest of others to build a truly meaningful collaborative work. She also taught me to frame any scientific question around "why should I care?" I'm still growing and learning how to be as good of a scientist as Anita, but she's set me in the right direction with a solid foundation.

I would like to thank the members of my committee for their expert advice, guidance, and patience. Specifically, Paul Garcia provided the absolutely required behavioral assays to assess the animals at the global level—which answers "why should I care?" about Zc3h14 in mice. He has also provided excellent mentorship, encouragement, and perspective as my MD-PhD advisor as well. Gary Bassell and his lab provided expertise at the other end of the spectrum and taught me the amazing technique to culture neurons in a dish. Kenneth Moberg and his lab also always provided new insights into the fly version of Zc3h14, which hinted at the function in the mouse Zc3h14. It was amazing to work on this protein through collaborations in different model organisms—the yeast in the Corbett lab and the fly in the Moberg lab. I would like to also thank Yue Feng for helpful edits to this thesis and her rigorous approach to the scientific method and emphasis on clear, logical, and methodical approaches to my sometimes far-flung goals and conclusions of the data. I could always depend on her as a sanity check back into sobering reality.

Stephanie Jones is an extremely talented graduate student who has been working on this project with me for two years and inherits this project. This work would not have been possible without her help. She is effectively the mouse technician, therapist, friend, and partner in crime. She is not only taking over all of the duties for taking care of the mice but also treading on paths that no other lab member including myself has gone, from 3D imaging of the whole brain, to Golgi staining, and to illustrating any scientific (and not-so-scientific) diagrams.

I also want to thank all of the Corbett lab members—Milo Fasken, Sara Leung, Ayan Banerjee, Katherine Mills, Annie McPherson, Callie Wigington, Sharon Soucek, Kevin Morris—for their expert advice and help throughout the project. I have especially enjoyed semi-depressed ruminations early in the morning or late at night when experiments failed or data did not make sense. They encouraged me through the rough times, and I continue with a hopeful love of science and experimentation despite the politics of publishing and unfairness of science gods.

The pursuit of understanding cognition necessitates an interdisciplinary approach—from neuroscientists, to biochemists, to cell and molecular biologists, to geneticists, to behaviorists. This work has been fortunately collaborative and owes its success to many individuals: Jonathan Fidler for graciously performing and analyzing the results of the WRAM, Wilfried Rossoll for technical assistance in locating the mouse genome sequence and providing early input to establish the *Zc3h14* mouse model, Katie Williams for technical assistance in primary neuronal culture, Alexa Mattheyses and Laura Fox-Goohariooon for instruction on confocal microscope imaging, Asheebo Rojas for thoughtful suggestions on analysis of serial histological sections, the William Tyor lab for providing

the WRAM apparatus, Su Yang and Xiao Jiang Li for assistance in using and providing the rotarod machine, D. J. Cutler for statistical guidance, and Ana Beain for help with genotyping. Special thanks to the following individuals of Emory University core facilities: Helen Zhang and Tamara Caspary of the Mouse Transgenic and Gene Targeting Core for blastocyst injection and production of chimeric mice, Eric Dammer, Duc Duong, Quidong Deng of the Proteomics Core for mass spectrometry analysis, Martha Gearing and Deborah Cooper at the Center for Neurodegenerative Diseases Histopathology Core for processing and staining tissues, and Division of Animal Resources, particularly Claude Pitt, for daily mouse colony maintenance.

Most importantly, I would like to thank my family who has supported (and endured) me throughout my life. My parents are my inspiration and example of diligence, discipline, honesty, kindness, and love. I have been blessed with a wonderful sister who has always accepted and supported me the way I am. I would like to thank my best friend and dedicated husband, Jon-Michael O'Bryan, who continues to inspire and encourage me. He provides me incredible strength and believes in me when I have trouble believing in myself. I dedicate this and future endeavors to him. I love you, Jon.

Table of Contents

List of Figures

Chapter 1:

Chapter 2:

Chapter 3:

Chapter 1

General Introduction

1.1 Molecular Basis of Learning and Memory

For centuries, humans have been fascinated by the mind. The field of neurobiology has come a long way from the insightful epistemological ruminations of Socrates, Plato, and Aristotle on the nature of knowledge and how it is acquired, to the Spanish neuroanatomist Santiago Ramón y Cajal who drew the first image of a neuron and conceptualized the idea of the synapse, to the experimental behavioral psychologist Ivan Pavlov who developed the fundamental learning and memory paradigm to condition dogs to salivate upon the ringing of a bell. What is learning and memory? The neurobiologist Larry Squire wrote that "learning is the *process* of acquiring new information, while memory refers to the *persistence* of learning in a state that can be revealed at a later time," (1). We continue to try to understand how the mind works, and in particular what learning and memory look like on the molecular and cellular level.

Where is memory stored in the brain? **Figure 1—1** shows the different parts of the brain that store different types of memory (2). For example, the emotional memories of the classically conditioned Pavlovian dog are stored in the amygdala. In our studies, we are specifically interested in explicit memories, those that can be brought into conscious awareness, such as the street name of our childhood home or how we celebrated our last birthday. PET scans of participants during an object location test show that there is high activity in hippocampus (3). The hippocampus is necessary for forming new explicit memories, as shown strikingly by one of the most widely known patients, HM. HM who suffered from epilepsy had his hippocampus removed and developed a severe memory deficit. He retained his ability to remember facts and events before the surgery but could not form new explicit memories. His ability to learn task-oriented activity like being able

to learn and remember how to play table tennis showed that as expected the other memory pathways were still intact (4). This observation also informs us that long-term storage of memory is in another part of the brain which is adjacent to the hippocampus (the medial temporal lobe and diencephalon).

What does learning and memory look like on the cellular level, and what are the basic molecular mechanisms underlying these processes? As insightfully predicted decades in advance by Santiago Ramon y Cajal, learning and memory involves synaptic plasticity, meaning dynamic changes of the synapse in response to activity or inactivity (5). Existing synapses can be strengthened to help retain information, whereas synapses may be weakened to divert resources elsewhere, which mediates forgetting. What does it mean molecularly to strengthen a synapse? An excitatory synapse is strengthened when the dendrite is more easily stimulated by the presynaptic terminal. This stronger connection between neurons is often brought about through an architectural change in the synapse, such as insertion of additional excitatory receptors. For example, the arrival of an action potential in the axon terminal induces release of glutamate, an excitatory neurotransmitter, into the synapse. Glutamate then binds to the AMPA receptor on the dendritic spine (5). This results in depolarization via a rush of sodium and calcium ions into the dendrite via the AMPA and NMDA receptors. Calcium ions activate Camk2a, which is a kinase that phosphorylates the AMPA receptor, increasing its conductance as well as stabilizing its synaptic localization in order to strengthen stimulatory events from the axon (5). Camk2a also phosphorylates transcription factors, activating genes for synthesis of new mRNA (6). Synapses may also be strengthened by N-cadherins which bind the presynaptic terminal to the postsynaptic spine (5). Synapses have develop

ped many different molecular mechanisms to facilitate efficient encoding of environmental stimuli and experience into learning and memory.

1.2 RNA regulation in the brain

In addition to transcription and post-translational modifications which are important for learning and memory, RNA-mediated mechanisms provide the rapid, localized, and long-lasting molecular changes needed to establish efficient learning and memory. *De novo* synthesis of proteins starting from DNA takes longer than local synthesis of protein from mRNA. To illustrate the time-intensive requirement of gene expression beginning from transcription, a well-studied, exemplary molecule is B-actin mRNA, which is expressed from an essential housekeeping gene and targeted to the moving edge of the cell (7). Transcription of β-actin mRNA in the human osteosarcoma cell line takes 1-2 minutes (3.3kb/min) plus 5-10 minutes for transcriptional initiation (8). Export of B-actin mRNA from the nucleus requires 6 minutes (8). B-actin active transport is rapid and requires just 8-33 seconds in primary neurons cultured from the embryonic chick forebrain (0.3-1.2 μm/s) if we assume the neurite is short and has a length of 10 μm (9). Translation is also very efficient and requires only 40 seconds (1.5 B-actin molecules produced per minute) in chick embryo fibroblasts (7, 10). Overall, expression of B-actin protein requires about 20 minutes. However, utilizing a reserve of already transcribed local B-actin mRNA, the protein can be synthesized in under one minute. Thus, post-transcriptional regulation of mRNA affords the brain some of the flexibility needed to respond quickly and pair coincident environmental signals, which is

important for learning and memory. Understanding post-transcriptional regulation and how it occurs will help us better understand the biology of the brain.

As shown in **Figure 1—2**, post-transcriptional regulation of mRNA begins co-transcriptionally, as numerous RNA-binding proteins associate from the pre-mRNA from the beginning of transcription. The mRNA molecule is modified at the 5'end by a 7-methylguanosine cap, splicing to remove introns, and 3'end cleavage and polyadenylation to add a polyadenosine (poly(A)) tail (11). Upon meeting certain quality control specifications, the mRNP (mRNA-protein complex) is exported through the nuclear pore into the cytoplasm (11). Once in the cytoplasm, the bound proteins, which can be dynamic and changing in composition, direct the fate of the mRNA (11). Some mRNA will be immediately translated, while others may be translationally silenced for future use (11). mRNA may diffuse throughout the cell or be carried by molecular motors and transported to targeted locations such as the dendritic spine or an axonal growth cone (11). mRNA is also degraded when it is no longer needed by the cell (11). Translation, localization, and degradation are mechanisms neurons use to achieve dynamic and efficient control of gene expression (12, 13). All of these different mechanisms are orchestrated by the different combinations of RNA-binding proteins that decorate the mRNA from its synthesis inside the nucleus (11).

One particular step in mRNA regulation has received heightened attention as a major player influencing the dynamics of gene expression (14). Following 3'end cleavage of mRNA, transcripts acquire a non-templated poly(A) tail of 250-300 adenosine nucleotides (15). Additionally, cellular mechanisms also regulate the length of the tail through deadenylation and polyadenylation even after the transcript is exported into the

cytoplasm (15, 16). Strikingly, the length of the poly(A) tail itself can affect the translation, localization, and stability of the transcript (16). To illustrate the importance of the poly(A) tail length, we can take the example of Camk2a mRNA regulation, which plays a crucial role in synaptic plasticity and learning and memory (17). Upon dendritic stimulation, CPEB (cytoplasmic polyadenylation element binding protein) binds to the 3'UTR of Camk2a mRNA located in dendrites, promoting polyadenylation and subsequent local translation (18). Thus, investigating how neurons regulate poly(A) tail length and the proteins that bind to mRNA is especially important to better understand the molecular mechanisms behind learning and memory.

Short poly(A) tail length is associated with repressed translational states, whereas elongation of the tail promotes translation (19). How exactly does modulation of poly(A) tail length affect translational efficiency? As shown in **Figure 1—3**, translational initiation generally takes places in three steps: 1) eIF4F (eukaryotic translation initiation factor-4F) complex associates with the 5'cap of the mRNA, 2) 40S ribosomal subunit is recruited, forms the pre-initiation complex, and scans to find the start codon on the transcript, 3) upon recognition of the AUG codon, 60S and 40S joins to form a translationally competent 80S ribosome and elongation begins (19). Importantly, the initial recruitment of 40S to the transcript is facilitated by the 3'end-bound PABP (polyadenosine tail-binding protein) and circularizes the transcript, forming a closed loop (19). An elongated 3'end tail helps to form a closed-loop formation to facilitate translational initiation, while a shortened tail would have limited ability to reach the other 5'end. Studies have shown that elongation of 3'end poly(A) tail activates translationally dormant transcripts in neurons and early embryos (19-22).

1.3 ZC3H14

1.3.1 Historical Background: From budding yeast to humans

ZC3H14 (Zinc finger CysCysCysHis-type containing 14) is the ubiquitously expressed human orthologue of a polyadenosine RNA-binding protein that has been characterized in a number of model organisms in which it is evolutionarily conserved. The most well characterized orthologue of ZC3H14 is *S. cerevisiae* (budding yeast) Nab2 (nuclear polyadenylated RNA-binding 2). Nab2 was identified in a screen for poly(A) RNA associated proteins in 1993 (23). Living yeast cells were UV-irradiated to crosslink RNA to protein. Polyadenylated RNAs were selectively purified using oligo(dT)-sepharose beads, and the polyadenylated RNA-protein complexes were used to immunize mice and raise antibodies, which were used to screen a yeast genomic expression library to identify several cross-linked proteins, including Nab2 (23). Since its discovery, Nab2 has emerged as a crucial regulator of RNA metabolism. Nab2 is an essential (23) protein, and mutant alleles show that it mediates several steps in RNA metabolism, including 3'end polyadenylation (24-27) and nuclear export (24, 28, 29).

More recently, investigations of the protein in multicellular organisms have also revealed its importance specifically in the brain, despite ubiquitous expression across all tissues (30). After reports characterizing the evolutionarily conserved functions of the mammalian orthologue, ZC3H14, in mice and in humans (30, 31), mutations in the gene were found to be responsible for causing autosomal recessive intellectual disability (32) in a large-scale study to identify novel genetic causes of recessive cognitive disorders (33). Subsequent studies in *Drosophila* (34-36) and mice (Chapter 2) have confirmed the importance of ZC3H14 in brain morphology and cognition. Furthermore, independent

investigations in *C. elegans* to screen for genes required for tau-induced neurotoxicity, which is a model for neurodegenerative disorders that form tau aggregates (37), identified the ZC3H14 orthologue in worms (named sut-2) as a modifier of tau pathology (38). Together, these studies establish ZC3H14 as an important regulator of RNA metabolism and a crucial protein necessary for proper brain function.

1.3.2 Phylogeny and Structure: Evolutionarily conserved functional domains

The structure of ZC3H14 is evolutionarily conserved across model organisms (**Figure 1—4**). In contrast to RNA-binding proteins that bind to RNA via the classical RRMs (RNA recognition motifs), ZC3H14/Nab2 is the founding member of the novel class of proteins that bind polyadenosine RNA via tandem Cys_3His zinc finger domains located at the C-terminus of the protein (25). The zinc finger domain is necessary and sufficient for direct binding to polyadenosine RNA (25, 31). Mammalian ZC3H14 has five tandem Cys_3His zinc fingers, whereas the yeast orthologue has seven Cys_3His zinc fingers. Each zinc finger is composed of the sequence, Cys-X_5-Cys-X_{4-6}-Cys-X_3-His, where X is any amino acid, and folds to hold one zinc ion each, which is also required for binding to RNA (39). Conserved aromatic residues after the first and third cysteines may help mediate base stacking interactions with polyadenosine RNA (27, 39, 40).

The N-terminal domain of Nab2/ZC3H14 contains a PWI-like fold (41), which is necessary for efficient polyA RNA export from the nucleus in budding yeast (29). The crystal structure of the N-terminal domain of Nab2 consists of five alpha-helices that pack to form a compact bundle (41). The structural arrangement of these helices is analogous to that of the PWI (Pro-Trp-Ile) fold. However, key differences between the

classic PWI fold and the PWI-like fold of ZC3H14/Nab2 exist. The ZC3H14 PWI-like fold lacks the characteristic residues Proline-Tryptophan-Isoleucine (PWI) and thus was not identified based on amino acid sequence identity. In Nab2, where the domain was initially characterized, the corresponding residues are instead Val12-Ile13-Val14. Furthermore, though the classic PWI fold is thought to bind nucleic acids (42, 43), the N-terminus of Nab2 does not bind to poly(N) RNA (41). Homology modeling reveals that the yeast Nab2 PWI-like fold aligns closely with the human N-terminal domain of ZC3H14 (30), showing that the N-termini of the two proteins are evolutionarily conserved.

As shown in **Figure 1—4**, between these two functional ends of Nab2/ZC3H14, at the center of the ZC3H14 sequence lies a domain important for ZC3H14 nuclear import: an RGG domain (Arg-Gly-Gly repeats) in Nab2 (25, 44, 45) and a classical nuclear localization signal (NLS) in the other model organisms, including mice (46). In yeast, the RGG domain binds to import factor Kap104 (44).

The *ZC3H14* gene is alternatively spliced in mice and humans, but not in yeast, flies, or worms (**Figure 1—4)** (30). All ZC3H14 isoforms contain the evolutionarily conserved C-terminal zinc finger domains (30) necessary for RNA binding. The first isoform is the longest variant. The second and third isoforms differentially include exons 10-12 (30) and still contain the N-terminal PWI-like fold and centrally located nuclear import signal. The fourth isoform expresses an alternative first exon and is truncated, lacking the N-terminal domain and import signal. These alternative isoforms may play differential roles both inside the cell nucleus and cytoplasm as well as inside various tissues as they are differentially expressed, including in the brain (30).

1.3.3 Molecular Function: ZC3H14 regulates poly(A) tail length

As a polyadenosine RNA-binding protein, ZC3H14 may be involved in any step of RNA metabolism. Extensive studies in yeast (24, 26, 27, 47, 48), *Drosophila* (32), and more recently mice (Chapter 2), reveal the evolutionarily conserved function of ZC3H14 orthologues in maintaining proper poly(A) tail length. Analysis of bulk RNA upon loss of Nab2/ZC3H14 function results in 3'end hyperadenlyation. The exact mechanism by which ZC3H14 regulates poly(A) tail length is not known. A possible model is that ZC3H14 binds to the poly(A) tail and recruits a 3'-5' RNA exonuclease (such as Rrp6 in yeast and Exosc10 in humans) for proper trimming of pre-mRNA, and thereby protects the RNA from excessive polyadenylation. Proper polyadenylation is a central step in pre-mRNA processing, one that is required for RNA to escape degradation by the RNA exosome that eliminates aberrantly processed transcripts (49). In addition to helping to produce export-competent mRNA, poly(A) tail length is also important in the cytoplasm in mRNA turnover and translational efficiency (50). Thus, by way of regulating the poly(A) tail length, ZC3H14 may potentially affect several steps in mRNA metabolism.

In budding yeast, Nab2 plays a central role in RNA export. Nab2 mutants accumulate poly(A) RNA in the nucleus (29). Furthermore, Nab2 physically interacts with several RNA export factors, including the mRNA export receptor Mex67 (51). In contrast to the conserved role of ZC3H14 orthologues in poly(A) tail length control, RNA export does not appear to be an evolutionarily conserved function in *Drosophila* or mice, probably due to redundant or compensatory mechanisms afforded by the larger genome of higher eukaryotes.

While ZC3H14 orthologues in budding yeast (23) and *Drosophila* (32) are essential, the worm (38), mouse (Chapter 2), and human (32) orthologues are not required for viability. Instead, patients who lack the expression of isoforms 1-3, the isoforms that most resemble the essential yeast and fly orthologues, develop into adulthood with only cognitive deficits (Pak). Furthermore, mutant worms (38) and mice (unpublished) that do not express corresponding ZC3H14 orthologues are viable and fertile.

An area of active investigation is the identification of RNA targets of ZC3H14. Some studies suggest that ZC3H14 orthologues are a general regulator of any RNA containing poly(A) stretches. High-throughput sequencing of Nab2 associated transcripts and subsequent GO analysis revealed that the mRNA largely follows the distribution of all yeast transcripts (52). Furthermore, Nab2 associates with the open reading frame of actively transcribed target genes of RNA polymerase II and RNA polymerase III (mRNA and tRNA/rRNA, respectively) (53). Nab2 is required for RNA polymerase III transcription (54). Interestingly, ribosome profiling of Nab2 mutants reveal problems with translational initiation and an overall decrease in polysomes (53), suggesting either an indirect or direct function in modulating translation.

Yet other studies suggest that ZC3H14 orthologues have specific target RNA. A genome-wide analysis by RNA-IP microarray showed that Nab2 in yeast binds to a unique spectrum of transcripts (55). Analysis of the target transcripts revealed an A-rich 12-nt sequence (AAAAAAAAAAAG). Additionally, in our unpublished studies, ZC3H14 knockdown in a human breast cancer cell line (MCF7) and subsequent microarray analysis reveal changes in the steady-state levels of only 1% of the transcriptome. One possible interpretation of this result is that ZC3H14 has a limited

number of targets (1% of the transcriptome) and knockdown of ZC3H14 affect the steady state expression those targets. A recent co-crystal structure of three zinc fingers of *C. thermophilum* Nab2 bound to an A_8 chain of RNA reveals that zinc fingers bind to only five of the eight adenosines (as shown in the following sequences: AAXAAXXA or AAXAXXAA), which would enable Nab2 to bind to general poly(A) RNA as well as specific transcripts with different nucleotides in the spacer positions within the transcript (40). Determining the targets of ZC3H14 will be important to study the exact mechanistic basis of how the protein works at the molecular level in regulating RNA.

1.3.4 ZC3H14 in Disease: Mutations in ZC3H14 cause autosomal recessive intellectual disability

Mammalian ZC3H14 is important for normal brain function. To date, two mutations in *ZC3H14* have been shown to cause a nonsyndromic form of autosomal recessive intellectual disability (32). The term "nonsyndromic" refers to the lack of any other signs or symptoms associated with the intellectual disability in patients. Patients develop a mild-moderate (IQ 50) to severe (IQ <35) form of intellectual disability and grow to a normal height with normal head circumference (32). One mutation is a nonsense mutation located in exon 6 (R154X), which eliminates expression of all three long isoforms of ZC3H14. The other mutation is a 25-bp deletion in the intron after the penultimate exon (exon 16) and disrupts expression of the last amino acid (unpublished data). Such an intronic mutation may interfere with splicing, resulting in exon skipping, activation of cryptic splice sites, or intron retention (56). Both *Drosophila* (32) and mouse (unpublished) models have been developed to further investigate the function of

ZC3H14 in the brain. Furthermore, evidence for the functional conservation across species was shown recently by Kelly *et al*. Expression of human ZC3H14 isoform 1 specifically in neurons can compensate for the loss of the *Drosophila* orthologue, dNab2, and rescue mutant *dnab2* flies (35).

Though ZC3H14 orthologues are necessary for normal brain function, the *C. elegans* ZC3H14 orthologue, sut-2 (suppressor of tau-2), is also implicated in potentiating tau-induced neurotoxicity in worms (38). Here, sut-2 is required for the development of tau-induced neurodegeneration. In worms, sut-2 is not essential, and loss of sut-2 suppresses tau-induced locomotion defects, possibly through activation of autophagic clearance of tau aggregates.

Many studies in these and other model organisms will aim to elucidate the mechanism by which ZC3H14 performs its RNA processing duties, especially in the context of neural cells.

1.4 Summary and prevailing questions

In this dissertation we explore the function of an evolutionarily conserved polyadenosine RNA-binding protein, ZC3H14, in the context of brain function. In particular, we investigate the hypothesis that **murine ZC3H14 plays an evolutionarily conserved role in polyadenylation and in learning and memory**. To address this hypothesis, we generated and characterized the first mouse model to study the function of ZC3H14 in the brain.

ZC3H14 is the evolutionarily conserved founding member of a novel class of RNA-binding proteins containing zinc finger domains that are necessary and sufficient for direct binding to polyadenosine sequences of RNA (31). An evolutionarily conserved

function of ZC3H14 is the regulation of poly(A) tail length, as shown extensively in yeast (24, 26, 27, 48), flies (32), and more recently in cultured mouse neuroblastoma cells (35). Reports of *ZC3H14* mutations in intellectually disabled patients have been instructive on the function and have guided investigations to include analysis of ZC3H14 in the brain.

The prevailing questions at the start of our investigations were: **1) Is ZC3H14 essential in mice?** While ZC3H14 orthologues in budding yeast (23) and in *Drosophila* (32) are essential, the ZC3H14 orthologue is not essential in worms (38). Patients who lack the expression of isoforms 1-3, the isoforms that most resemble the essential yeast and fly orthologues, develop into adulthood with only cognitive deficits (32), which suggest that ZC3H14 in humans is nonessential. **2) Is ZC3H14 important for learning and memory in mice?** Loss of ZC3H14 in patients causes intellectual disability, and a ZC3H14 RNAi knockdown in a fly model develops short-term memory dysfunction (34). Lethality caused by a loss of the ZC3H14 orthologue, dNab2, in flies can be rescued by the neuron-specific expression of human ZC3H14 isoform 1 (35). Together, these data suggest that the role ZC3H14 plays in the brain is functionally conserved across species. **3) Is ZC3H14 important for development of normal overall morphology of the brain?** Though brain morphology data from patients is lacking, studies in the *Drosophila* model reveal abnormal mushroom body architecture (34). **4) Is ZC3H14 necessary for the proper control of poly(A) tail length in a brain structure critical for learning and memory such as the hippocampus?** Extensive studies in various model organisms (24, 26, 27, 32, 35, 48) suggest that poly(A) tail length control is a conserved function of ZC3H14 orthologues. **5) What is the localization of ZC3H14 in cultured murine primary neurons?** Though the ZC3H14 orthologue in yeast is enriched in the nucleus

(23), studies in yeast have also shown that Nab2 shuttles (28) and delivers transcripts to the bud site during mitosis far from the nuclear envelope (57). Furthermore, preliminary unpublished studies in rat hippocampal neurons reveal that in addition to enrichment in the nucleus, ZC3H14 may be enriched in the axon of cultured young developing primary hippocampal neurons. Localization of ZC3H14 to specific cytoplasmic compartments is significant because it opens up possible regulatory functions ZC3H14 may play as a cytoplasmic RNA-binding protein, which brings us to the next question. **6) Does ZC3H14 play a role in translation?** *ZC3H14* shares some similarities with the gene, *FMR1* (fragile X mental retardation 1), which also encodes for an RNA-binding protein, that is mutated in patients who develop intellectual disability and plays a critical role in translational inhibition at the synapse (58). **7) What are some RNA targets of ZC3H14?** Identification of RNA targets is necessary to address the exact regulatory mechanism of ZC3H14 in RNA metabolism.

The following chapters delve into addressing these and other related questions. In **Chapter 2**, we present the generation and initial characterization of the first ZC3H14 knockout mouse and answers to the first four questions. **Chapter 3** is a collaborative study with Kenneth H. Moberg's laboratory using the *Drosophila* model organism to study the role of dNab2 (the ZC3H14 fly orthologue) in translation, with a correlate study using the mouse model organism. Here, we discuss responses to questions 5-7. **Chapter 4** offers preliminary evidence for the slowed neuronal growth and abnormal synaptogenesis of ZC3H14 deficient neurons *in vitro*. For clarity responses to these questions are explicitly outlined in the discussion (**Chapter 5**) of this dissertation.

1.5 Figures

Figure 1—1

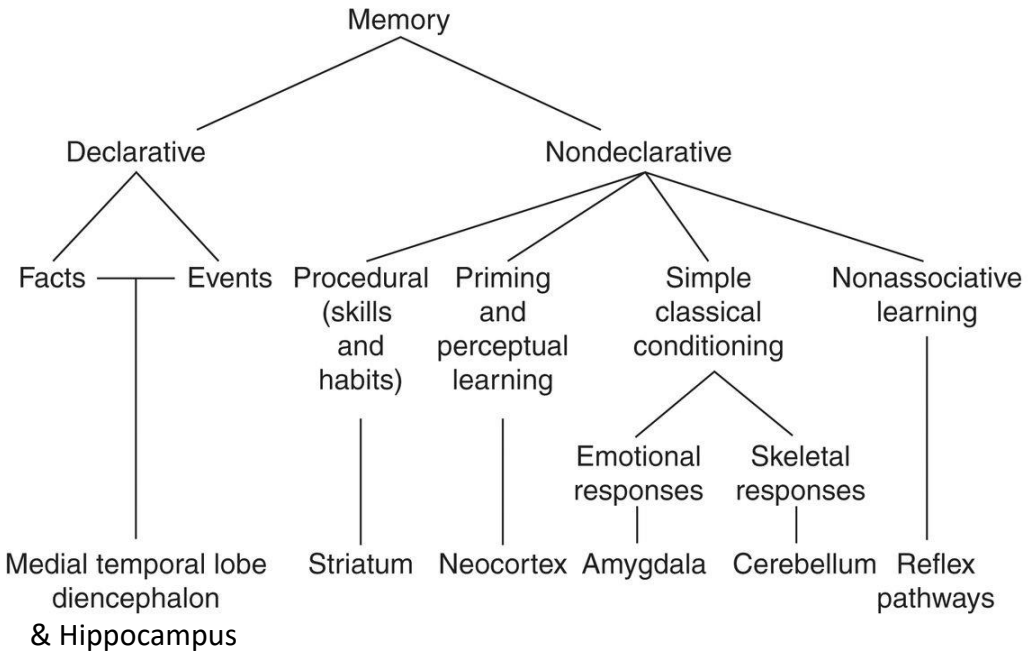

Figure 1—1. Organization of the mammalian long-term memory system and the brain structures thought to be specifically important for each form of memory.

The medial temporal lobe includes the hippocampus. This figure is modified from Squire and Dede (2015) (2).

Figure 1—2

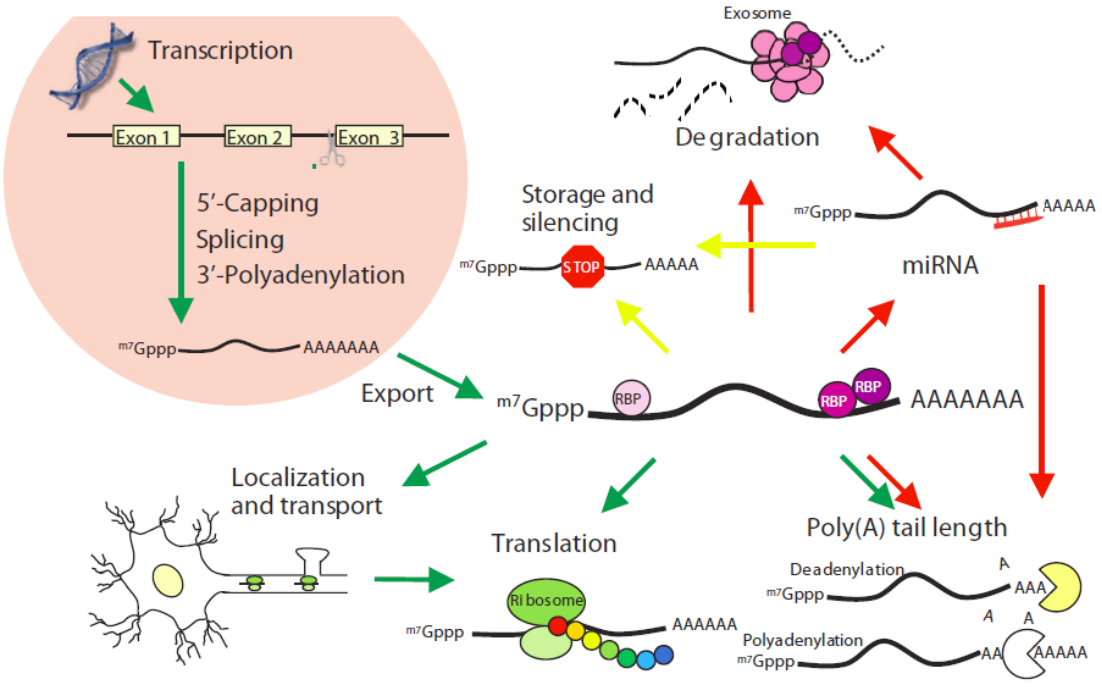
Transcription
Exon 1
Exon 2
Exon 3
5′-Capping
Splicing
3′-Polyadenylation
m7Gppp
AAAAAAA
Exosome
Degradation
Storage and
silencing
m7Gppp
STOP
AAAAA
m7Gppp
AAAAA
miRNA
Export
m7Gppp
RBP
RBP
RBP
AAAAAAA
Localization
and transport
Translation
Ribosome
m7Gppp
AAAAAA
Poly(A) tail length
Deadenylation
m7Gppp
AAA
Polyadenylation
m7Gppp
AA
AAAAA

Figure 1—2. Post-transcriptional control mediated by RNA-binding proteins. Regulation of mRNA expression involves nuclear 5'-capping, splicing, and 3'-polyadenylation. RNA-bound transcripts are then exported into the cytoplasm where they are immediately translated, transported, silenced, or degraded. The transcripts also undergo further regulation of their poly(A) tail length which affects transcript stability and translation initiation. Green arrows indicate pathways leading towards translation, yellow arrows toward translational silencing, and red arrows towards mRNA degrdation pathways. RBP, RNA-binding protein. This figure is adapted from Kojima *et al.* (2011) (59).

Figure 1—3

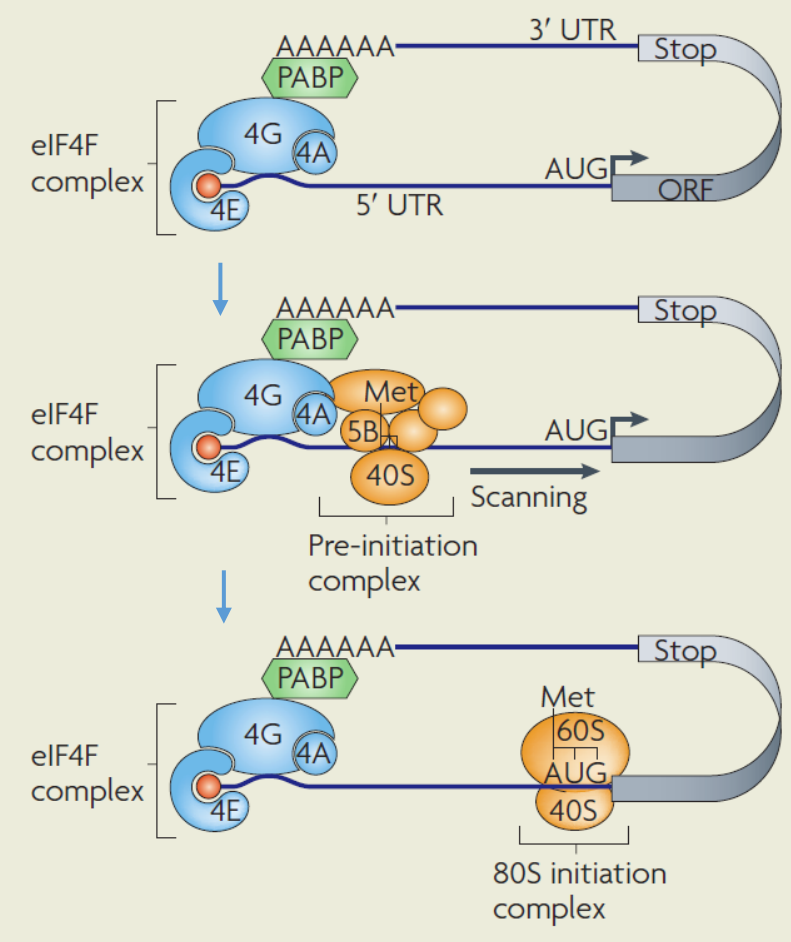
AAAAAA
PABP
3′ UTR
Stop
eIF4F
complex
4G
4A
4E
AUG
ORF
5′ UTR
AAAAAA
PABP
Stop
eIF4F
complex
4G
4A
Met
5B
4E
40S
AUG
Scanning
Pre-initiation
complex
AAAAAA
PABP
Stop
Met
60S
eIF4F
complex
4G
4A
AUG
4E
40S
80S initiation
complex

Figure 1—3. Translational initiation facilitated by closed-loop formation.

The closed-loop formation joining the 3'- and 5'-end of the transcript is thought to faciliate recruitment of the pre-initiation complex, which includes the 40S ribosomal subunit. The closed-loop is formed when PABP (poly(A) binding protein) bound to the poly(A) tail also binds to the eIF4F (eukaryotic translation initiation factor-4F) which is bound to the 5'-cap. After initiation, translation proceeds through elognation and termination (not shown). This figure is modified from Besse and Ephrussi (2008) (19).

Figure 1—4

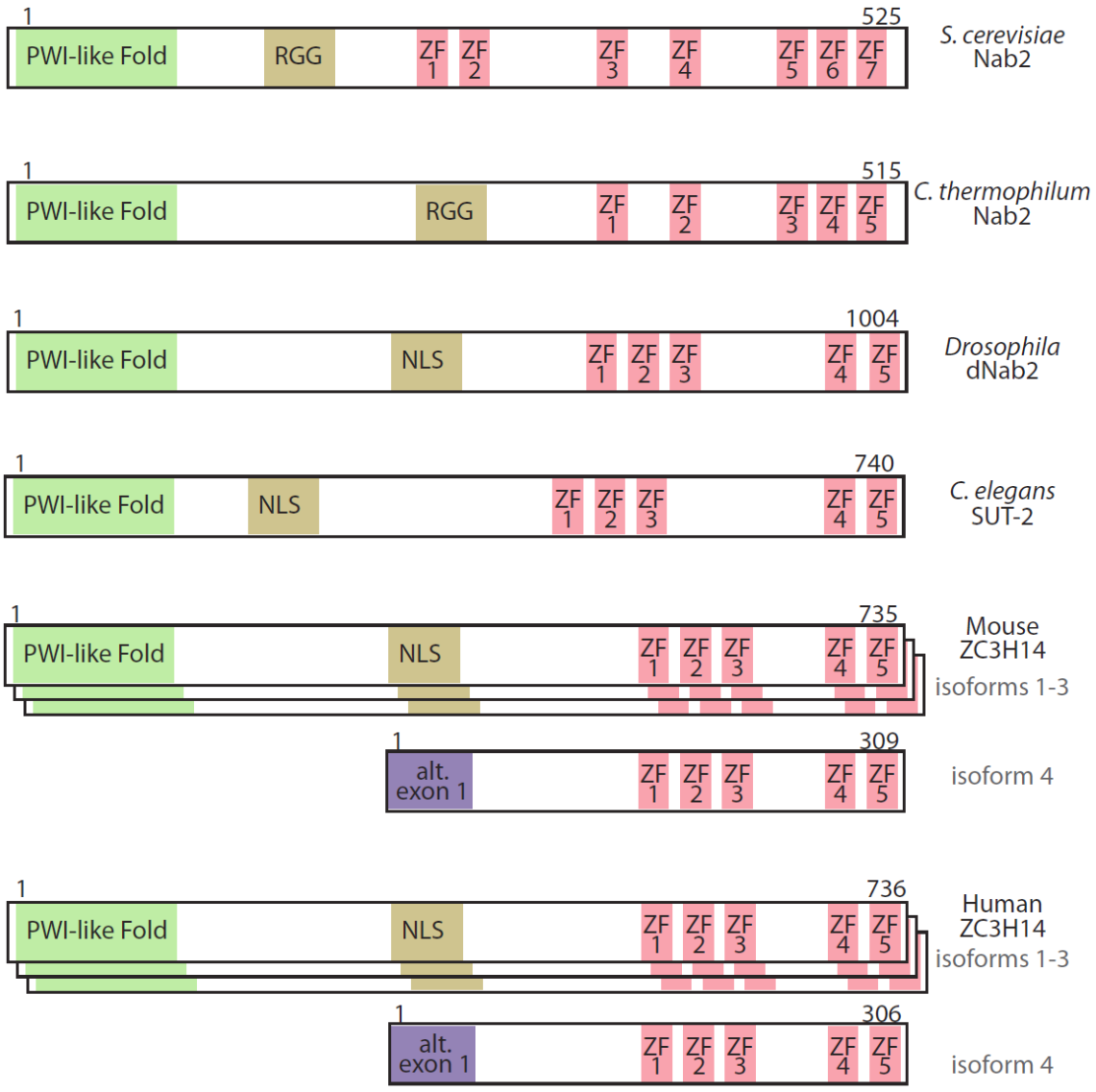
1
525
PWI-like Fold
RGG
ZF 1
ZF 2
ZF 3
ZF 4
ZF 5
ZF 6
ZF 7
S. cerevisiae Nab2
1
515
PWI-like Fold
RGG
ZF 1
ZF 2
ZF 3
ZF 4
ZF 5
C. thermophilum Nab2
1
1004
PWI-like Fold
NLS
ZF 1
ZF 2
ZF 3
ZF 4
ZF 5
Drosophila dNab2
1
740
PWI-like Fold
NLS
ZF 1
ZF 2
ZF 3
ZF 4
ZF 5
C. elegans SUT-2
1
735
PWI-like Fold
NLS
ZF 1
ZF 2
ZF 3
ZF 4
ZF 5
Mouse ZC3H14 isoforms 1-3
1
309
alt. exon 1
ZF 1
ZF 2
ZF 3
ZF 4
ZF 5
isoform 4
1
736
PWI-like Fold
NLS
ZF 1
ZF 2
ZF 3
ZF 4
ZF 5
Human ZC3H14 isoforms 1-3
1
306
alt. exon 1
ZF 1
ZF 2
ZF 3
ZF 4
ZF 5
isoform 4

Figure 1—4. Conservation of functional domains of ZC3H14 orthologues across species.

ZC3H14 are studied in numerous organisms, ranging from budding yeast to mice and humans. ZC3H14 orthologues are composed of three functional domains: PWI-like fold, NLS (nuclear localization signal), and the RNA-binding domain composed of five to seven zinc fingers (ZF). Mammalian orthologues of ZC3H14 are alternatively spliced. Numbers above each schematic indicates number of amino acids in the protein. The spacing between domains is not drawn to scale. The clustered spacing of ZFs within the RNA-binding domain reflects actual spacing.

Chapter 2

The RNA-binding protein, ZC3H14, is required for proper polyadenylation, expression of synaptic proteins, and brain function in mice

***Nota bene*:**

Jonathan Fidler, a listed co-author of the manuscript, performed and analyzed the data from the Water Radial Arm Maze (Figure 2—5) experiment in the current chapter.

This chapter has been submitted for review as:

Jennifer Rha, Stephanie K. Jones, Jonathan Fidler, Kevin J. Morris, Ayan Banerjee, Jennifer C. Wong, George Andrew S. Inglis, Lindsey Shapiro, Qiudong Deng, Adam M. Hanif, Machelle T. Pardue, Nicholas T. Seyfried, Kenneth H. Moberg, Gary J. Bassell, Andrew Escayg, Paul S. Garcia, and Anita H. Corbett, "The RNA-binding protein, ZC3H14, is required for proper polyadenylation, expression of synaptic proteins, and brain function in mice" (2016).

2.1 Introduction

Post-transcriptional processing of mRNA, which is critical to ensure proper gene expression, is mediated by numerous RNA-binding proteins that associate with RNA from the start of transcription in the nucleus to degradation in the cytoplasm (60, 61). There are a growing number of examples where mutations in genes that encode ubiquitously expressed RNA-binding proteins required for post-transcriptional processing cause tissue-specific human disease (62). Many of these mutations cause diseases of the nervous system such as fragile X syndrome (63) and spinal muscular atrophy (64). Understanding the functions of these RNA-binding proteins within the nervous system is an important step towards defining the molecular mechanism underlying these tissue-specific diseases.

Fine-tuning of the size and number of synaptic connections in the brain is critical for cognition and underlies fundamental processes such as learning and memory (65). One key mechanism by which neurons finely tune synapses is through spatio-temporal regulation of gene expression at the site of the synapse (12, 13). Much of this regulation is mediated by RNA-binding proteins that modulate steps in post-transcriptional processing of mRNAs to achieve local protein synthesis in neurites (12). A number of mRNA binding proteins, such as Fragile X Mental Retardation Protein (FMRP) and Zipcode Binding Protein 1 (ZBP1), regulate local protein synthesis (13) in neurons. FMRP binds to target mRNAs and represses their local translation, allowing for finely-tuned expression of key synaptic plasticity proteins (66). ZBP1 guides target mRNAs to the growth cone and synchronizes their translation in response to external stimuli (13). Such specific functions that may be most essential in neurons could explain why mutations in genes encoding ubiquitously expressed RNA-binding proteins cause neurological defects.

Recently, mutations in the gene encoding the evolutionarily conserved polyadenosine RNA-binding protein, ZC3H14 (Zinc finger CysCysCysHis protein 14), were identified as the cause of a form of nonsyndromic, autosomal recessive intellectual disability (32). ZC3H14 is conserved through evolution (30-32, 34, 35), and orthologues are essential in budding yeast (23) and flies (32). Patients that suffer from intellectual disability caused by mutation of *ZC3H14* are homozygous for a *ZC3H14* allele with a premature stop codon in exon 6 that eliminates expression of the protein isoforms that most resemble the essential orthologues found in yeast (23) and flies (32). Alternative splicing of mammalian *ZC3H14* produces multiple protein isoforms (Fig. 2-1A) including isoform 4 (isoform d in mice), a short isoform of ZC3H14, which lacks exon 6 and is thus unaffected by the mutation (30), that might fulfill an essential function in these patients (36). Alternatively, ZC3H14 function may not be essential in mammals. Prior to the current study there was no way to assess the requirement for mammalian ZC3H14.

The ZC3H14 protein contains C-terminal zinc finger motifs that mediate high-affinity binding to polyadenosine RNA (31, 32). Studies in cultured human cell lines show that ZC3H14 is localized primarily to nuclear speckles (30, 67) suggesting functions within the nucleus. In fact, characterization of ZC3H14 orthologues in model organisms reveals a number of nuclear functions for this zinc finger polyadenosine RNA-binding protein including transcription (54), control of poly(A) tail length (24, 35), and RNA export from the nucleus (25). These functions are consistent with the steady-state localization of the protein to the nucleus and the confirmed nucleocytoplasmic shuttling of the *S. cerevisiae* orthologue (28, 29, 68). However, such functions alone cannot readily explain why loss of ZC3H14 in patients leads to brain-specific deficits. The specific cellular requirement for

ZC3H14 has been addressed by studies exploiting loss-of-function models of the *Drosophila* orthologue, dNab2. Flies lacking both zygotic and maternally-deposited dNab2 are not viable (32) while zygotic mutants show reduced viability as well as defects in brain morphology (34). Neuron-specific knockdown of dNab2 impairs short-term memory as determined in a courtship conditioning assay (34). Furthermore, neuron-specific re-expression of dNab2 or expression of human ZC3H14 is sufficient to rescue behavioral defects in *dNab2* zygotic mutant flies (32, 35). These studies establish a critical, functionally conserved requirement for dNab2 in neurons.

To examine the function of ZC3H14 in a mammalian brain and provide insight into why a loss-of-function mutation in *ZC3H14* causes brain-specific defects in humans, we generated mice that are deficient for all isoforms encoded by the *Zc3h14* gene (denoted as $Zc3h14^{\Delta/\Delta}$). Here, we report an evolutionarily conserved function of ZC3H14 in poly(A) tail length control in the mammalian brain. Furthermore, $Zc3h14^{\Delta/\Delta}$ mice show morphological deformities in the brain as well as a deficit in working memory. Quantitative label-free proteomic analysis reveals key pathways with roles in synaptic function affected upon the loss of ZC3H14. The $Zc3h14^{\Delta/\Delta}$ mouse and these findings reveal the importance of ZC3H14 in the mammalian brain and help shed light on understanding the pathogenesis in patients who lack ZC3H14.

2.2 Results

2.2.1 Generation and confirmation of $Zc3h14^{\Delta/\Delta}$ mice. As with humans (30), mice express multiple splice variants of the *Zc3h14* gene, which encodes four protein isoforms termed ZC3H14 isoforms a-d (Fig. 2—1A). These isoforms share 90% amino acid

sequence identity with the human ZC3H14 isoforms. Exon 13 is the first common exon among the *Zc3h14* splice variants. This exon encodes the start of the zinc finger domain that mediates binding to RNA (27, 30-32, 39, 40) and is essential for the function of the budding yeast ZC3H14 orthologue, Nab2 (25). As described in Materials and Methods, we obtained embryonic stem cells from the Knockout Mouse Project where *Zc3h14* exon 13 is flanked by *loxP* sites (Fig. 2—1B). These cells were utilized to generate a floxed allele for *Zc3h14* which was induced to create an out-of-frame deletion of *Zc3h14* exon 13 upon Cre-mediated recombination.

To examine the function of ZC3H14, we inactivated *Zc3h14* by mating homozygous floxed $Zc3h14^{F/F}$ mice to *EIIa-Cre* transgenic mice, which express Cre-recombinase under the control of a strong adenovirus EIIa promoter in a wide range of tissues in the mouse embryo including germ cells (69, 70). *EIIa-Cre* transgenic mice are commonly used to generate germ-line deletion of *loxP*-flanked genes (71-77). Following several generations of breeding as described in Materials and Methods, the floxed *Zc3h14* conditional allele was efficiently recombined to yield *EIIa-*$Zc3h14^{\Delta/\Delta}$ mice as determined by genomic PCR analysis (primers indicated in Fig. 2—1B) to detect the control, floxed, and recombined alleles. The recombination event was confirmed by the appearance of a lower molecular weight band at the predicted size (230 bp) upon Cre-mediated deletion of exon 13 (Fig. 2—1C, *top* panel). Additional PCR analyses confirmed the loss of exon 13 in the recombined mice (Fig. 2—1C, *bottom* panel). Mice with confirmed proper recombination were mated to wildtype mice to breed out the *EIIa-Cre* allele. *EIIa-Cre*-negative, $Zc3h14^{\Delta/+}$ were mated to generate $Zc3h14^{\Delta/\Delta}$ homozygous mice for at least four generations for subsequent analyses.

To validate the loss of ZC3H14 protein in these mice, we immunoblotted tissue isolated from the hippocampus, cerebral cortex, cerebellum, and spinal cord, using an antibody that detects the N-terminal PWI-like domain of ZC3H14 (30). As shown in Figure 2—1D, the *Zc3h14*$^{\Delta/\Delta}$ mice show no detectable expression of ZC3H14 isoforms a-c, which are readily detectable in the *Zc3h14*$^{+/+}$ control mice. Note that we did observe a small amount of a lower molecular weight band (asterisk in Figure 2—1D) specifically detected by the N-terminal ZC3H14 antibody. Using mass spectrometry, we determined that this lower molecular weight band corresponds to a truncated form of ZC3H14. Peptides of ZC3H14 from the *Zc3h14*$^{\Delta/\Delta}$ mouse map only to the N-terminal region of the ZC3H14 protein within exons 5 and 6 (see Supplementary Material, Fig. 2—S1), suggesting low-level expression of a truncated protein that lacks the essential RNA-binding domain (25). In contrast, peptides from the control mouse map to both the N- and C-terminal regions of the ZC3H14 protein (Supplementary Material, Fig. 2—S1). Furthermore, ZC3H14 isolated from *Zc3h14*$^{+/+}$ mice is at least ten-fold more abundant than the truncated protein in the immunoprecipitated sample, indicating that *Zc3h14*$^{\Delta/\Delta}$ mice do express a small amount of truncated ZC3H14, which is devoid of the functionally essential RNA-binding zinc finger domain (25, 31). As no antibody is available to detect ZC3H14 isoform d by immunoblotting, we performed real-time PCR analysis of mouse brain to confirm that this variant was also absent from the *Zc3h14*$^{\Delta/\Delta}$ mice. The *Zc3h14 isoform d* transcript was not detectable above background in *Zc3h14*$^{\Delta/\Delta}$ mice, but was readily detected in *Zc3h14*$^{+/+}$ mice (Fig. 2—1E). Taken together, these analyses confirm that we have generated mice lacking any full-length ZC3H14 isoform.

2.2.2 ZC3H14 is not essential but is required for normal litter and testis size. To assess the requirement for ZC3H14 in mice, we bred heterozygous *Zc3h14*$^{\Delta/+}$ mice to one another, calculated ratios of the genotypes produced, and compared them to expected Mendelian ratios. *Zc3h14*$^{\Delta/\Delta}$ mice are viable. Furthermore, there was no statistically significant difference between the expected and observed ratios of the genotypes produced (Fig. 2—2A). To assess differences in litter size, we bred homozygous *Zc3h14*$^{\Delta/\Delta}$ mice to one another. We detected a modest but statistically significant decrease in average litter size (4.3 pups/litter) generated from these *Zc3h14*$^{\Delta/\Delta}$ pairings when compared with *Zc3h14*$^{+/+}$ pairings (5.7 pups/litter) (Fig. 2—2B). This decrease in litter size may at least partially be due to a statistically significant decrease in the number of male *Zc3h14*$^{\Delta/\Delta}$ births as shown in Fig. 2—2C. Together, these data indicate that although *Zc3h14* is not essential for viability, but loss of ZC3H14 may impair survivability *in utero*.

As a general indication of overall health and development, we periodically measured the body weight of the mice starting at 3 weeks after birth and continuing until they were 5 months old (Supplementary Material, Fig. 2—S2A). This analysis of mean values for body weight of male and female mice for *Zc3h14*$^{+/+}$ and *Zc3h14*$^{\Delta/\Delta}$ showed no statistically significant difference between the two genotypes. The sample size, standard error of the means (SEMs), and *p* values are reported in Supplementary Material, Fig. 2—S2B-D. We also observed no statistically significant difference between the mean values for whole brain weight (Fig. 2—2E) or individual hippocampal weight (Fig. 2—2F) when we compared male *Zc3h14*$^{+/+}$ and *Zc3h14*$^{\Delta/\Delta}$ adult mice.

As the testes express high levels of ZC3H14 (30), we compared testis weight in *Zc3h14*$^{+/+}$ versus *Zc3h14*$^{\Delta/\Delta}$ mice. Although no gross differences in body weight or brain weight were detected, *Zc3h14*$^{\Delta/\Delta}$ mice had testes that were half the size of *Zc3h14*$^{+/+}$ testes (Fig. 2—2G). ZC3H14 is thus required for normal litter size and important for normal testis size.

2.2.3 Zc3h14 is required for proper poly(A) tail length control. Our previous work demonstrates that one evolutionarily conserved molecular function of ZC3H14 is to restrict poly(A) tail length of bulk RNAs (23, 24, 32, 35). However, no studies have been previously performed to assess the molecular function of vertebrate ZC3H14 *in vivo*. To assess the functional consequence of loss of ZC3H14 in the brain, we examined poly(A) tail length of bulk RNA isolated from either *Zc3h14*$^{+/+}$ or *Zc3h14*$^{\Delta/\Delta}$ mouse hippocampi. As shown in Figure 2—3A and quantified in Figure 2—3B, the *Zc3h14*$^{\Delta/\Delta}$ mice show an increase in bulk poly(A) tail length compared to *Zc3h14*$^{+/+}$ mice. This result provides molecular and *in vivo* evidence that ZC3H14 plays a role in poly(A) tail length control in a region of the mouse brain that is important for learning and memory.

2.2.4 *Zc3h14*$^{\Delta/\Delta}$ mice show structural defects in the brain. Although the brain and hippocampi of *Zc3h14*$^{\Delta/\Delta}$ mice showed no overall change in weight as compared to *Zc3h14*$^{+/+}$ mice, we examined brain morphology by histology to provide a more detailed analysis. We analyzed coronal histological sections (as diagrammed in Fig. 2—4A) comparing *Zc3h14*$^{+/+}$ and *Zc3h14*$^{\Delta/\Delta}$ mouse brains. Haematoxylin and eosin (H&E) stains revealed that the anterior portion of the lateral ventricles is enlarged in *Zc3h14*$^{\Delta/\Delta}$ mice as compared to *Zc3h14*$^{+/+}$ mice (Fig. 2—4 B and C). In contrast, there was no detectable

effect on the size of the lateral ventricles at a more caudal level at the hippocampus proper (Fig. 2—4D). Thus, ZC3H14 is required for normal ventricle morphology.

2.2.5 *Zc3h14*$^{\Delta/\Delta}$ mice have impaired working memory but intact learning. Loss of the ZC3H14 orthologue in *Drosophila* causes defects in short-term memory while learning remains intact (34). To determine whether ZC3H14 is required for learning and memory in mice, we used the water radial arm maze (WRAM), a well-established assay that assesses hippocampus-dependent spatio-temporal learning and working memory (78-81). As illustrated in Figure 2—5A, the WRAM is an eight-arm arena in which mice *learn* to locate submerged platforms to escape from having to swim and *remember* the location of the hidden platforms. Learning is indicated, across nine days of testing, by a decrease in the amount of time required to find all four platforms and a decrease in the number of errors made. Errors include mistakes in which a mouse enters an arm that: (a) does not contain a platform, (b) contains a platform but the mouse does not locate it, (c) contained a platform on a previous trial on the same day, or (d) has already been entered previously during the trial (i.e. deficit in working memory). Both *Zc3h14*$^{+/+}$ and *Zc3h14*$^{\Delta/\Delta}$ adult mice were able to learn the locations of the hidden platforms, as evidenced by a decrease in the time required for mice to locate the platforms (Fig. 2—5B, $p<0.0001$), a decrease in the number of overall total errors (Fig. 2—5C, $p<0.0001$), and a decrease in the number of working memory errors (Fig. 2—5D, $p<0.0001$), across the course of the nine-day testing period.

Though both *Zc3h14*$^{+/+}$ and *Zc3h14*$^{\Delta/\Delta}$ mice show the ability to *learn* as assessed in the WRAM (Fig. 2—5B-D), data uniformly indicate a trend toward an impairment in efficient learning by the *Zc3h14*$^{\Delta/\Delta}$ mice, which require one to three additional days to

perform at a similar level to *Zc3h14*$^{+/+}$ mice. Furthermore, analyzing the WRAM data to assess *working memory* function in test subjects, *Zc3h14*$^{\Delta/\Delta}$ mice showed a statistically significant deficit in working memory when compared with *Zc3h14*$^{+/+}$ mice (Fig. 2—5D). Specifically, working memory errors are repeated entries into any arm on a given trial, indicating the subject's inability to remember which arm was explored within the previous two minutes (the length of a single trial). As illustrated in Fig. 2—5D, *Zc3h14*$^{\Delta/\Delta}$ mice exhibited a statistically significant (p=0.035) persistence in the number of working memory errors that is not exhibited by control mice. *Zc3h14*$^{\Delta/\Delta}$ mice require two additional days of trials to perform as well as the control mice in locating all platforms. The WRAM results indicate that ZC3H14 is required in adult mice for proper cognitive function, particularly spatio-temporal working memory, which is consistent with the cognitive deficits seen in patients (32) and the behavioral defects observed in the *dNab2* mutant flies (34).

2.2.6 *Zc3h14*$^{\Delta/\Delta}$ mice have normal visual function and exhibit normal motor function and coordination. The WRAM test requires vision to locate environmental cues and motor coordination to swim efficiently. To rule out possible confounding variables that could lead to impaired performance of *Zc3h14*$^{\Delta/\Delta}$ mice in the WRAM test, we conducted a battery of tests to examine visual function (Supplementary Material, Fig. 2—S3 A-C*)*, motor function and coordination (Supplementary Material, Fig. 2—S3 D-G), general activity, and exploratory behaviors (Supplemental Material, Table 2—S1). *Zc3h14*$^{\Delta/\Delta}$ mice performed at least as well as the *Zc3h14*$^{+/+}$ mice performed on the visual and motor coordination assays. We measured visual acuity and contrast sensitivity by using an optokinetic test apparatus (depicted in Supplementary Material, Fig. 2—S3A)

for rodents, which elicits a head- and body-turning response to a rotating visual field (82). *Zc3h14*$^{\Delta/\Delta}$ mice showed no obvious deficit in their visual acuity represented by their ability to distinguish similar spatial frequencies of black and white gratings when compared to control mice (Supplementary Material, Fig. 2—S3B). Furthermore, *Zc3h14*$^{\Delta/\Delta}$ mice showed no evidence of impaired contrast sensitivity, as measured by their ability to distinguish between gradients of dark- and light-gray gratings (Supplementary Material, Fig. 2—S3C), when compared to *Zc3h14*$^{+/+}$ mice.

Next, we challenged mice using two assays to assess general motor function and coordination. *Zc3h14*$^{\Delta/\Delta}$ mice did not show a statistically significant difference in their ability to grip a wire mesh while up-side down (depicted in Supplementary Material, Fig. 2—S3D) when compared to *Zc3h14*$^{+/+}$ mice (Supplementary Material, Fig. vS3E). Additionally, when challenged to balance on a rotarod apparatus (depicted in Supplementary Material, Fig. 2—S3F), *Zc3h14*$^{\Delta/\Delta}$ mice performed at least as well as the *Zc3h14*$^{+/+}$ mice (Supplementary Material, Fig. 2—S3G). These data together indicate that, along with vision, general motor function, sensorimotor coordination, and motor learning are intact in *Zc3h14*$^{\Delta/\Delta}$ mice, and thus would not contribute to differences in performance on the WRAM.

Furthermore, consistent with normal baseline behavior, *Zc3h14*$^{+/+}$ and *Zc3h14*$^{\Delta/\Delta}$ mice were comparable in measures of activity (open field), exploratory behavior (novel cage), and anxiety (light/dark box) (Supplementary Material, Table 2—S1). Together, these results indicate that the working memory deficit detected in the *Zc3h14*$^{\Delta/\Delta}$ mice through WRAM analysis is not confounded by these variables.

2.2.7 *Zc3h14*$^{\Delta/\Delta}$ mice exhibit increased resistance to seizures. A well-known comorbidity of intellectual disability is epilepsy. Epidemiologically, about 5-10% of people with intellectual disability also suffer from seizures (83). In individuals with autism, epilepsy occurs in 10-50% (83). To assess whether *Zc3h14*$^{\Delta/\Delta}$ mice show altered seizure susceptibility, we subjected mice to two seizure-induction paradigms, the 6-Hz psychomotor seizure model (84) and the chemical convulsant, flurothyl (85). Seizures induced by the 6-Hz paradigm were scored on a modified Racine scale (RS): RS0, no seizure; RS1, staring; RS2, forelimb clonus or paw waving; RS3, rearing and falling. In this paradigm, seizures were observed in 15 of 24 (63%) female *Zc3h14*$^{+/+}$ mice (11 RS2, 4 RS3). Seizure occurrence and severity were significantly lower in the female *Zc3h14*$^{\Delta/\Delta}$ mice, which showed seizures in only 5 of 24 (21%) mice (4 RS2, 1 RS3, Fig. 2—6A). Similar results were obtained when male mice were examined (Fig. 2—6B). Seizures were observed in 16 of 23 (70%, 7 RS2, 9 RS3) male *Zc3h14*$^{+/+}$ mice, and in 10 of 22 (45%, RS2 only) male *Zc3h14*$^{\Delta/\Delta}$ mice. Fewer and less severe 6-Hz seizures were therefore observed in the *Zc3h14*$^{\Delta/\Delta}$ mice compared to *Zc3h14*$^{+/+}$ mice.

A separate cohort of mice were exposed to the chemical convulsant flurothyl to induce seizure via a distinct paradigm. Although the latency to myoclonic jerk was comparable between *Zc3h14*$^{+/+}$ and *Zc3h14*$^{\Delta/\Delta}$ mice of both sexes (female data shown in Fig. 2—6C), consistent with the increased resistance to 6 Hz-induced seizures, female *Zc3h14*$^{\Delta/\Delta}$ mice displayed an increased latency to the flurothyl-induced generalized tonic-clonic seizure (GTCS) ($p < 0.01$, Fig. 2—6D) when compared to *Zc3h14*$^{+/+}$ mice. However, the average latency to GTCS was comparable between male *Zc3h14*$^{+/+}$ and

Zc3h14$^{\Delta/\Delta}$ mice (data not shown). Thus, the loss of ZC3H14 contributes to increased seizure resistance in these mice.

2.2.8 Increased expression of synaptic proteins in *Zc3h14*$^{\Delta/\Delta}$ mice. Our results show differences in the function and morphology of the brain in mice lacking ZC3H14. To begin to understand the mechanism underlying these functional changes, we performed a quantitative proteomic analysis to compare the hippocampi of *Zc3h14*$^{+/+}$ and *Zc3h14*$^{\Delta/\Delta}$ mice (n = 4 each group). Following tissue homogenization and trypsin digestion, peptides from each sample were analyzed by LC-MS/MS on an Orbitrap Fusion mass spectrometer. Relative protein abundance was determined by peptide ion-intensity measurements across LC-MS runs using the label-free quantification (LFQ) algorithm in the MaxQuant computational platform (86). In total, 56,423 peptides mapping to 4,450 protein groups were identified across *Zc3h14*$^{+/+}$ and *Zc3h14*$^{\Delta/\Delta}$ mice hippocampi each in technical replicate. The stochastic nature of LC-MS/MS based peptide sequencing required us to limit the number of missing protein measurements to no more than two per condition, resulting in the final quantification of 4,161 protein groups (henceforth referred to as proteins) mapping to 4,052 unique gene symbols. Figure 2—7A shows a volcano plot where each protein that has any change in steady state expression level between *Zc3h14*$^{+/+}$ and *Zc3h14*$^{\Delta/\Delta}$ hippocampi is represented by a colored dot. In total 113 proteins had at least a ±1.25 fold change (i.e., $|\log_2(Zc3h14^{+/+}/Zc3h14^{\Delta/\Delta})| \geq 0.32$) and a p value < 0.05 are highlighted as green (decreased) or red (increased) dots, while those proteins (shown as teal dots) that do not meet these criteria are omitted from further analysis and fall within the shaded nonsignificant boundaries of the plot. The identities of the top 10 decreased and top 10 increased proteins are listed, and their corresponding

positions are labeled (with Roman or Arabic numerals, respectively) on the plot. Note that the top protein with decreased expression is ZC3H14, which further validates the absence of the ZC3H14 protein from *Zc3h14*$^{\Delta/\Delta}$ mice and highlights the reliability of our proteomics approach to quantify proteins due to loss of *Zc3h14*$^{\Delta/\Delta}$ function.

To analyze enrichment of proteins that participate in the same cellular components, biological processes, or molecular functions, we performed a GO (gene ontology) analysis of the decreased and increased protein sets of only those proteins significantly increased or decreased in *Zc3h14*$^{\Delta/\Delta}$ mice. The criteria to cluster into a GO term were Z-score ≥ 1.96, p value < 0.05, and ≥ 3 gene symbols per GO term. As shown in Fig. 2—7B, only two GO terms were identified using the decreased protein set (n = 50), as most of these proteins do not cluster into GO terms. These GO terms are nuclear-specific and suggest these pathways are most affected in the nucleus at the protein level as a result of loss of ZC3H14. The small number of proteins that do cluster into common GO terms are depicted in Fig. 2—7C. Thus, the majority of proteins with decreased expression do not cluster into common pathways recognized by GO terms.

We then analyzed the increased protein set (n = 63) for GO enrichment. In striking contrast to the decreased protein set, we observed that many of the increased proteins cluster into several biologically meaningful GO terms. In fact, this result holds true even after we applied more stringent inclusion criteria (Z-score ≥ 2.58, p value < 0.01, and ≥ 5 gene symbols per GO term) than that used for analyzing the decreased gene set (Fig. 2—7D). Many of the GO terms, such as “synapse,” “signal transduction,” and “behavior,” have neuronal or brain-specific functions. For example, the top GO term categorized under cellular component is “synapse” (large green asterisk in Fig. 2—7E),

which contains the following genes that increase in expression in *Zc3h14*$^{\Delta/\Delta}$ hippocampi when compared to *Zc3h14*$^{+/+}$ hippocampi: Atp1a2, Camk2a, Nrgn, Psd3, Slc1a2, Slc1a3, Sparcl1, Sv2a (small green asterisks). Furthermore, the majority of the top 10 increased proteins cluster into the GO terms "signal transduction" and/or "membrane." In contrast, none of the top 10 decreased proteins cluster into common GO terms. This global GO term analysis of the increased protein set suggests that mutation of *Zc3h14* causes increased steady state levels of proteins in cellular components or processes important for brain function such as the synapse and signal transduction.

2.3 Discussion

We have generated a *Zc3h14*$^{\Delta/\Delta}$ mouse to study the function of the evolutionarily conserved, ubiquitously expressed polyadenosine RNA-binding protein, ZC3H14. Results demonstrate that *Zc3h14* is not essential for viability. However, the *Zc3h14*$^{\Delta/\Delta}$ mice show morphological and behavioral defects. Quantitative proteomic analysis reveals enrichment of proteins involved in for synaptic plasticity and function. Taken together, this work provides a mouse model in which to study the function of ZC3H14 in the mammalian brain as well as a potential model for why ZC3H14 is critical for proper brain function.

ZC3H14 orthologues in *S. cerevisiae* (23) and *Drosophila* (32) are essential for full viability. However, patients who lack expression of ZC3H14 isoforms (isoforms 1-3), which most closely resemble the evolutionarily conserved gene product shared by the yeast and flies, are alive (32). Furthermore, the patients are diagnosed with nonsyndromic intellectual disability indicating that major impairment is limited to the brain despite the

fact that ZC3H14 isoforms 1-3 are ubiquitously expressed (30). The *Zc3h14*$^{\Delta/\Delta}$ mouse, which lacks expression of all ZC3H14 isoforms, allows us to address the question of whether the gene is essential in a mammalian model organism. *Zc3h14*$^{\Delta/\Delta}$ mice are indeed viable, fertile, and appear to show normal growth. Similar to the nonsyndromic characteristics of *ZC3H14* patients who grow to a normal height and have a normal head circumference (32), *Zc3h14*$^{\Delta/\Delta}$ mice have normal overall body weight as well as normal brain and hippocampal weights. Furthermore, *Zc3h14*$^{\Delta/\Delta}$ mice pass tests of visual acuity and contrast sensitivity as well as exhibit normal general motor function and coordination. However, consistent with the nonsyndromic intellectual disability diagnosed in patients, the *Zc3h14*$^{\Delta/\Delta}$ mice show defects in working memory indicative of impaired higher-order brain function.

Results of the behavioral analyses reveal that the *Zc3h14*$^{\Delta/\Delta}$ mice are capable of spatio-temporal learning. However, they show defects in working memory. These data are remarkably consistent with studies in a *Drosophila* model, in which flies depleted of the ZC3H14 orthologue (dNab2) specifically in neurons, show defects in short-term memory but preserved learning ability (34). Working memory is closely related to attention (87), and measures of working memory capacity predict higher performance on executive function tasks (88). Not only is working memory critical to brain development (89), but it is also a marker for age-related declines in cognitive function (90). Taken together, it is possible that the human phenotype is, at least in part, recapitulated by the behavioral results in our rodent model.

Both the *Drosophila* and mouse models show morphological defects in the brain upon loss of dNab2/ZC3H14. In *dNab2* mutant flies, the lobes of the mushroom bodies,

neuropil which are essential for learning in flies (91), are malformed and show crossing-over defects of axons across the midline (34). Interestingly, such defects have also been reported in the fragile X syndrome fly model (92). The *Zc3h14*$^{\Delta/\Delta}$ mice show enlarged lateral ventricles, which are anatomically adjacent to the hippocampi. Such enlargement of lateral ventricles has been reported in a mouse model of an autism spectrum disorder, Smith-Lemli-Opitz syndrome (93) as well as mouse models of Down syndrome (94). Furthermore, enlargement of lateral ventricles is a hallmark of developmental disability (95) and age-related cognitive decline (96, 97) in humans. *Zc3h14*$^{\Delta/\Delta}$ mice thus have in common with several developmental disorders of the brain this enlargement of lateral ventricles. Further studies will be required to determine the causes and consequences of this morphological change.

Two tissues that are highly dependent on spatial and temporal control of gene expression are the brain (64, 98, 99) and the testes (100, 101). Consequently, changes in testis size are commonly associated with disorders of intellectual disability (102-106). A striking phenotype we observe in the *Zc3h14*$^{\Delta/\Delta}$ mice is the decreased size of the testes, which suggests a requirement for ZC3H14 in proper testes development or maintenance. In fact the testes have high expression of all ZC3H14 isoforms including the testes-enriched isoform d (30). The testes themselves are rich in RNA-binding proteins (100, 101), many of which are expressed as testes-specific isoforms (107, 108). Furthermore, spermatogenesis is highly dependent on post-transcriptional processing (109). Additional studies are necessary to understand the requirement for ZC3H14 in the testes and the role ZC3H14, in particular the mammalian-specific isoform 4, plays in the testes.

With respect to the key function of ZC3H14, previous studies established that ZC3H14 and its orthologues play an evolutionarily conserved role in regulating polyadenylation of RNAs in budding yeast (24), in *Drosophila* (32), and in a murine neuroblastoma cell line (35). Utilizing the *Zc3h14*$^{\Delta/\Delta}$ mice, we present the first functional characterization of the mammalian ZC3H14 protein *in vivo*. Our results reveal that ZC3H14 is required for proper control of poly(A) tail length in the hippocampus. Proper control of poly(A) tail length is crucial for regulation of mRNA (50), especially in neurons that require precise temporal and spatial control of gene expression (110). Several studies highlight the importance of poly(A) tail length control in maintaining this precise mRNA expression in neurons (111-114). The elongated poly(A) tail may increase the half-life (50) of specific target RNAs and/or increase translation through a CPEB (cytoplasmic polyadenylation element binding protein) mechanism (15, 115). Either mechanism could lead to an increased steady state level of these proteins. Furthermore, GO-term analysis of our mass spectrometry results reveals a unilateral increase in the expression of proteins (e.g. Camk2a) important for processes such as signal transduction and synaptic functioning. Disruption of ZC3H14-mediated control of polyadenylation and/or translation may cause aberrations in memory formation and neuronal circuitry, as observed in the *Zc3h14*$^{\Delta/\Delta}$ mice on the WRAM and seizure-induction paradigms, respectively. These data suggest that ZC3H14 may directly or indirectly play a role in translational regulation of key target transcripts necessary for proper brain function.

In conclusion, we have generated a *Zc3h14*$^{\Delta/\Delta}$ mouse as a tool to study the role ZC3H14 plays in the mammalian brain. We establish here that ZC3H14 is required for proper brain function in mice and also demonstrate the ZC3H14 plays a conserved role in

polyadenylation within the hippocampus. Based on our proteomic analysis, we present a model where ZC3H14 regulates the expression of proteins critical for brain function. Utilizing this mouse model, future work will focus on identifying specific target mRNAs for which ZC3H14 regulates polyadenylation and/or translational control that are important for the brain.

2.4 Figures

Figure 2—1

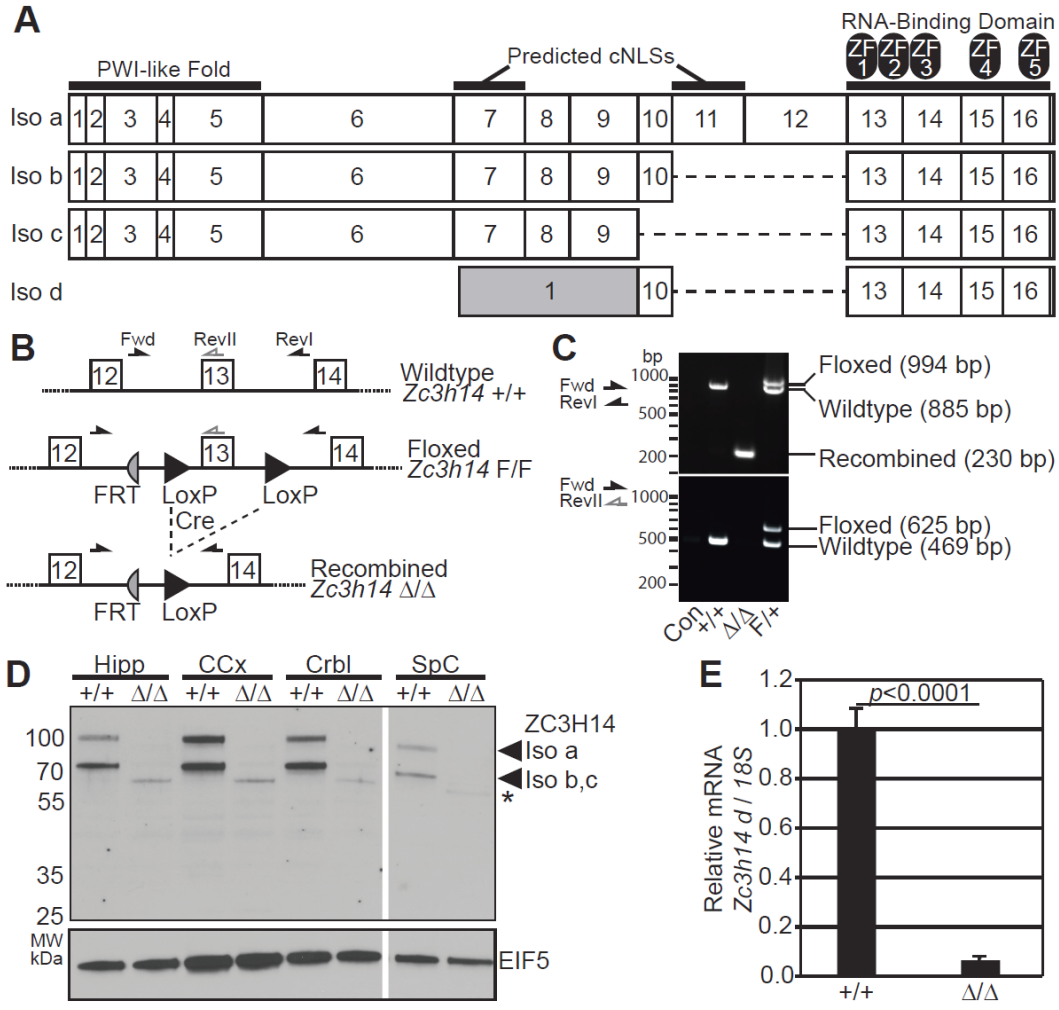

Figure 2—1: Generation of *Zc3h14*$^{\Delta/\Delta}$ mice.

(A) Schematic of four protein isoforms of murine *Zc3h14* gene (Isoforms a-d). All isoforms generated contain the C-terminal RNA-binding domain, composed of five CCCH (Cys-Cys-Cys-His) zinc fingers (labelled as ZF1-5). Isoforms a-c contain the N-terminal PWI-like fold, important for poly(A) RNA export from nucleus in budding yeast (39) and predicted classical nuclear localization signal (NLS) motifs. Isoform d contains an alternative first exon (gray) that splices directly to exon 10 encoding a smaller protein isoform. Note that exon 13 is the first common exon among all *Zc3h14* splice variants and encodes the beginning of the critical RNA-binding domain (27, 31). **(B)** A map illustrating the location of the *loxP* and *FRT* sites adjacent to *Zc3h14* exon 13 in the floxed allele. The recombined allele illustrates the removal of *Zc3h14* exon 13 following Cre-mediated recombination. The position of the forward (Fwd) and reverse (RevI, RevII) primers used for genotyping are indicated. FRT, Flippase Recognition Target; +, control allele; F, floxed allele; Δ, recombined allele lacking exon 13. **(C)** Genotyping of the *Zc3h14* allele by PCR using primers illustrated in (B). Representative agarose gels are shown for PCR (*top gel*) using the primers flanking *Zc3h14* exon 13, including *LoxP* sites (Fwd and RevI, black arrows), or (*bottom gel*) using the Fwd primer and reverse primer located in exon 13 (RevII, grey reverse arrow). Results are shown for no genomic DNA control (Con); a +/+ control mouse; a Δ/Δ homozygous recombined mouse; and a heterozygously floxed/+ (F/+) mouse. The size of the products generated is indicated to the right, and markers in bp are shown on the left. **(D)** ZC3H14 protein was analyzed in tissue samples collected from *Zc3h14*$^{+/+}$ or *Zc3h14*$^{\Delta/\Delta}$ mouse hippocampus (Hipp), cerebral cortex (CCx), cerebellum (Crbl), and spinal cord (SpC). The top panel shows an

immunoblot for ZC3H14 using an N-terminal antibody that recognizes the PWI-like fold (30). The band corresponding to isoform a is located at ~100 kDa; and the shorter isoforms, b and c, are detected as a single band at ~70 kDa. The bottom panel shows an immunoblot for EIF5, eukaryotic Initiation Factor 5, as a loading control (116). (*) denotes a truncated N-terminal fragment of ZC3H14 (see Supplementary Material, Fig. 2—S1). **(E)** Quantitative PCR analysis of *Zc3h14* splice variant d (which lacks the PWI-like Fold recognized by the antibody), normalized to 18S rRNA as an internal control, isolated from $Zc3h14^{+/+}$ or $Zc3h14^{\Delta/\Delta}$ mouse brain. Error bars indicate SEM. $P < 0.0001$.

Figure 2—2

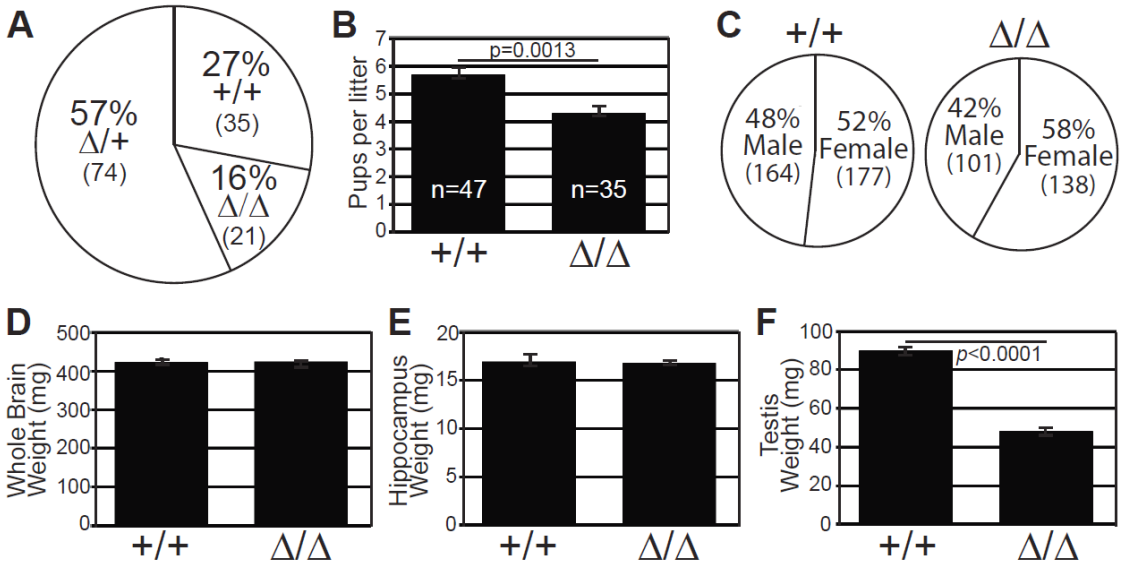
A
27%
+/+
(35)
57%
Δ/+
(74)
16%
Δ/Δ
(21)
B
Pups per litter
p=0.0013
n=47
n=35
+/+
Δ/Δ
C
+/+
Δ/Δ
48%
Male
(164)
52%
Female
(177)
42%
Male
(101)
58%
Female
(138)
D
Whole Brain
Weight (mg)
+/+
Δ/Δ
E
Hippocampus
Weight (mg)
+/+
Δ/Δ
F
Testis
Weight (mg)
p<0.0001
+/+
Δ/Δ

Figure 2—2: *Zc3h14*$^{\Delta/\Delta}$ mice are viable.

(A) *Zc3h14* genotype percentages produced by heterozygous *Zc3h14*$^{\Delta/+}$ breeding pairs. The total numbers of mice obtained for each genotype are indicated in parentheses. $P<0.0825$. **(B)** The average number of pups per litter generated from *Zc3h14*$^{+/+}$ pairings or *Zc3h14*$^{\Delta/\Delta}$ parings are indicated in the bar graph. $P=0.0013$. **(C)** The percent of males and females of *Zc3h14*$^{+/+}$ and *Zc3h14*$^{\Delta/\Delta}$ mice born from *Zc3h14*$^{+/+}$ pairings or *Zc3h14*$^{\Delta/\Delta}$ parings is presented by genotype. Means of **(D)** whole brain weight and **(E)** hippocampus weight for *Zc3h14*$^{+/+}$ and *Zc3h14*$^{\Delta/\Delta}$ adult male mice. *Zc3h14*$^{+/+}$, n=3; *Zc3h14*$^{\Delta/\Delta}$, n=3. **(F)** Testis weight (mg) comparison between *Zc3h14*$^{+/+}$ and *Zc3h14*$^{\Delta/\Delta}$ adult mice. $P<0.0001$. *Zc3h14*$^{+/+}$, n=9; *Zc3h14*$^{\Delta/\Delta}$, n=9. Error bars indicate SEM for (B), (D), (E), (F).

Figure 2—3

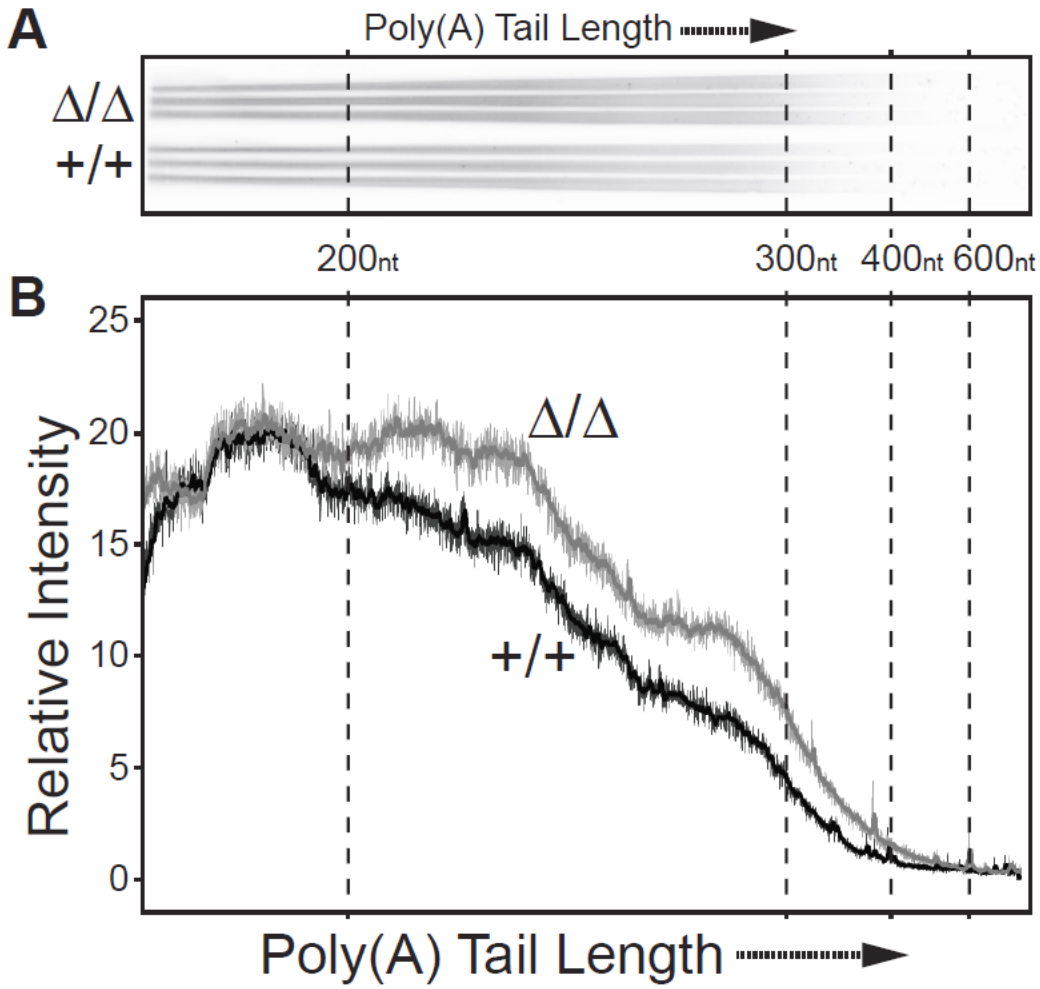
A
Poly(A) Tail Length
Δ/Δ
+/+
200nt
300nt
400nt
600nt
B
25
20
15
10
5
0
Relative Intensity
Δ/Δ
+/+
Poly(A) Tail Length

Figure 2—3: ZC3H14 is required for proper poly(A) tail length control in mice.

(A) A gel of the resolved bulk poly(A) samples is shown for *Zc3h14*$^{\Delta/\Delta}$ (Δ/Δ) and *Zc3h14*$^{+/+}$ (+/+) hippocampal samples isolated from 3 independent mice. Approximate positions of nucleotide size markers (nt) are indicated. **(B)** To provide a quantitative measure of poly(A) tail length across samples, the Relative Intensity of the signal is plotted along the length of the poly(A) tail as determined by the size markers. The positions of the scan corresponding to 200, 300, 400, and 600 nucleotides (nt) are indicated.

Figure 2—4

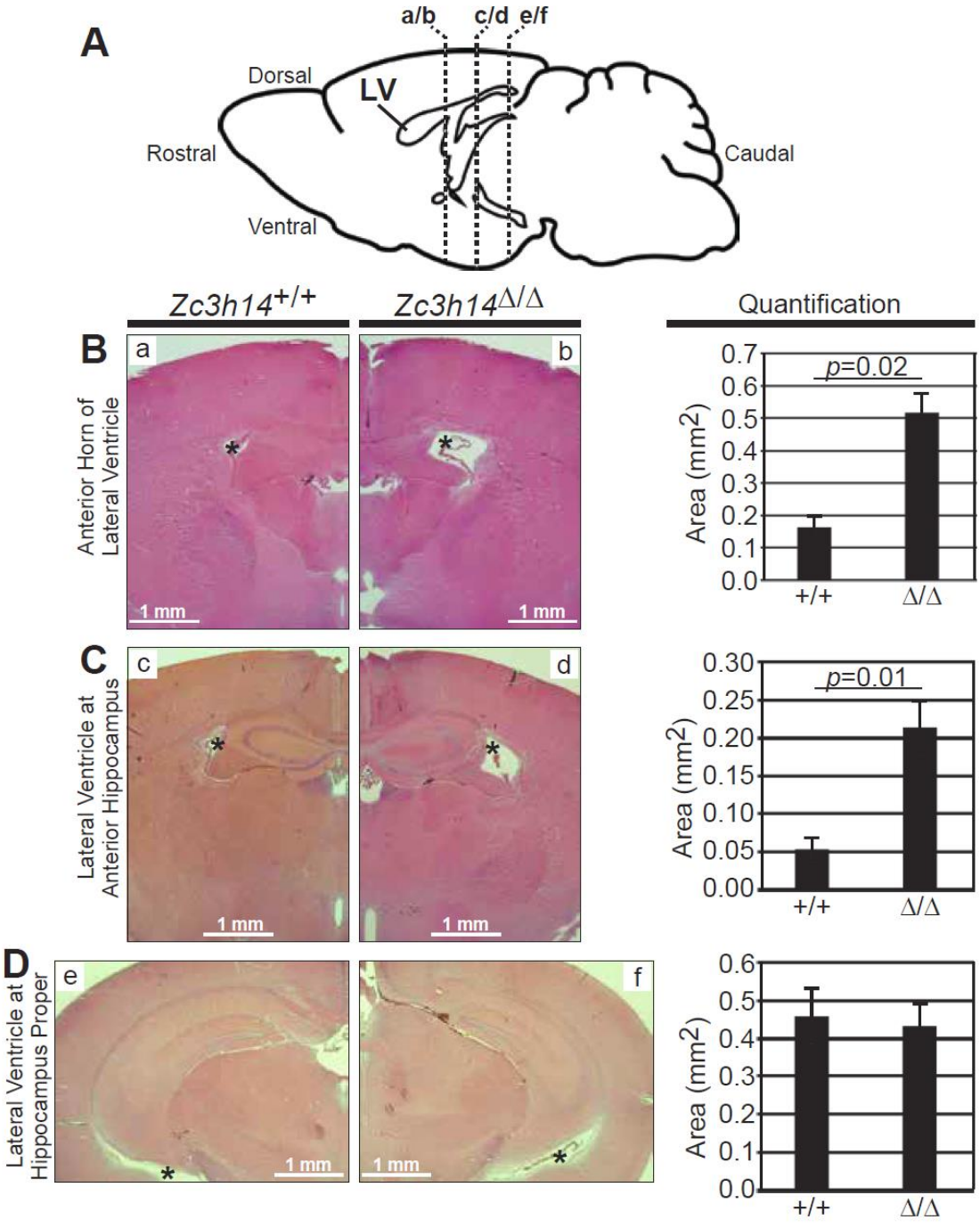
A
a/b
c/d
e/f
Dorsal
LV
Rostral
Caudal
Ventral
Zc3h14+/+
Zc3h14Δ/Δ
Quantification
B
Anterior Horn of Lateral Ventricle
a
b
1 mm
1 mm
p=0.02
Area (mm2)
0.7
0.6
0.5
0.4
0.3
0.2
0.1
0.0
+/+
Δ/Δ
C
Lateral Ventricle at Anterior Hippocampus
c
d
1 mm
1 mm
p=0.01
Area (mm2)
0.30
0.25
0.20
0.15
0.10
0.05
0.00
+/+
Δ/Δ
D
Lateral Ventricle at Hippocampus Proper
e
f
1 mm
1 mm
Area (mm2)
0.6
0.5
0.4
0.3
0.2
0.1
0.0
+/+
Δ/Δ

Figure 2—4: Brain ventricular size defect in *Zc3h14*$^{\Delta/\Delta}$ mice.

(A) Diagram of lateral view of mouse brain and location of coronal sections shown in the following histological images. LV, lateral ventricle. Representative H&E stains of lateral ventricles of *Zc3h14*$^{+/+}$ (+/+) and *Zc3h14*$^{\Delta/\Delta}$ (Δ/Δ) adult mice at the following level of slices: **(B)** anterior horns of ventricles (***a***/***b*** in diagram), **(C)** anterior hippocampus (***c***/***d*** in diagram), and **(D)** hippocampus proper (***e***/***f*** in diagram). Magnification x2. Scale bars, 1 mm. *, lateral ventricle. H, hippocampus. Shown to the right are the corresponding quantifications of the area (mm^2) of the lateral ventricles at the indicated levels for *Zc3h14*$^{+/+}$ and *Zc3h14*$^{\Delta/\Delta}$ mice. Error bars indicate SEM. For quantification of anterior horns of lateral ventricles; *Zc3h14*$^{+/+}$, n=3; *Zc3h14*$^{\Delta/\Delta}$, n=5. For quantification of lateral ventricles at anterior hippocampus; *Zc3h14*$^{+/+}$, n=3; *Zc3h14*$^{\Delta/\Delta}$, n=3. For quantification of lateral ventricles at hippocampus proper; *Zc3h14*$^{+/+}$, n=6; *Zc3h14*$^{\Delta/\Delta}$, n=6.

Figure 2—5

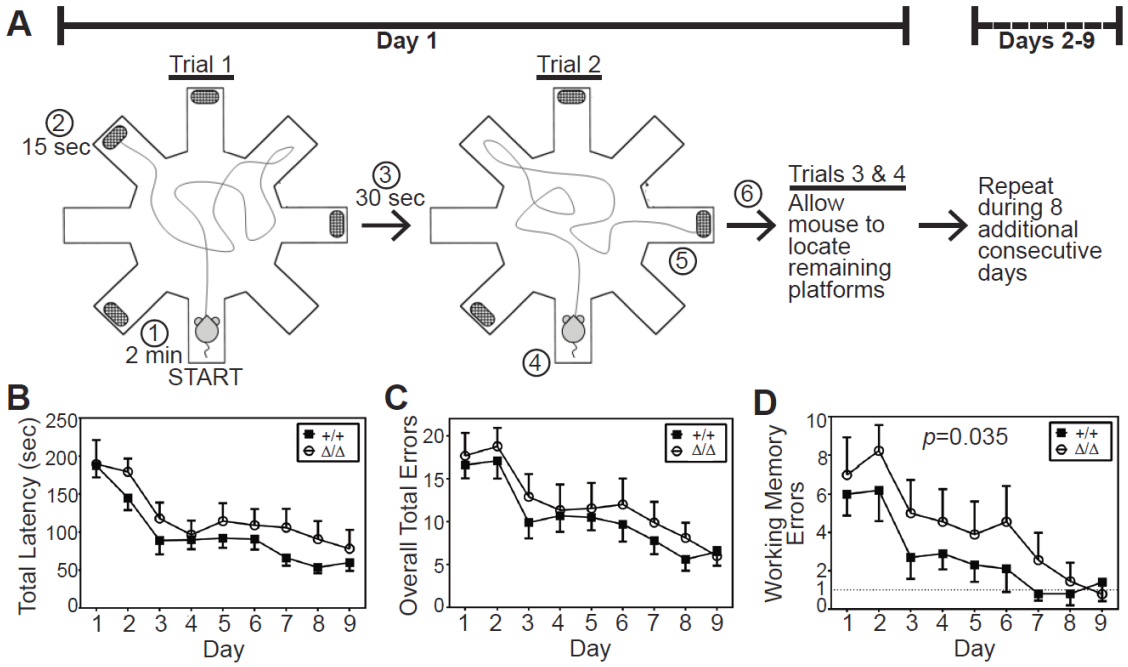
A
Day 1
Days 2-9
Trial 1
Trial 2
② 15 sec
③ 30 sec
⑥
Trials 3 & 4
Allow mouse to locate remaining platforms
Repeat during 8 additional consecutive days
⑤
① 2 min START
④
B
Total Latency (sec)
250
200
150
100
50
0
1 2 3 4 5 6 7 8 9
Day
+/+
Δ/Δ
C
Overall Total Errors
20
15
10
5
0
1 2 3 4 5 6 7 8 9
Day
+/+
Δ/Δ
D
Working Memory Errors
p=0.035
10
8
6
4
2
1
0
1 2 3 4 5 6 7 8 9
Day
+/+
Δ/Δ

Figure 2—5: WRAM (water radial arm maze) analysis of learning and working memory.

(A) Schematic of apparatus and 9-day testing procedure (80). Mice are given two minutes to locate a hidden platform positioned at the far ends of four of eight arms. If a mouse is unable to locate a platform within two minutes of beginning the trial, it is gently guided to the nearest platform. Upon successful escape from water onto platform, mice are rewarded with 15 sec of rest on platform, followed by 30 sec of rest in a heated, dry cage. At the start of trial 2, the previously located platform is taken away and mice proceed to find one of the remaining hidden platforms. This process is repeated until all platforms are found, one in each trial. These four trials are repeated daily for a total of 9 consecutive days. Circled numbers indicate sequence of events in trials. The experiment compares *Zc3h14*$^{+/+}$ (+/+, closed squares) to *Zc3h14*$^{\Delta/\Delta}$ (Δ/Δ, open circles) mice. **(B)** Total latency is the average time (seconds) required per subject to complete all four trials for a specified day of testing. Comparing by test day, $p<0.0001$; comparing by genotype, $p=0.11$, indicating no difference. **(C)** Overall total errors is the average number of errors made per subject for all four trials for a specified day. Comparing by test day, $p<0.0001$; comparing by genotype, $p=0.20$, indicating no difference. **(D)** The average number of working memory errors, represented by reentry into any maze arm during a given trial, per subject for a specified day, is shown. Dashed line at 1 working memory error represents sufficient performance on WRAM. Comparing by test day, $p<0.0001$; comparing by genotype, $p=0.035$, revealing a statistically significant difference. Open circles indicate *Zc3h14*$^{\Delta/\Delta}$. Closed squares indicate *Zc3h14*$^{+/+}$. All tested mice were male. *Zc3h14*$^{+/+}$, n=10; *Zc3h14*$^{\Delta/\Delta}$, n=9. Error bars indicate SEM for (B), (C), (D).

Figure 2—6

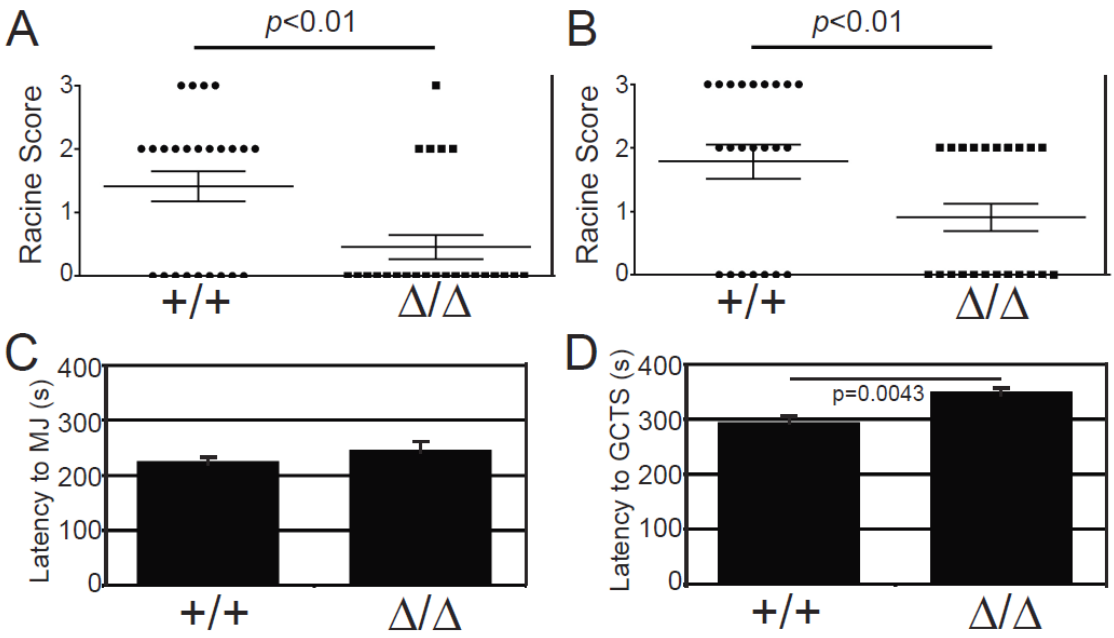
A
p<0.01
Racine Score
3
2
1
0
+/+
Δ/Δ
B
p<0.01
Racine Score
3
2
1
0
+/+
Δ/Δ
C
Latency to MJ (s)
400
300
200
100
0
+/+
Δ/Δ
D
Latency to GCTS (s)
p=0.0043
400
300
200
100
0
+/+
Δ/Δ

Figure 2—6: *Zc3h14*$^{\Delta/\Delta}$ mice are resistant to induced seizures.

Mice, *Zc3h14*$^{+/+}$ (+/+) and *Zc3h14*$^{\Delta/\Delta}$ (Δ/Δ), were subjected to the 6-Hz paradigm. Results are plotted as Racine Score for each mouse tested. **(A)** Female mice were tested at a current intensity of 13 mA. **(B)** Male mice were subjected to a current intensity of 15 mA. For both (A) and (B), $p < 0.01$. **(C)** Female mice were exposed to the chemical convulsant flurothyl. Latency to initial myoclonic jerk (MJ) was not significantly different between *Zc3h14*$^{+/+}$ and *Zc3h14*$^{\Delta/\Delta}$ mice. **(D)** Latency to first generalized tonic-clonic seizure (GTCS) was significantly higher in *Zc3h14*$^{\Delta/\Delta}$ mice compared to *Zc3h14*$^{+/+}$ mice ($p = 0.0043$).

Figure 2—7

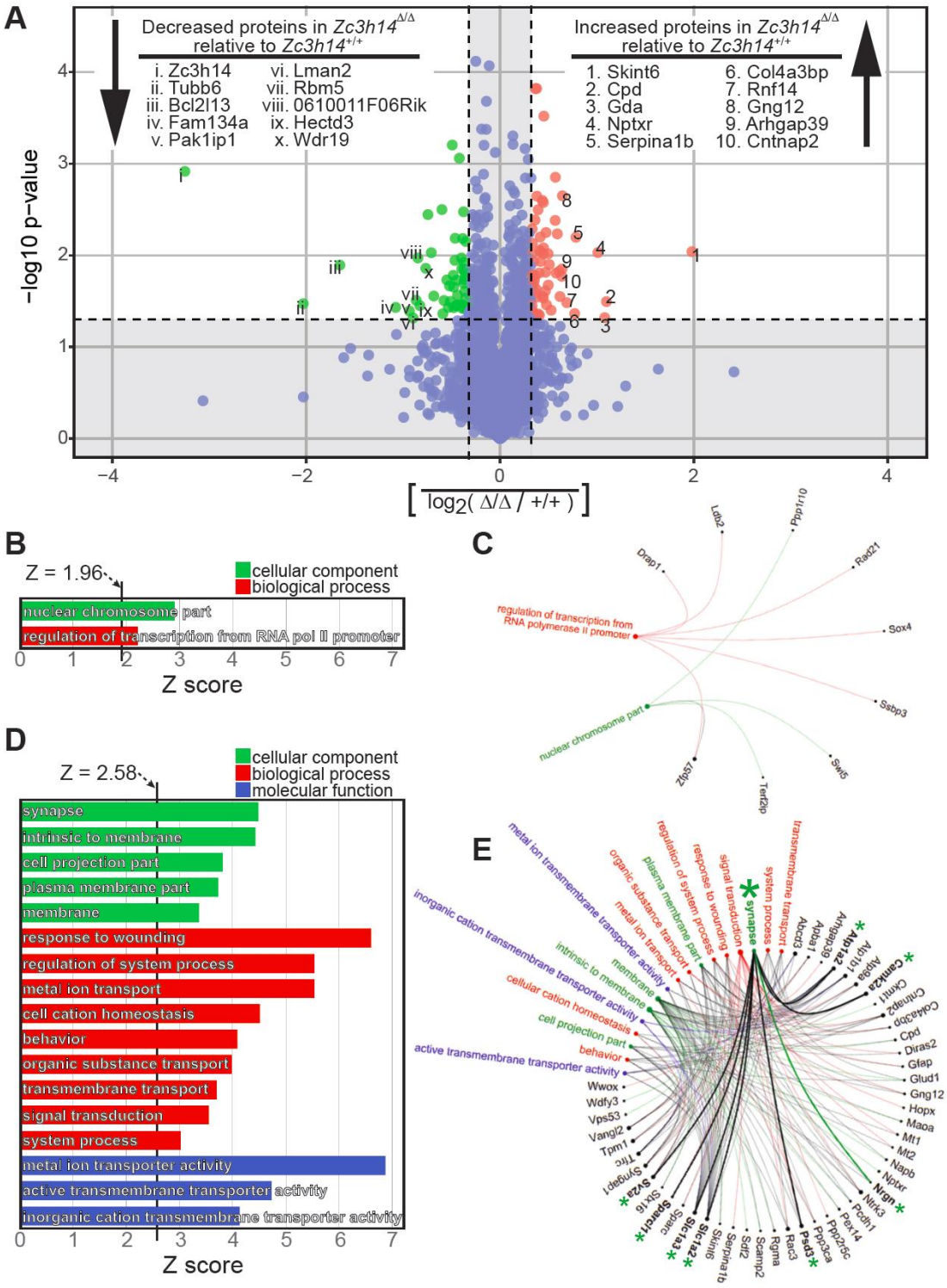
A
Decreased proteins in Zc3h14Δ/Δ relative to Zc3h14+/+
i. Zc3h14
ii. Tubb6
iii. Bcl2l13
iv. Fam134a
v. Pak1ip1
vi. Lman2
vii. Rbm5
viii. 0610011F06Rik
ix. Hectd3
x. Wdr19
Increased proteins in Zc3h14Δ/Δ relative to Zc3h14+/+
1. Skint6
2. Cpd
3. Gda
4. Nptxr
5. Serpina1b
6. Col4a3bp
7. Rnf14
8. Gng12
9. Arhgap39
10. Cntnap2
−log10 p−value
log2(Δ/Δ / +/+)
B
Z = 1.96
cellular component
biological process
nuclear chromosome part
regulation of transcription from RNA pol II promoter
Z score
C
Lab2
Ppp1r10
Drap1
Rad21
regulation of transcription from RNA polymerase II promoter
Sox4
Ssbp3
nuclear chromosome part
Zfp57
Swi5
Terf2ip
D
Z = 2.58
cellular component
biological process
molecular function
synapse
intrinsic to membrane
cell projection part
plasma membrane part
membrane
response to wounding
regulation of system process
metal ion transport
cell cation homeostasis
behavior
organic substance transport
transmembrane transport
signal transduction
system process
metal ion transporter activity
active transmembrane transporter activity
inorganic cation transmembrane transporter activity
Z score
E
metal ion transmembrane transporter activity
inorganic cation transmembrane transporter activity
active transmembrane transporter activity
synapse
intrinsic to membrane
cell projection part
cellular cation homeostasis
behavior
plasma membrane part
organic substance transport
metal ion transport
regulation of system process
response to wounding
signal transduction
system process
transmembrane transport
Abcd3
Ap1ar
Arhgap39
Ap1b1
Ap3s1
Cntnap2
Cpd
Diras2
Gfap
Glud1
Gng12
Hopx
Maoa
Mt1
Mt2
Napb
Nptxr
Nrgn
Ntrk3
Pcdh1
Pex14
Ppp2r5c
Ppp3ca
Rab3
Rgma
Scamp2
Sdf2
Serpina1b
Skint6
Slc17a3
Slc17a7
Sparcl1
Sparc
Stx16
Syt4
Syngap1
Ttc
Tpm1
Vangl2
Vps53
Wdfy3
Wwox

Figure 2—7: Proteomic analysis of *Zc3h14*$^{+/+}$ versus *Zc3h14*$^{\Delta/\Delta}$ hippocampi.

(A) Volcano plot of all proteins with changed expression levels between *Zc3h14*$^{+/+}$ *and* *Zc3h14*$^{\Delta/\Delta}$ hippocampi, represented as colored dots. Statistically significantly changed proteins are highlighted as green dots and red dots. Among these, 50 proteins have decreased expression (green dots) in *Zc3h14*$^{\Delta/\Delta}$ hippocampi when compared to *Zc3h14*$^{+/+}$ hippocampi, and 63 proteins have increased expression (red dots). Inclusion criteria for statistically significance are 1.25 fold change and $p < 0.05$. The top 10 hits for decreased and increased proteins are listed, along with their relative positions (Roman or Arabic numerals, respectively) on the volcano plot. The remaining proteins that did not meet statistical significance are represented as teal dots and fall within the shaded region of the plot, the boundaries of which are set by the aforementioned inclusion criteria. **(B)** For the decreased gene set, the two GO terms along with their Z-scores are listed. Inclusion criteria for this analysis are Z-score ≥ 1.96, *p* value < 0.05, and ≥ 3 genes per GO term. **(C)** The nine decreased genes that cluster and their corresponding GO terms are shown by a connecting line. **(D)** For the increased gene set, the list of GO terms along with their Z-scores are listed. Inclusion criteria for this analysis are Z-score ≥ 2.58, *p* value < 0.01, and ≥ 5 genes per GO term. **(E)** The increased genes that cluster into the listed GO terms in (D) are depicted. The corresponding GO terms are shown by a connecting line. For example, the large green asterisk indicates a GO term (synapse) and small green asterisks indicates the genes (Atp1a2, Camk2a, Nrgn, Psd3, Slc1a2, Slc1a3, Sparcl1, Sv2a) that cluster to the GO term, also shown by connecting lines.

2.5 Supplementary Figures

Figure 2—S1

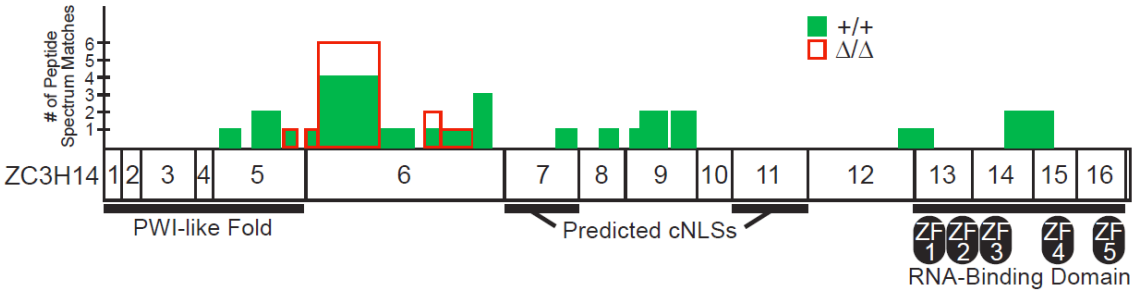

Figure 2—S1: Mass spectrometry analysis of *Zc3h14*$^{\Delta/\Delta}$ truncation products.

A schematic of ZC3H14 with individual exons denoted is shown. The functional domains are indicated on the bottom of the schematic. The top shows peptide spectrum matches (PSM) for immunoprecipitation using an N-terminal ZC3H14 antibody of ZC3H14 isolated from *Zc3h14*$^{+/+}$ (green) or *Zc3h14*$^{\Delta/\Delta}$ (red) mouse whole brain lysate. The total number of identified PSMs for ZC3H14 is indicated. The location of the peptides identified is indicated by the position on the schematic. A scale bar to the left indicates the number of times fragment was identified. ZF, zinc finger.

Figure 2—S2

A

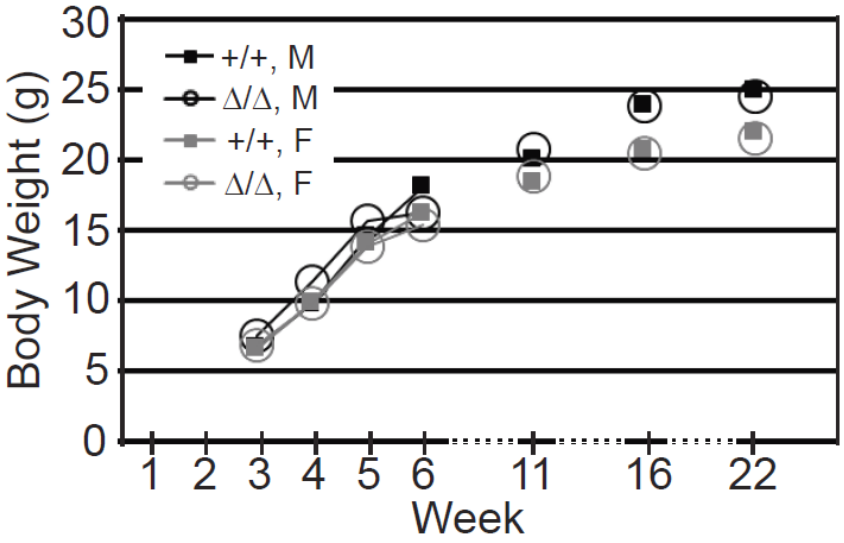

B

N values for Body Weight							
Week	3	4	5	6	11	16	22
Male +/+	7	7	8	5	7	8	6
Male Δ/Δ	3	9	8	4	5	10	6
Female +/+	6	6	8	7	6	9	5
Female Δ/Δ	4	13	9	7	8	13	9

C

SEM for Body Weight							
Week	3	4	5	6	11	16	22
Male +/+	0.46	0.96	0.93	0.32	1.07	0.40	0.60
Male Δ/Δ	1.63	0.94	0.81	1.23	1.66	0.91	1.84
Female +/+	0.33	0.43	0.33	0.32	0.44	0.44	0.73
Female Δ/Δ	0.98	0.63	0.65	0.61	0.73	0.49	0.56

D

P values for Body Weight							
Week	3	4	5	6	11	16	22
Male	0.49	0.26	0.41	0.16	0.87	0.97	0.82
Female	0.73	0.94	0.75	0.26	0.67	0.7	0.63

Figure 2—S2: Statistical values for body weight.

(A) Mean weight (grams) of animals measured from juvenile to adult age is shown. M, male. F, female. For individual data points on mouse body weight reported, the following tables show **(B)** n values, **(C)** standard error of the means (SEMs), and **(D)** *p* values.

Figure 2—S3

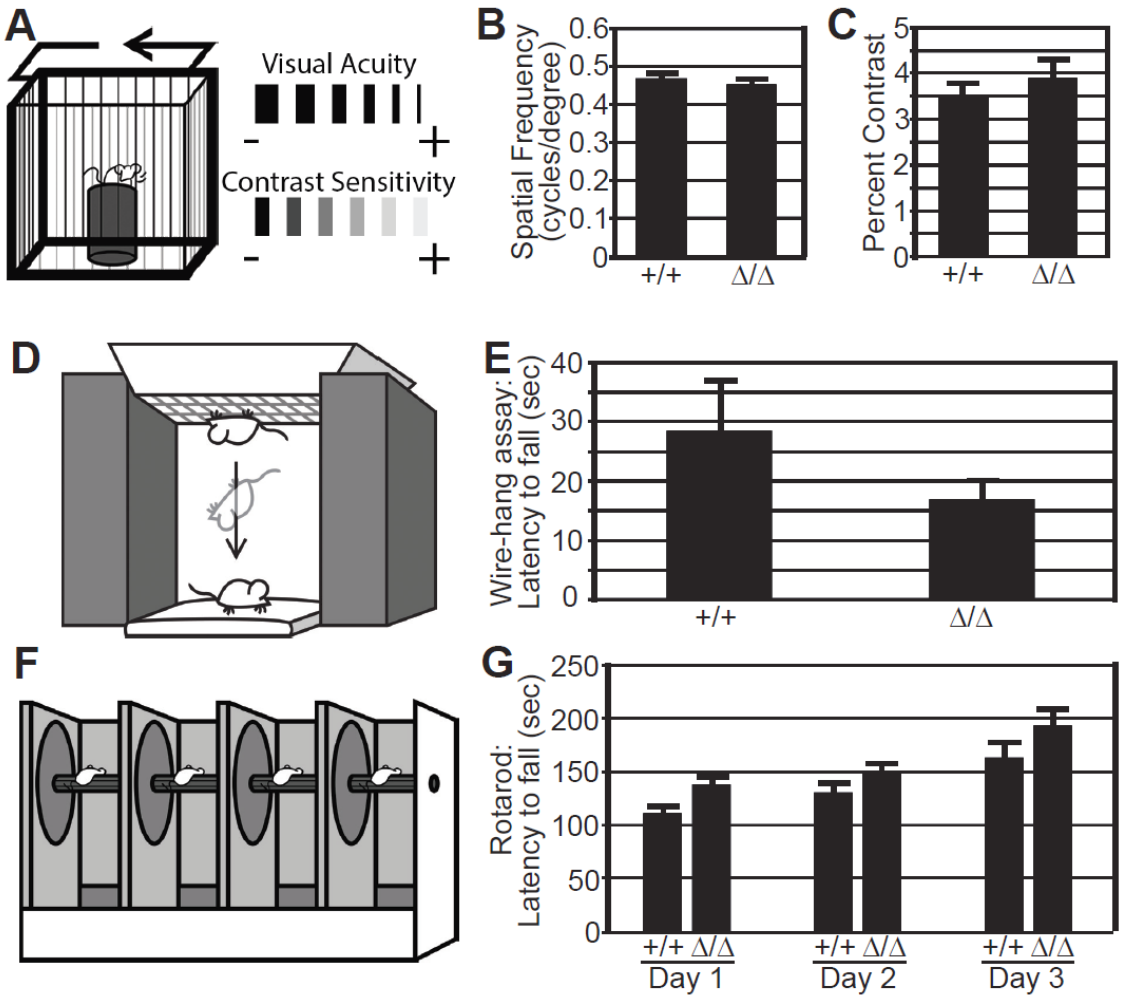
A
Visual Acuity
-
+
Contrast Sensitivity
-
+
B
Spatial Frequency (cycles/degree)
0.6
0.5
0.4
0.3
0.2
0.1
0
+/+
Δ/Δ
C
Percent Contrast
5
4
3
2
1
0
+/+
Δ/Δ
D
E
Wire-hang assay: Latency to fall (sec)
40
30
20
10
0
+/+
Δ/Δ
F
G
Rotarod: Latency to fall (sec)
250
200
150
100
50
0
+/+ Δ/Δ
Day 1
+/+ Δ/Δ
Day 2
+/+ Δ/Δ
Day 3

Figure 2—S3: Visual function and motor coordination assessments.

To rule out possible visual or motor coordination deficits that could interfere with performance during water radial arm maze, we tested the visual and motor capabilities of the mice. When compared to controls (+/+), mutant (Δ/Δ) mice performed at least as well on all visual and motor coordination assays. **(A)** Illustration of Optokinetic apparatus and visual cues. Visual acuity was measured by the ability of the mice to discern small spatial frequencies of white and black bars (117-119). Contrast sensitivity was measured by the ability of the mice to discern alternating bars of similar shades of gray (117-119). **(B)** Average of lowest spatial frequencies able to be detected by mice by genotype is shown. **(C)** Average of lowest percent contrast able to be detected by mice by genotype is shown. For (B) and (C) *Zc3h14*$^{+/+}$, n=4; *Zc3h14*$^{\Delta/\Delta}$, n=4. **(D)** Illustration of wire-hang assay setup. **(E)** Latency to fall is the average time in seconds for mice, by genotype, to fall from a wire mesh when placed upside down against gravity. *Zc3h14*$^{+/+}$, n=9; *Zc3h14*$^{\Delta/\Delta}$, n=14. Comparing by genotype, p=0.1828. **(F)** Illustration of rotarod apparatus, which measures the ability of mice to balance on a rotating rod, tested across three days. **(G)** Latency to fall is the average time for mice to fall from the rotating rod, grouped by genotype. *Zc3h14*$^{+/+}$, n=9; *Zc3h14*$^{\Delta/\Delta}$, n=10. Differences between *Zc3h14*$^{+/+}$ and *Zc3h14*$^{\Delta/\Delta}$ on a given test day were not statistically significant after applying the Bonferroni correction for repeated measures. Error bars indicate SEM for all panels in figure.

Table 2—S1

Test	Measurement	Genotype	Average	SEM	*P*
Open Field	Time in center (sec)	+/+	35.10	5.18	0.03
		Δ/Δ	77.00	17.54	
	Number of entries into the center	+/+	18.20	9.38	0.05
		Δ/Δ	27.70	12.37	
	Total distance traveled (cm)	+/+	36.60	2.67	0.62
		Δ/Δ	34.50	3.28	
	Average speed (cm/sec)	+/+	0.10	0.00	0.61
		Δ/Δ	0.10	0.01	
Novel Cage	Time spent rearing (sec)	+/+	133.00	14.05	0.38
		Δ/Δ	117.40	10.27	
	Time spent digging (sec)	+/+	44.50	10.96	0.45
		Δ/Δ	34.30	7.38	
	Time spent grooming (sec)	+/+	13.80	1.81	0.81
		Δ/Δ	13.00	2.48	
Light-Dark Box	Latency to first dark entry (sec)	+/+	15.70	4.28	0.56
		Δ/Δ	21.20	8.34	
	Number of transitions between light/dark	+/+	23.80	1.79	0.22
		Δ/Δ	26.80	1.63	
	Time in dark (sec)	+/+	393.60	19.63	0.86
		Δ/Δ	386.60	33.20	
	Time in light (sec)	+/+	206.30	19.62	0.86
		Δ/Δ	213.40	33.21	

Table 2—S1: General behavioral tests.

Twelve male *Zc3h14*$^{+/+}$ and twelve *Zc3h14*$^{\Delta/\Delta}$ mice were evaluated using several paradigms as described in Materials and Methods to assess general activity in open field, exploratory behavior in novel cage, and anxiety in light-dark box.

Chapter 3

The evolutionarily conserved RNA-binding protein dNab2 interacts with the Fragile X protein homolog and mediates translational repression in *Drosophila* neurons

***Nota bene*:**

In the current chapter, Jennifer Rha contributed only to the experiments and the associated text for Figure 3—7, showing axonal localization and polysome association of ZC3H14 in murine cells.

All *Drosophila* experiments were performed and associated text written by the remaining co-authors, primarily Rick S. Bienkowski and Kenneth H. Moberg.

This chapter has been submitted for review as:

Rick S. Bienkowski, **Jennifer Rha**, Ayan Banerjee, J. Christopher Rounds, Christina Gross, ChangHui Pak, Kevin J. Morris, Stephanie K. Jones, Michael R. Santoro, Stephen T. Warren, Gary J. Bassell, Anita H. Corbett, and Kenneth H. Moberg, "The evolutionarily conserved RNA-binding protein dNab2 interacts with the Fragile X protein homolog and mediates translational repression in *Drosophila* neurons" (2016).

3.1 Introduction

RNA-binding proteins play critical roles in the transcription, processing, and translation of mRNAs to ensure proper gene expression (60). Consistent with the importance of this class of proteins, mutations in a number of genes that encode ubiquitously expressed RNA-binding proteins have been linked to human disease (63), and in many cases, these diseases present with tissue-specific pathology (63, 120). Neurological disorders are quite prevalent among diseases linked to RNA-binding proteins (120), likely due to the requirement for finely tuned control of gene expression in neurons. The challenge in such cases is to define the tissue-specific requirements and mechanisms of action for these factors that underlie their neuronal roles.

The *ZC3H14* (zinc finger CCCH-type 14) gene encodes an RNA-binding protein that is lost in an inherited form of autosomal recessive, non-syndromic intellectual disability (32, 35). Patients homozygous for nonsense mutations in the *ZC3H14* gene have very low IQ but lack dysmorphic features (32), suggesting a specific role for the ZC3H14 protein in nervous system development or function. In support of this idea, *Drosophila* lacking dNab2, the functional orthologue of ZC3H14 (35), show reduced viability, impaired motor function, and defects in brain morphology (32, 34), phenotypes that are rescued upon neuronal re-expression of dNab2 (34, 35). Despite evidence indicating an important role in the brain, the function of this protein that is critical in neurons remains largely undefined. *Drosophila* have been used extensively to model tissue-specific human disease (121) and provide an excellent system to define molecular roles of the dNab2/ZC3H14 protein family *in vivo*.

The *Drosophila* dNab2 and human ZC3H14 proteins share a domain structure and significant sequence homology, with an N-terminal PWI (proline/tryptophan/isoleucine)-like domain, a centrally located nuclear-localization sequence, and a C-terminal domain of five CysCysCysHis (CCCH)-type zinc fingers that mediates RNA binding (32, 122). Each protein is found predominantly in the nucleus at steady-state and is widely expressed in many tissues, including the brain (32, 122). Fly dNab2 and human ZC3H14 each bind with high affinity to polyadenosine (poly(A)) RNA *in vitro* (32, 123), suggesting an interaction with the poly(A) tail of mRNAs *in vivo*. Consistent with this model, ZC3H14 colocalizes with poly(A) mRNA speckles in mouse hippocampal pyramidal neurons and cultured rat hippocampal neurons (32). In addition, RNAs harvested from the heads of adult *Drosophila* lacking dNab2, or from a mammalian neuronal cell line depleted for ZC3H14, show elongated poly(A) tails among a subset of total cellular RNA (32, 35). This elongated poly(A) tail phenotype is also observed in *S. cerevisiae* cells depleted of the Nab2 protein (24). The conserved nature of the poly(A) defect implies that dysregulated polyadenylation may drive altered patterns of mRNA stability and/or impact translation within the developing brains of flies and humans lacking dNab2/ZC3H14 that, in turn, impair neural function.

Genetic analysis in *Drosophila* has confirmed a critical and conserved requirement for dNab2 in neurons and specifically in neurons that extend axons into the mushroom bodies (34), twin neuropil structures required for associative olfactory learning and memory (91). Pan-neuronal dNab2 depletion in otherwise wildtype *Drosophila* is sufficient to replicate almost all phenotypes resulting from organism-wide loss of dNab2, including impaired adult viability, locomotor and flight defects, and a wings-held-out

phenotype (32). Reciprocally, dNab2 re-expression solely in the neurons of *dNab2* mutants rescues these same phenotypes (32). Importantly, pan-neuronal expression of a major isoform of human ZC3H14 (isoform 1) in *dNab2* mutant *Drosophila* is also sufficient to rescue a number of these defects, demonstrating a high degree of functional conservation between the dNab2 and ZC3H14 proteins in neurons (35). Notably, the *dNab2* mutant wing-posture and locomotor defects are not phenocopied by dNab2 depletion from motor neurons that innervate adult muscle (32), implying a requirement for dNab2 within central nervous system (CNS) neurons. Consistent with this observation, neuronal depletion of dNab2 impairs short-term memory in a courtship-conditioning paradigm (34) and at a structural level, dNab2 loss alters developmentally programmed patterns of axon projection into the α and β lobes of the mushroom bodies: β-lobe axons misproject across the brain midline and α-lobe axons show a high frequency of branching defects (34). Selective depletion or re-expression of dNab2 only in Kenyon cell neurons, which give rise to α and β axons, is sufficient to respectively phenocopy or rescue these defects (35). These findings confirm a critical and conserved role for dNab2 in neurons.

In aggregate, these genetic data provide strong evidence that dNab2 acts within neurons to control mushroom body morphology and behavior, but do not provide insight into molecular pathways that dNab2 uses to control these processes. The dNab2 protein likely modulates gene expression by binding to target mRNAs, perhaps in cooperation with other RNA-binding proteins. The near ubiquitous expression combined with the steady-state nuclear localization implies that dNab2 may rely on nuclear interactions to regulate mRNA processing. However the yeast Nab2 protein shuttles between the nucleus and cytoplasm (28), opening the possibility that dNab2/ZC3H14 could also play a role within

the cytoplasm. A number of other RNA-binding proteins play critical roles in the neuronal cytoplasm. For example, the most commonly inherited form of intellectual disability, fragile X syndrome, is caused by loss of expression of the RNA-binding protein FMRP (Fragile X Mental Retardation Protein). FMRP localizes to axons, dendrites and dendritic spines, and binds to target mRNAs to repress their local translation allowing for finely tuned post-synaptic, local protein translation (124, 125). FMRP is also localized to subcompartments within axons where it appears to play an important role in growth cone dynamics (126, 127) and presynaptic function during the development of neural circuits (128, 129). Thus, FMRP serves as a paradigm for how RNA-binding proteins can perform specialized critical functions within neurons.

Here, we describe a genetic screen for *dNab2* interacting loci in neurons that has uncovered a role for dNab2 as a translational repressor in association with the *Drosophila* FMRP homolog, dFMRP. We find extensive genetic interactions between *dNab2* and *dfmr1* in neuronal development and behavior that are paralleled by a physical interaction between the dNab2 and dFMRP proteins in the neuronal cytoplasm. We also provide evidence that dNab2 can engage in translational repression of specific neuronal mRNAs *in vivo* that are also targets of dFMRP. We extend these studies to demonstrate that murine ZC3H14 is also present in cytoplasmic foci and associated with translational machinery providing evidence that this translational regulatory role in the cytoplasm is conserved for ZC3H14. These data represent a critical first step in defining a molecular role for the conserved dNab2/ZC3H14 protein in neurodevelopment and neurological disease.

3.2 Results

3.2.1 *dfmr1* is a dominant modifier of *dNab2* overexpression in the eye. To probe the function of *dNab2* in neurons, we exploited our prior finding that dNab2 overexpression in *Drosophila* retinal cells (*GMR-Gal4,UAS-dNab2*, or '*GMR>dNab2'*) leads to an adult rough-eye phenotype that is modified by alleles of the *PABP2* nuclear poly(A) binding protein and the *hiiragi* poly(A) polymerase (32). The *GMR>dNab2* rough-eye is characterized by a small adult eye field, loss of pigmentation and disorganized ommatidia (Figure 3—1A), all of which presumably reflect the ability of exogenous dNab2 to interact with cellular RNAs and engage endogenous RNA regulatory mechanisms. In this candidate-based approach, genes with established roles in neurodevelopment, neuronal function, that encode RNA-binding proteins, or that autonomously regulate axonogenesis in the brain mushroom bodies in a manner similar to dNab2 (34) were analyzed for modification of the *GMR>dNab2* rough-eye phenotype. Available alleles for these candidate genes (200 in total) included loss-of-function alleles, RNAi depletion lines, and EP-type overexpression lines (130). Each candidate modifier allele was crossed into the *GMR>dNab2* background and evaluated for suppression or enhancement of the rough eye phenotype (Figure 3—1A). Of 200 alleles tested, 14 enhanced the rough eye phenotype and 30 suppressed (Figure 3—1A and Table 3—S1); some of these 44 modifiers correspond to loss-of-function alleles and others are EP-type insertions (130), confirming that the effect of dNab2 expression in eye cells is readily modified by altering gene-dosage of multiple factors among the selected group of candidates.

Multiple *GMR>dNab2* modifier alleles recovered from the genetic screen correspond to factors that function within translational regulatory pathways that involve

dfmr1, which encodes the *Drosophila* homolog of the fragile X syndrome mental retardation protein (dFMRP) (Table 3—S1). A null allele of *dfmr1*, $dfmr1^{\Delta 50}$, dominantly suppresses the *GMR>dNab2* eye phenotype, indicating that a diploid dose of *dfmr1* is required for dNab2 to disrupt eye morphology (Figure 3—1B). In addition, alleles of the miR pathway components *Argonaute-1* (*Ago1*) and *Gw182*, the *Rm62/dmp68* RNA helicase, the RNA-binding proteins *Staufen* and *Ataxin-2*, and the matrix metalloproteinase *Timp*, also modify the *GMR-dNab2* adult eye phenotype. Each of these genes interacts genetically with *dfmr1* in *Drosophila* (131-135). Furthermore, *dNab2* and *dfmr1* transgenes exhibit synthetic lethality when co-expressed in the developing eye. Transgenic overexpression of *dfmr1* in *Drosophila* causes apoptosis and a dominant rough eye phenotype (136, 137). Flies that overexpress *fmr1* in the eye (*GMR>dfmr1) are* viable in a wildtype background (*GMR-Gal4,UAS-dfmr1*) but this overexpression is lethal when *dNab2* is also overexpressed (*GMR-Gal4,UAS-dNab2,UAS-dfmr1*) (Table 3—S1). The recovery of *dfmr1* and *dfmr1*-interacting genes as *GMR-dNab2* modifiers led us to explore whether dNab2 and dFMRP function within similar neuronal pathways and/or complexes.

3.2.2 *dfmr1* interacts with *dNab2* in locomotor behavior and mushroom body development. To further explore interactions between dNab2 and dFMRP in neurons, we examined neuronally encoded locomotor behavior and development of the mushroom bodies, twin neuropil structures in the brain that are essential for olfactory learning and memory (91). Pan-neuronal RNAi-mediated depletion of dNab2 causes a locomotor defect in adult flies that is not replicated by depletion solely in motor neurons (32), implying a requirement for dNab2 in central nervous system (CNS) circuits that support locomotion. This dNab2-RNAi locomotor defect is dominantly enhanced by the $dfmr1^{\Delta 113M}$ null allele

(*C155-Gal4,UAS-dNab2-RNAi;dfmr1*$^{\Delta 113M}$/+) (Figure 3—1F). This effect of a second, independent *dfmr1* allele, *dfmr1*$^{\Delta 113M}$, parallels the suppressing effect of *dfmr1*$^{\Delta 50}$ on the gain-of-function *GMR-dNab2* model and provides additional evidence of a tight link between *dNab2* and *dfmr1* gene dosage.

dNab2 and dFMRP each act cell-autonomously within the Kenyon cell neurons of the mushroom bodies to pattern axon projection (34, 92). Loss of either factor elicits similar mushroom body defects, including misprojection of β-lobe axons across the brain midline (ß-lobe fusion) and missing or thinned α-lobes [(34, 92) and Figure 3—2]. These α/β-lobe defects appear with similar severity and penetrance in each homozygous null background (*dNab2*^{ex3} or *dfmr1*$^{\Delta 50}$) ((92) and Figure 3—2A,B), suggesting the potential for shared effects on downstream pathways. Consistent with this idea, heterozygosity for either gene has no detectable effect on mushroom body morphology in isolation, but dominantly modifies mushroom body phenotypes caused by loss of the other gene. *dfmr1* heterozygosity significantly increases the frequency of α-lobe defects (i.e. missing or thinned α-lobes as judged by anti-Fas2 staining) in *dNab2* null brains without a corresponding effect on β-lobe defects (Figure 3—2D,G,H). Reciprocally, *dNab2* heterozygosity rescues the frequency of α-lobe defects in *dfmr1* null brains with no discernable effect on β-lobes (Figure 3—2E,H). Thus, although removing dNab2 from otherwise wildtype Kenyon cells leads to highly penetrant defects in α-lobe development (34), reducing dNab2 dosage in *dfmr1* null neurons has the opposite effect of rescuing α-lobe development (Figure 3—2G). This remarkable pattern of opposing effects of *dNab2* alleles on α-lobe structure implies that dNab2 can either promote or disrupt α-lobe

development depending on *dfmr1* status, perhaps via linked roles for dNab2 and dFMRP proteins on an overlapping cohort of transcripts with roles in α-lobe development.

3.2.3 dNab2 co-localizes with dFMRP RNPs in neurites. The abundant and complex genetic links between *dNab2* and *dfmr1* in retinal and CNS neurons suggest that the two RNA-binding proteins may associate with one another within RNA-protein complexes. A dNab2-dFMRP association would be somewhat surprising, given that the majority of each protein localizes to distinct cellular compartments at steady-state: dNab2 is localized to the nucleus at steady state (32, 138) while dFMRP is primarily cytoplasmic (139). However, orthologs of dNab2 and dFMRP undergo dynamic nucleocytoplasmic shuttling (140, 141). Human FMRP binds mRNA transcripts in the nucleus and accompanies them to the cytoplasm (142) and *S. cerevisiae* Nab2 also shuttles between the nucleus and the cytoplasm in a manner that depends on poly(A) RNA export (141). To examine the subcellular distribution of dNab2 in single neurons, we utilized an anti-dNab2 antibody (32) to track dNab2 protein in 3-day old cultured primary *Drosophila* brain neurons (Figure 3—3). These neuronal cultures were co-stained with an anti-HRP antibody to visualize neuronal membranes and illuminate neurite arbors (Figure 3—3A). As previously reported (32), the dNab2 protein is enriched in the nucleus of all neurons examined; however, two-thirds of these neurons also contain cytoplasmic dNab2 in the form of discrete puncta distributed along the length of neurites (Figure 3—3A,C). To confirm that the cytoplasmic signal is due to dNab2, we demonstrated that it is lost in cultured neurons derived from dNab2 null brains (Figure 3—3B). Of the cultured cells examined, only 2/3 have detectable dNab2 in the cytoplasm. This diversity could reflect the fact that the cultured neurons contain a mixture of types of neurons that are not readily distinguished *in vitro*. We

hypothesized that cell-to-cell variation in the presence of dNab2 cytoplasmic puncta in mixed brain cultures could be due to differences in dNab2 localization between specific types of neurons. To test this hypothesis, the distribution of dNab2 protein was examined in neuronal cultures expressing membrane-tethered GFP in Kenyon cells (*OK107-Gal4,UAS-CD8:GFP*), which extend axons into the mushroom body lobes (143). This approach labels Kenyon cells with GFP and allows for identification of these cells in the mixed culture. Among these CD8:GFP-positive Kenyon cells examined, 80% (8 of 10) contained dNab2 cytoplasmic puncta (Figure 3—4E). Thus, even within a single neuronal cell type, there is cell-to-cell variation in whether or not dNab2 can be detected in cytoplasmic puncta. The reason for this variation is not clear, however it could be stochastic or due to Kenyon cell subtype (e.g. α, α', β, β' or γ) or developmental age (e.g. 'early' vs 'late' born mushroom body neurons). In sum, these fluorescence data identify a previously undefined pool of dNab2 present within neurites.

We next tested whether dFMRP co-localizes with cytoplasmic dNab2 puncta in neuronal processes of wildtype brain neurons illuminated by anti-HRP (Figure 3—4A). As described by others (132, 133), dFMRP is detected in the soma cytoplasm and in puncta that distribute along the length of neurites (Fig 3—4A), which correspond to dFMRP-containing ribonucleoprotein (RNP) granules (132, 133). Importantly, when dNab2 localization is analyzed in these same neurites, dNab2 and dFMRP co-localize within a subset of these neurite puncta (Figure 3—4A, arrows). Mander's Coefficient was used to quantitate dNab2-dFMRP co-localization specifically in neurites distal from the cell body (Figure 3—4A). By this analysis, approximately 20% of total dNab2 signal in neurites overlaps with dFMRP-positive puncta and approximately 25% of the dFMRP signal in

neurites overlaps with dNab2-positive puncta. This co-localization of subsets of dNab2 and dFMRP protein in neurites suggests that dNab2 may be a component of a subset of dFMRP-containing RNP granules in brain neurons. These data also provide a potential molecular context for the strong genetic interactions between *dNab2* and *dfmr1* in retinal cells and brains neurons.

3.2.4 The dNab2 and dFMRP proteins physically associate in neurons. To assess whether dNab2 and dFMRP physically interact and corroborate the immunofluoresence data, the RNA-tagging technique (144) was used to precipitate N-terminally Flag-epitope tagged Nab2 from brain neurons. Briefly, lysates generated from heads of flies with pan-neuronal expression of Flag-dNab2 (*C155-Gal4;UAS-Flag-Nab2*) were immunoprecipitated with anti-Flag antibody-conjugated agarose beads. This technique effectively enriches for Flag-tagged dNab2 or a control Flag-tagged RNA-binding protein, human PABP (Flag-hPABP) (144), from head lysates (Figure 3—4B). Negative control lysates prepared from flies expressing the *C155-Gal4* driver alone did not immunoprecipitate detectable anti-Flag reactive epitopes. Immunoblot of these anti-Flag precipitates with anti-dFMRP antibody (145) specifically detects dFMRP protein only in the Flag-dNab2 sample and not in the Flag-hPABP or Gal4-alone samples, indicating that dNab2 may be part of protein-RNA complex that includes dFMRP.

To biochemically localize the dNab2-dFMRP association within cells, we exploited a muscle-specific driver (*MHC-Gal4*) in order to provide sufficient starting tissue for biochemical fractionation. The immunoprecipitation protocol was repeated with lysate prepared from *MHC>Flag-dNab2* adult flies that was fractionated into nuclear and cytoplasmic fractions. Immunoblotting these lysates with an antibody to the nuclear protein

Lamin D confirms the separation of soluble nuclear and cytoplasmic proteins (Figure 3—4C, bottom panel). Immunoblot analysis of total lysates prior to immunoprecipitation reveals the expected nuclear enrichment of Nab2 and cytoplasmic enrichment of dFMRP, but also detects pools of each protein in the reciprocal compartment (i.e. dNab2 in the cytoplasm and dFMRP in the nucleus). Significantly, upon anti-Flag immunoprecipitation, dFMRP is detected in association with cytoplasmic dNab2 but not the considerably more abundant pool of nuclear dNab2. The dNab2-dFMRP association is not disrupted by addition of RNAse, indicating that co-immunoprecipitation of the two proteins is not RNA-dependent (Supplemental Figure 3—S1). This biochemical evidence of a dNab2-dFMRP complex in the cytoplasm parallels the co-localization of dNab2 and dFMRP in neurites and provides further a correlate to the genetic evidence that these proteins co-regulate mushroom body development. Thus, dNab2 may be a component of dFMRP-containing RNA-protein granules in the neuronal cytoplasm.

3.2.5 dFMRP and dNab2 co-regulate target RNAs. The conserved requirement for dNab2/ZC3H14 in supporting higher cognitive function (32, 34, 146) indicates that the RNAs bound and regulated by this RNA-binding protein are important for neural development and/or function. The spectrum of dNab2-regulated RNAs is not known, but the dNab2-dFMRP association implies that dNab2 could play a role in regulating mRNAs that are also regulated by dFMRP. Two well-conserved mRNA targets of dFMRP/FMRP are *futsch*, the *Drosophila* homolog of *microtubule-associated protein-1B* (*Map1B*) (147), and the *Calmodulin-dependent protein Kinase II* (*CaMKII*) (134). dFMRP interacts with the *futsch* and *CamKII* mRNAs and represses their translation (147, 148); consequently

both proteins are elevated in *Drosophila* neurons lacking dFMRP (134, 147). Similarly, FMRP represses translation of CamKIIα and MAP1b mRNAs in mouse brain (149, 150).

To assess the requirement for dNab2 in dFMRP-mediated translational repression, we took advantage of the ability of overexpressed dFMRP to repress Futsch protein levels in neurons (147). In control cultured brain neurons, Futsch protein is located both in the cell body and distributed along the central shaft of major neuronal processes (Figure 3—5A). In dFMRP over-expressing neurons (*C155>dfmr1*), Futsch levels drop in the cell body and become nearly undetectable in the neuronal shafts (Figure 3—5A). When these effects are quantified across all compartments, Futsch levels are reduced by approximately 2-fold in dFMRP-overexpressing neurons (Figure 3—5C). When we analyzed the requirement for dNab2 in this system, we observed an interesting pattern: although Futsch levels are unaltered in *dNab2* null neurons relative to control neurons, the absence of dNab2 nonetheless effectively suppresses the ability of excess dFMRP to repress Futsch levels (Figures 3—6B-E). We confirmed that similar levels of exogenous dFMRP are expressed in control and *dNab2* null neurons (Figure 3—5B,D), indicating that the epistatic effect of dNab2 is not due to differences in *dfmr1* transgene expression between control and *dNab2* null neurons. These genetic data argue that endogenous dNab2 is not strictly required to repress Futsch translation, but that dNab2 is required by exogenous dFMRP to repress Futsch.

We next examined the requirement for dNab2 in control of *CaMKII* mRNA translation in neurons. The *CaMKII* mRNA encodes a post-synaptically localized kinase involved in synaptic plasticity and learning and memory (151) that is repressed by dFMRP *in vivo* (134). To assess translational inputs into the *CaMKII* mRNA, we utilized a

previously described *CaMKII* translational reporter that contains a Gal4-inducible *eYFP* coding-sequence fused to the *CaMKII* 3'UTR (152). This reporter was co-expressed with *dNab2* and *dfmr1* RNAi transgenes in olfactory projection neurons (*GH146-Gal4*) that innervate the antennal lobe (153, 154). In control flies, *eYFP:CaMKII-3'UTR* is expressed in the cell bodies and dendrites of *GH146*-positive projection neurons (PNs) of the antennal lobe (Figure 3—6A). As observed in prior work (134), RNAi-mediated depletion of dFMRP in these neurons increases *CaMKII-3'UTR* reporter expression as shown by elevated eYFP fluorescence (Figure 3—6A). Significantly, RNAi-mediated knockdown of *dNab2* in *GH146* PNs elevates expression of the *CaMKII-3'UTR* reporter to a nearly identical extent as knockdown of *dfmr1* (Figure 3—6A,C). RNAi knockdown of the unrelated NMDA receptor (NR1) does not affect *CaMKII-3'UTR* reporter expression (Figure 3—6A), confirming the specificity of the effects of dNab2 and dFMRP knockdown. Moreover, RNAi knockdown of *dNab2* in *GH146* antennal lobe neurons did not affect expression of a second unrelated translational reporter comprised of eGFP fused to the *SV40-3'UTR* (Figure 3—6B). These *in vivo* data indicate that dNab2 is required in neurons to inhibit expression of a *CaMKII-3'UTR* translational reporter in a manner similar to dFMRP.

3.2.6 ZC3H14 localizes to axons and associates with the translational machinery. Our prior finding that a neuron-specific isoform of human ZC3H14 (isoform1) rescues *dNab2* null fly phenotypes (35) implies that vertebrate ZC3H14 may also display properties of a cytoplasmic translational regulator. To test this hypothesis, the localization of endogenous ZC3H14 was assayed in primary cultured murine hippocampal neurons with an antibody that recognizes ZC3H14-isoform1 (iso1) and the closely related ZC3H14-iso2

and iso3 proteins (122). As previously reported (30, 67), these ZC3H14 isoforms are located within nuclear speckles (Fig. 3—7A), but they are also detected in the cytoplasm of neuronal extensions consistent with the finding in cultured *Drosophila* neurons. Importantly, this cytoplasmic anti-ZC3H14 signal is absent from hippocampal neurons cultured from *ZC3H14*$^{\Delta/\Delta}$ mice that were recently generated (146) (Figure 3—7B), confirming that the signal corresponds to endogenous ZC3H14-iso1-3 proteins. As with *Drosophila* dNab2, the cytoplasmic pool of murine ZC3H14 is also detected following biochemical fractionation into nuclear and cytoplasmic lysates (Figure 3—7C). Nuclear/cytoplasmic fractionation was confirmed with antibodies to the nuclear-specific marker, Histone H3, and the cytoplasmic-specific marker, α-Tubulin (155). As a control, we also examined another nuclear RNA-binding protein, THOC1, which aids in the processing and export of polyadenylated mRNA (156, 157). As expected, THOC1 was only detected in the nuclear fraction (Figure 3—7C), which provides evidence that detection of the RNA-binding protein, ZC3H14, in the cytoplasm does not reflect a pattern common to all RNA-binding proteins.

Closer inspection of the anti-ZC3H14 immunofluorescence pattern revealed that the protein is enriched in a single neurite from each hippocampal neuron. To assess the distribution of ZC3H14 in axons and dendrites, antibodies for a dendritic marker, Map2 (158, 159), or an axonal marker, Tau (158, 159), were used in co-staining experiments. ZC3H14 immunofluorescence is generally excluded from Map2-labeled dendrites but is present throughout the Tau-positive axon, including the growth cone (Figure 3—7D,E). These results provide evidence that ZC3H14 is enriched specifically in axonal extensions of cultured hippocampal neurons.

To determine whether ZC3H14 physically associates with translation machinery, we performed a polyribosome fractionation experiment using a linear sucrose density gradient and probed for ZC3H14 by immunoblotting. As shown in Figure 3—7F, we found that in cytoplasmic brain lysates isolated from P13 mice, ZC3H14 co-sediments with fractions containing monosomes and polyribosomes. To provide additional evidence that ZC3H14 co-sedimentation with polyribosomes is specific to intact translational machinery, we also generated cytoplasmic P13 brain lysates in the presence of the magnesium ion chelator, EDTA, which disrupts ribosomes into large and small ribosomal subunits (160). EDTA-mediated disruption of ribosomes is indicated by the absence of polyribosome peaks in the RNA absorption profile and a shift of the ribosomal S6 protein, a component of the 40S subunit (161), to the lighter density sucrose fractions (Figure 3—7G). Following EDTA treatment, ZC3H14 also shifted to the lighter fractions (Figure 3—7G), indicating that ZC3H14 is specifically associated with intact ribosomes. In aggregate, these data indicate that ZC3H14 isoforms 1-3 are enriched in hippocampal axons and associated with ribosomes in brain lysates, which is consistent with a role in spatial regulation of translation in neurons.

3.3 Discussion

Here we report that the dNab2 RNA-binding protein, the sole *Drosophila* ortholog of human ZC3H14, functionally and physically interacts with the homolog of Fragile X Mental Retardation Protein, dFMRP, in the development of the mushroom bodies as well as in the translational repression of mRNA target transcripts. Evidence from both *Drosophila* and mouse reveal a pool of dNab2/ZC3H14 present in the neuronal cytoplasm and associated with the translational machinery. This work suggests that the requirement

for this class of protein to support proper brain function could reflect a critical role in the regulation of translation.

The dNab2-dFMRP interaction provides new insight into how dNab2 affects neuronal gene expression, but our data also suggest that the two proteins may not always act in redundant or identical ways on all RNA targets. *dNab2* and *dfmr1* are independently required for proper mushroom body development (34, 92) and loss of either factor induces β-lobe overgrowth and α-lobe thinning/loss. However, *dNab2* and *dfmr1* show dosage sensitive interactions only in the context of α-lobe development. One interpretation of these data is that dNab2 and dFMRP may co-regulate RNA transcripts required for proper projection of α-axons, perhaps by acting within common RNP granules, but that these relationships are not conserved in β-lobe projections. Moreover, the observation that dFMRP status determines the phenotypic outcome of *dNab2* alleles in α-lobes implies that dFMRP is, to a degree, epistatic to dNab2: *dNab2* loss leads to α-lobe defects that can be enhanced by *dfmr1* heterozygosity, but *dNab2* heterozygosity rescues α-lobe defects in *dfmr1* null flies. These results imply that dNab2 and dFMRP co-regulate an overlapping set of transcripts, but not in precisely the same manner.

The molecular effects of dNab2 on Futsch and CaMKII reveal additional complexity in the manner in which *dNab2* can modulate translation. Knockdown of *dNab2* is sufficient to increase expression of a *CaMKII* translational reporter to an almost identical degree as knockdown of *dfmr1*, but it is not sufficient to dysregulate steady-state levels of Futsch protein, whose mRNA is bound and regulated by dFMRP (147). Rather, dNab2 is required for repression of Futsch by overexpressed *dfmr1*. Thus, dNab2 is independently required to regulate some target transcripts (e.g. *CaMKII),* while other transcripts *(*e.g.

futsch) appear to be regulated in a manner that is dependent on dFMRP, implying that dNab2 may be required for dFMRP to properly regulate some target RNAs.

The genetic and biochemical evidence linking dNab2/ZC3H14 to translational repression in the cytoplasm of neurons does not distinguish the molecular process these RNA-binding proteins use to control bound RNAs. Although there are a number of mechanisms through which this regulation could occur, the interaction of dNab2 and dFMRP in fly cells raises the possibility that dNab2-dependent repression might involve dFMRP. dFMRP physically interacts with the RNA-induced silencing complex (RISC) in the cytoplasm of cultured *Drosophila* neurons that is closely linked with miRNA-mediated repression (162). Notably, the *CaMKII 3'UTR* GFP sensor which responds to dNab2 loss is also a target of the miRNA pathway (134, 152), and multiple miRNA-RISC components, including *Ago1, Dcr1,* and *gawky* (GW182), were recovered in our *GMR-dNab2* rough eye screen. One explanation of these genetic links is that dNab2 loss extends poly(A) tails (32), which in turn facilitate enhanced recruitment of the RISC component GW182 by the poly(A) binding protein PABP (163). Alternatively, dNab2 may interact with dFMRP and block translation-coupled circularization of mRNAs. Poly(A) binding proteins are also emerging as important regulators of local translation in the cytoplasm of neurons (164). Yet while most cytoplasmic PABPs enhance polyadenylation of their bound mRNAs, dNab2/ZC3H14 appears to repress this process, suggesting that antagonism between two types of cytoplasmic PABPs may directly affect the translation of key neuronal mRNAs.

Consistent with the apparent role of dNab2 in translational regulation in *Drosophila*, the orthologous protein ZC3H14 localizes to axons and the growth cone in cultured murine hippocampal neurons and co-sediments with polyribosomes in the mouse

brain, suggesting a potential role in regulation of local protein synthesis. FMRP is localized to polysomes as well, and has been suggested to inhibit translation by polysome stalling (148). Intriguingly, CamKIIa is one of a group of synaptic proteins that increase in abundance in the hippocampus of *Zc3h14* knockout mice compared to control *Zc3h14*$^{+/+}$ mice (146), implying that CamKIIa is a conserved target of dNab2/ZC3H14. *CamKIIa* mRNA is also a well-validated target of FMRP (165). FMRP localizes to both axons and dendrites (126), and two other mammalian FMRP family members Fxr1 and Fxr2 are enriched pre-synaptically in axons (145, 166). We speculate that the dNab2-dFMRP interaction observed in flies may be conserved in mammals as a ZC3H14-Fxr1 or Fxr2 interaction. In support of this hypothesis, Fxr1 co-precipitates with the zinc-finger domain of ZC3H14 (167). Although functional and biochemical studies will be required to confirm the significance of this interaction in mammals, the significant body of genetic, biochemical and functional data in fly neurons, together with the findings that murine ZC3H14 is enriched in hippocampal axons and co-sediments with polyribosomes supports a model in which a newly defined cytoplasmic pool of dNab2/ZC3H14 plays a required role in the translational repression of key neuronal target mRNAs.

Here we show that the dNab2 and ZC3H14 poly(A) RNA-binding proteins localize to the nucleus and cytoplasm of neurons, that the cytoplasmic pools of these proteins interact with both dFMRP and polyribosomes, and that dNab2/ZC3H14 modulates neuronal translation. Given the clear link between FMRP and intellectual disease in humans, these interactions raise the question of whether defects in translational silencing of mRNAs transported to distal sites within neuronal processes contribute to intellectual disability in humans lacking ZC3H14.

Figure 3—1

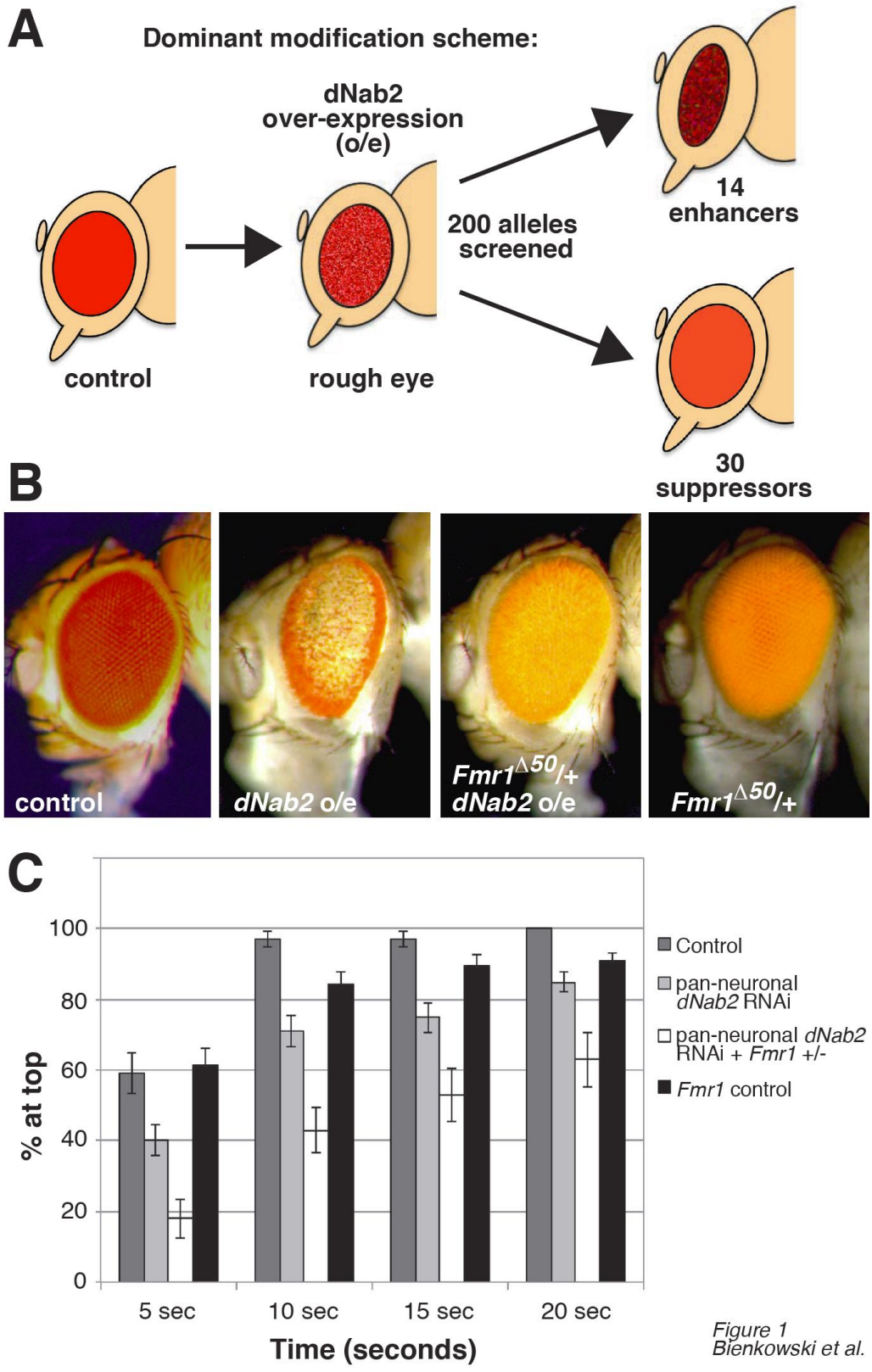

Figure 1
Bienkowski et al.

3.4 Figures

Figure 3—1: Genetic interactions between dNab2 and dfmr1.

(**A**) Schematic of the screen for genetic modifiers of a *dNab2* gain-of-function phenotype. *GMR-Gal4* driven overexpression (o/e) of dNab2 from the $dNab2^{EP3716}$ allele (*GMR>dNab2*) in the developing eye field leads to a "rough" adult eye phenotype that was screened against a pre-selected group of 200 candidate alleles. Of these, 14 enhanced and 30 suppressed *GMR>dNab2* rough eyes. (**B**) Light microscopic images of eyes from control (*GMR-Gal4/+*), *dNab2* transgenic (*GMR-Gal4/+;*$dNab2^{EP3716}$*/+*), *dNab2* transgenic+*dfmr1* heterozygous (*GMR-Gal4/+;+,*$dfmr1^{\Delta 50}$*/* $dNab2^{EP371}$*,+*), and *dfmr1* heterozygous (*GMR-Gal4/+;*$dfmr1^{\Delta 50}$*/+*) adult females. (**C**) Quantitation of a negative geotaxis assay among groups of 5-day old adult control flies (*C155-Gal4*), flies with pan-neuronal dNab2 RNAi (*C155-Gal4,UAS-dNab2-IR*), flies with pan-neuronal dNab2 RNAi in combination with *dfmr1* heterozygosity (*C155-Gal4,UAS-dNab2-IR,*$dfmr1^{\Delta 113M}$*/+*) or *dfmr1* heterozygotes alone (*C155-Gal4,*$dfmr1^{\Delta 113}$*/+*). Data are presented as the percentage of flies that reach the top of a cylinder at each time interval. Flies were assayed in groups of 10 and measured in at least 10 independent trials. Error bars represent SD.

Figure 3—2

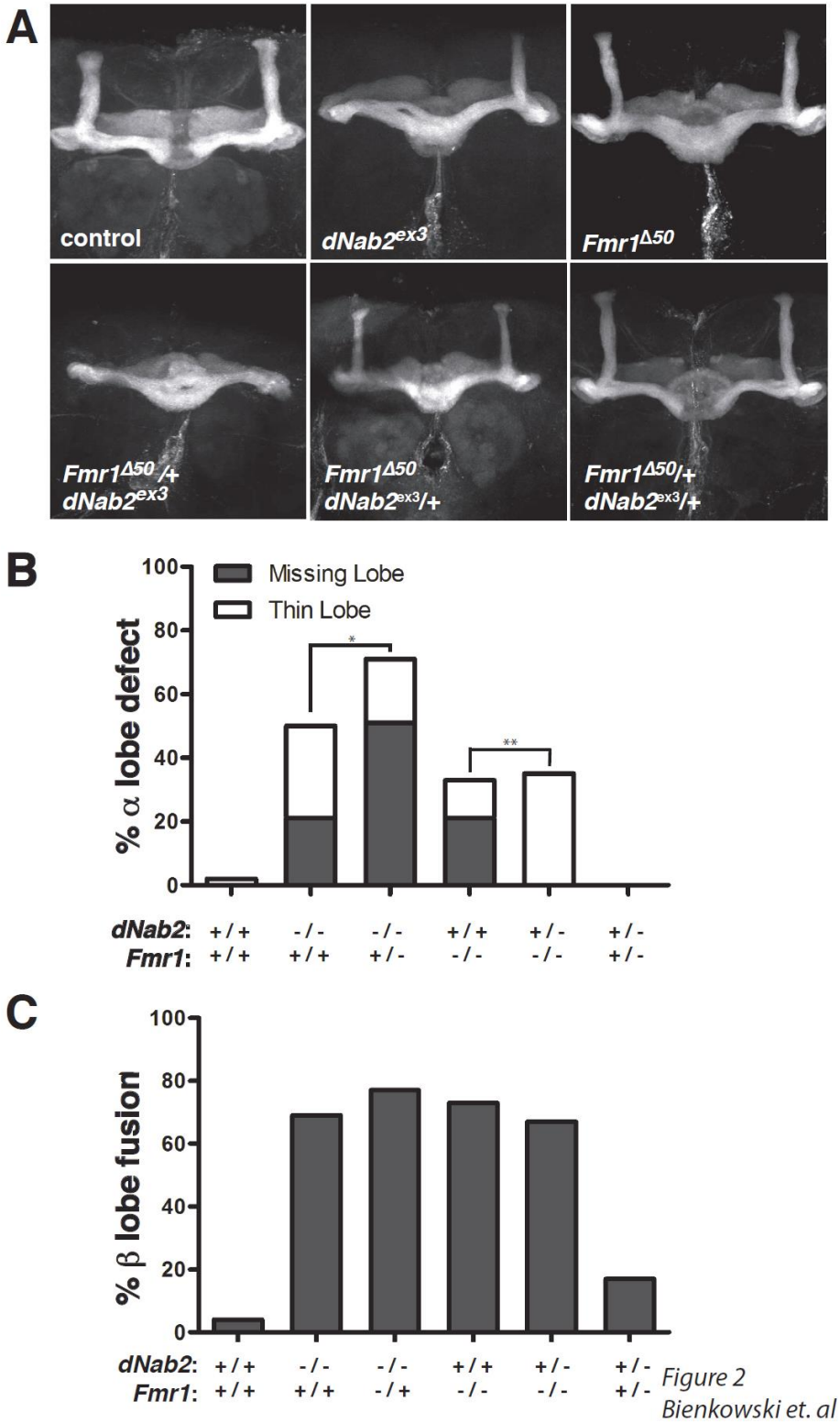

Figure 2
Bienkowski et. al

Figure 3—2: *dNab2* and *dfmr1* interact genetically in the process of mushroom body (MB) α-lobe development.

(**A**) Maximum intensity projections of a *dNab2* wildtype brain (*pex41/pex41* isogenic control), a *dNab2* null brain (*ex3/ex3* null homozygotes), a *dfmr1* null brain (Δ*50/*Δ*50* null homozygotes), a *dNab2* null brain lacking on copy of *dfmr1* (*ex3,*Δ*50/ex3,+*), an *dfmr1* null lacking one copy of *dNab2* (*ex3,*Δ*50/+,*Δ*50*), or a *trans*-heterozygote brain (*ex3,* Δ*50/+*). Quantitation of (**B**) the percentage of α-lobe defects (missing or thinned) and (**C**) fused β-lobe defects in the same genotypes as in (**A**) with individual lobes counted as discrete events. At least 24 brains of each genotype were examined. Significance was determined via the Chi-squared test (* p=0.000482 and ** p=0.0000150).

Figure 3—3

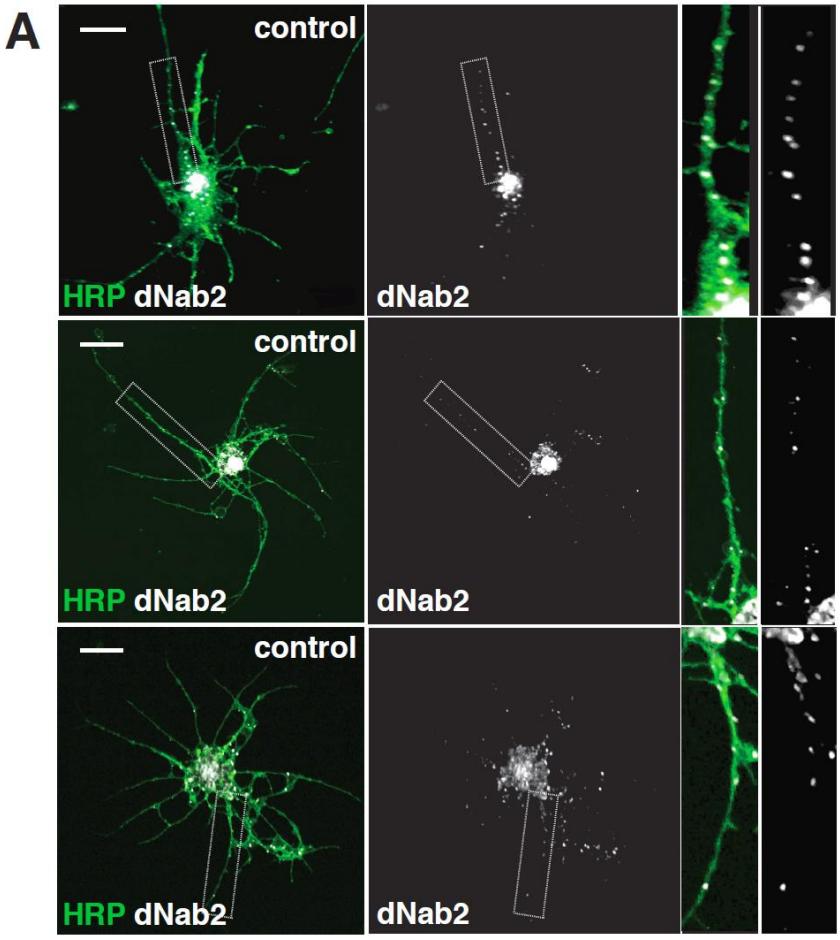

C

	Cytoplasmic dNab2 positive	Cytoplasmic dNab2 negative
cultured brain neurons	27/40	13/40
	67.5%	32.5%
cultured Kenyon cells	8/10	2/10
	80%	20%

Figure 3
Bienkowski et al.

Figure 3—3: dNab2 localizes to neurites of primary brain neurons.

Confocal images of representative (**A**) control (*pex41*) or (**B**) dNab2 null (*ex3*) brain neurons from 24h APF pupae cultured 72h *in vitro* and labeled with anti-HRP (green) to highlight neuronal membranes, and anti-dNab2 protein (grey). Rightmost panels in (**A**) show magnified views of dNab2 puncta in HRP-positive neurites (dotted boxes). (**C**) Quantification of the frequency of cytoplasmic dNab2 in neurites of wild type (*pex41*) brain neurons (top) or Kenyon cells (bottom) labeled CD8:GFP expression (*CD8-GFP/+;;OK107>Gal4/+).* Scale bars=10μm.

Figure 3—4

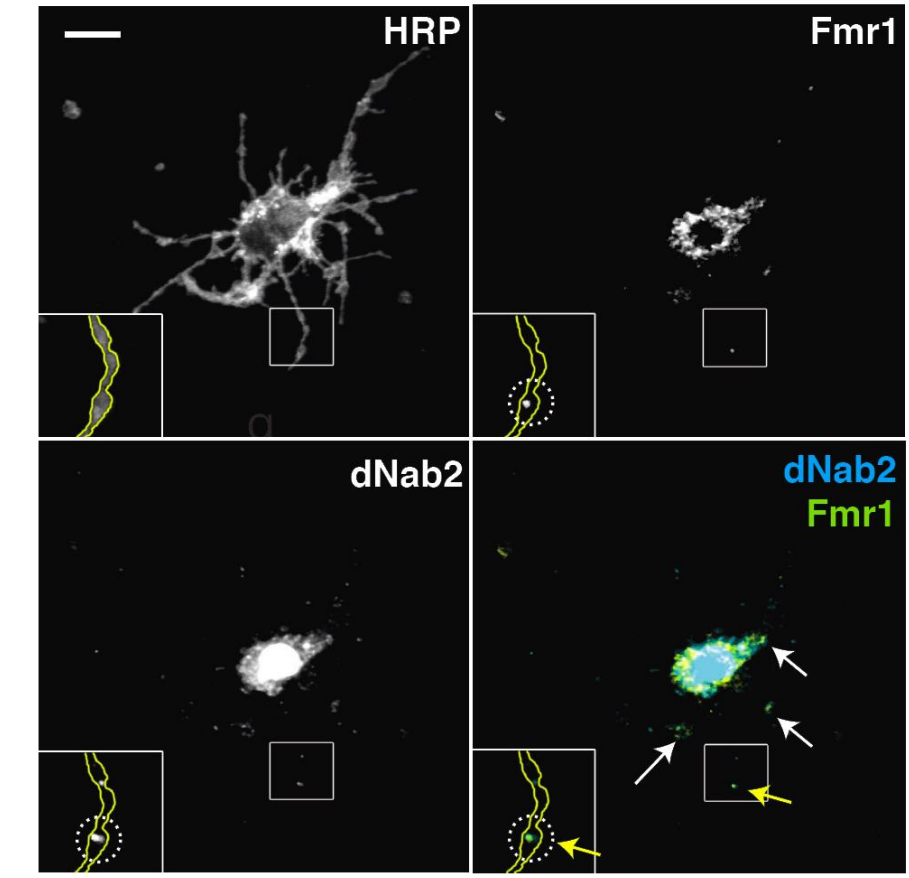

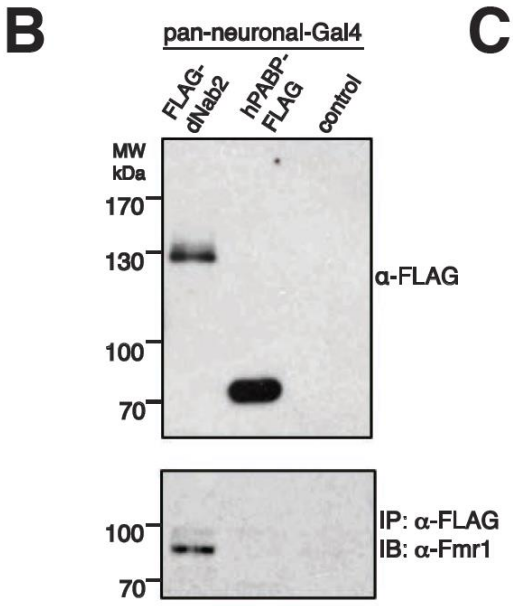

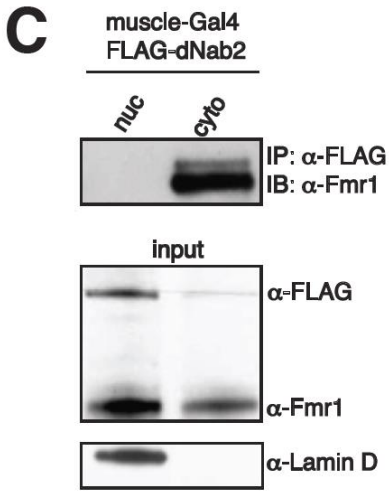

Figure 4
Bienkowski et al.

Figure 3—4: dNab2 physically associates with dFMRP in the neuronal cytoplasm.

(**A**) Confocal image of a single control (*pex41*) 24h APF brain neuron labeled with anti-HRP to mark membranes (top left panel), anti-dFMRP (top right panel), anti-dNab2 (bottom left panel), and double labeled with anti-dFMRP (green) and anti-dNab2 (blue) (bottom right panel). White arrows denote dNab2/dFMRP-double positive puncta. Boxed insert shows a high magnification view of a dNab2/dFMRP-positive speckle localized to a distal neurite (yellow arrow & dotted circle). Scale bars=10μm. (**B**) Anti-Flag (top panel) or anti-dFMRP (bottom panel) Western blot analysis of anti-Flag immunoprecipitates (IPs) from adult heads expressing neuronal Flag-dNab2 (*C155-Gal4;;UAS-Flag-dNab2/+*), hPABP-Flag (*C155-Gal4;UAS-hPABP-Flag/+*), or Gal4 alone (*C155-Gal4*). Note that endogenous dFMRP is only enriched in Flag-dNab2 precipitates. (**C**) Bulk lysates of adults expressing Flag-dNab2 from the muscle-specific driver *Mhc-Gal4* were separated into nuclear (nuc) and cytoplasmic (cyto) fractions and subject to anti-Flag IP/anti-dFMRP Western blot (upper panel). Input lysates were blotted to detect nuclear and cytoplasmic distribution of Flag-dNab2 and endogenous dFMRP. An antibody to nuclear Lamin was used to assess biochemical fractionation.

Figure 3—5

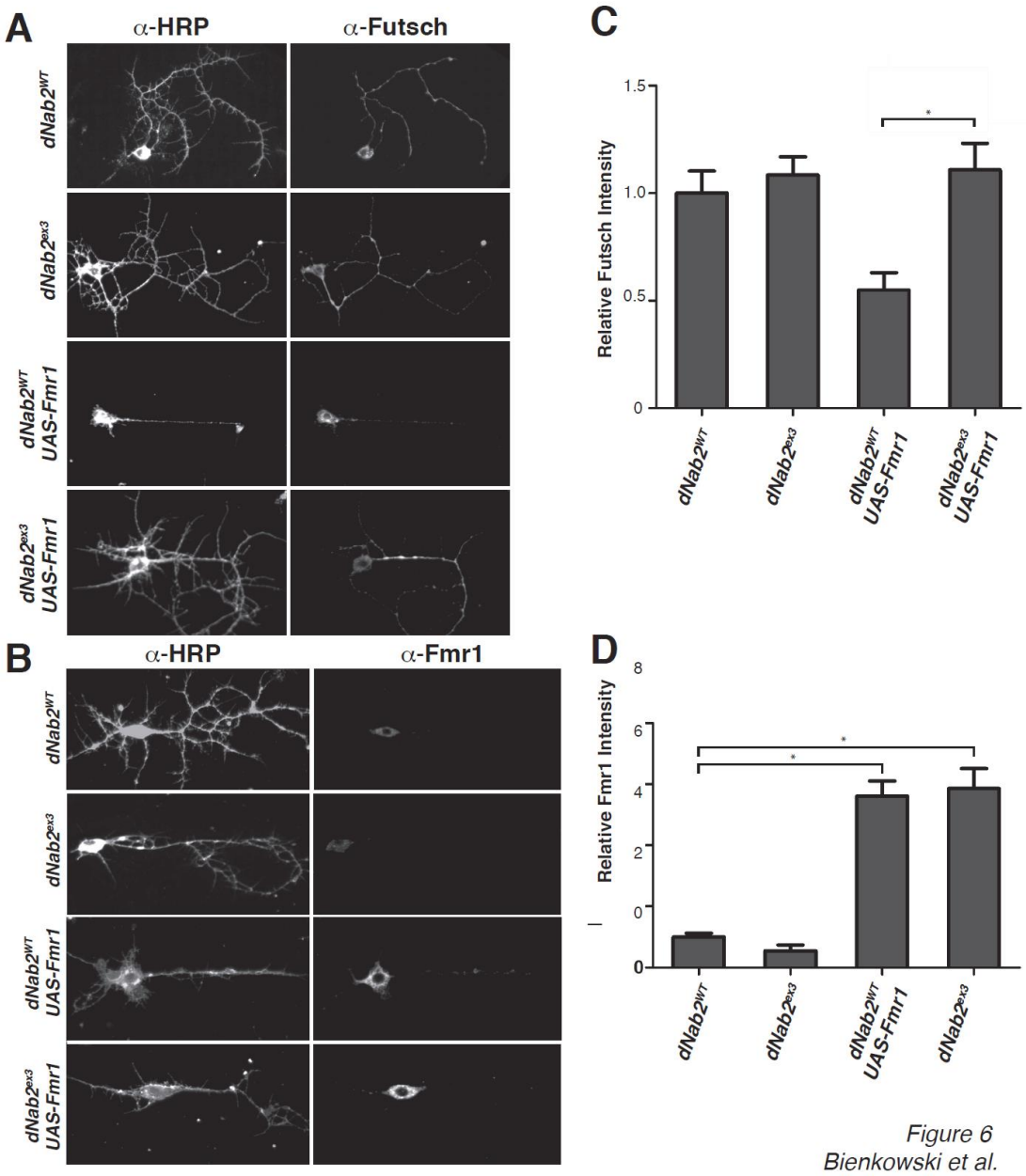

Figure 6
Bienkowski et al.

Figure 3—5: dNab2 is required for translational suppression of *futsch* by exogenous dFMRP.

Paired confocal images of (**A**) anti-Futsch or (**B**) anti-dFMRP stained 24h APF brain neurons co-stained with anti-HRP to illuminate neuronal membranes. Indicated genotypes: wildtype Nab2 (*dNab2^{wt}*), mutant dNab2 (*dNab2^{ex3}*), transgenic dFMRP (*UAS-dfmr1;dNab2^{wt}*), or mutant dNab2 + transgenic dFMRP (*UAS-dfmr1;dNab2^{ex3}*). The *C155-Gal4* neuronal driver is present in all neurons. Quantitation of (**C**) Futsch or (**D**) dFMRP protein levels presented as mean fluorescence intensity among the same genotypes as in (**A)** and (**B**). Data are normalized to *C155-Gal4;dNab2^{wt}* (lane 1) (n=15 in **C**; n=12 in **D**). Error bars represent SEM ($*$ $p<0.05$)

Figure 3—6

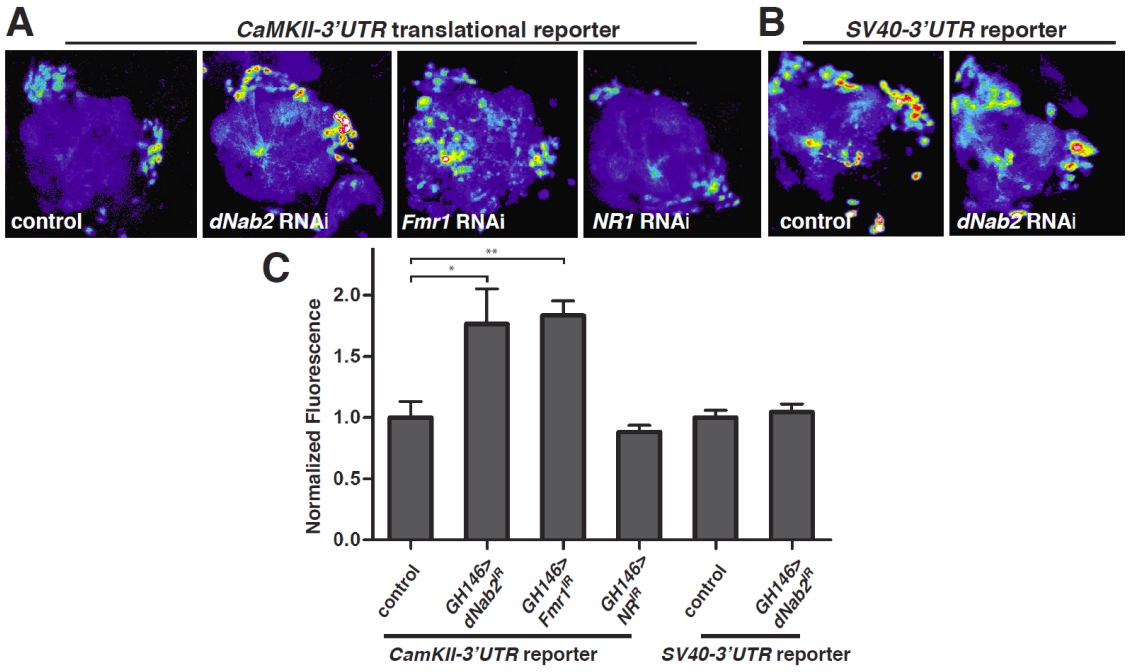

Figure 6
Bienkowski et al.

Figure 3—6: *dNab2* regulates expression of a CaMKII translational reporter.

Confocal images of (**A**) *UAS-eYFP:CaMKII-3'UTR* and (**B**) *UAS-eYFP:SV40-3'UTR* expression in *GH146-Gal4* antennal lobe neurons expressing the indicated RNAi transgenes. Expression levels are represented as a 16-color intensity scale. RNAi genotypes: no RNAi (*control*), *UAS-dNab2-RNAi* (*dNab2* RNAi), *UAS-dfmr1-RNAi* (*dfmr1* RNAi), *UAS-NMDA Receptor-1-RNAi* (*NR1* RNAi). (**C**) Mean eYFP fluorescence from the *CaMKII-3'UTR* and *SV40-3'UTR* reporters for each indicated genotype. Data are normalized to the mean fluorescence of control (*GH146-Gal4,UAS-eYFP:CaMKII-3'UTR* or *GH146-Gal4,UAS-eYFP:SV40-3'UTR*) antennal lobes. Error bars represent SEM. $*$ $p<0.05$, $**p<0.01$.

Figure 3—7

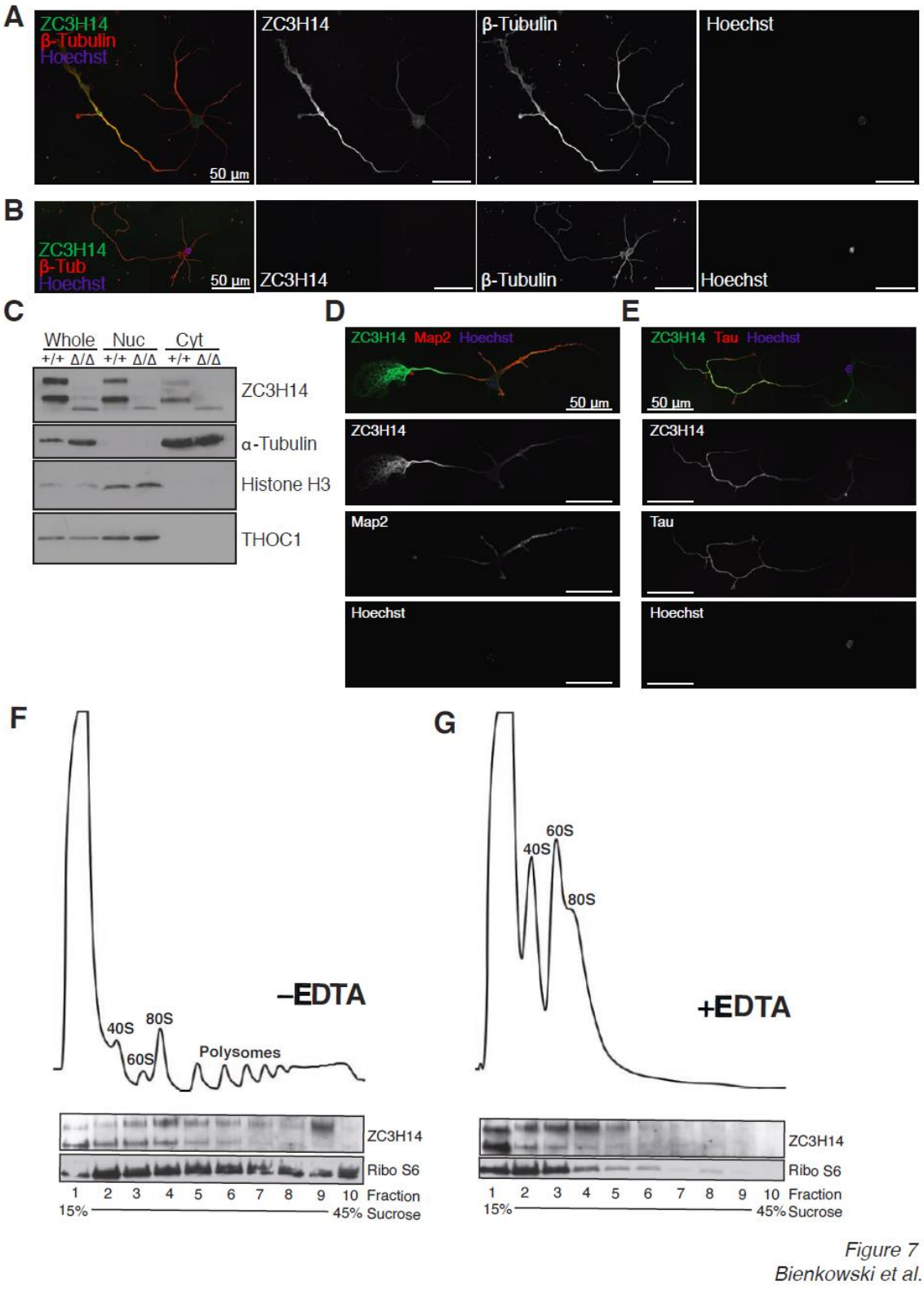

Figure 7
Bienkowski et al.

Figure 3—7: ZC3H14 localizes to axons in primary hippocampal neurons and associates with polyribosomes in mouse cortical lysates.

(A, B) Immunofluorescence images of 5 days *in vitro* (DIV) cultures of primary hippocampal neurons collected from P1 (**A**) *Zc3h14*$^{+/+}$ or (**B**) *Zc3h14*$^{\Delta/\Delta}$ pups and stained with anti-ZC3H14 (green), anti-β-tubulin (red), and Hoechst to detect DNA (blue). Scale bars=50 μm. (**C**) Nuclear and cytoplasmic fractions of *Zc3h14*$^{+/+}$ and *Zc3h14*$^{\Delta/\Delta}$ brains immunoblotted to detect the ZC3H14 RNA-binding proteins, α-tubulin (cytoplasmic marker), Histone H3 (nuclear marker), and THOC1, a second RNA-binding protein that localizes exclusively in nuclei. (**D**, **E**) Wildtype P1 hippocampal neurons (5 DIV) were co-stained with antibodies to (**D**) ZC3H14 (green) and the dendritic marker Map2 (blue), or (**E**) ZC3H14 (green) and the axonal marker Tau (blue). Hoechst (blue) marks neuronal nuclei. Scale bars=50 μm. (**F**, **G**) Polysome profiles across a 15-45% linear sucrose gradient of cytoplasmic extracts of the P13 brain cortex of wildtype mice prepared in the (**F**) absence or (**G**) presence of EDTA, which dissociates the 40S and 60S ribosomal subunits. Linear traces denote 254nm absorption profiles (RNA) of representative gradients, with the positions of ribosome peaks and polysomes indicated. Lower panels show the distribution of ZC3H14 and the S6 ribosomal protein (Ribo S6) across the indicated fractions as detected by immunoblot.

3.5 Supplementary Figures

Figure 3—S1

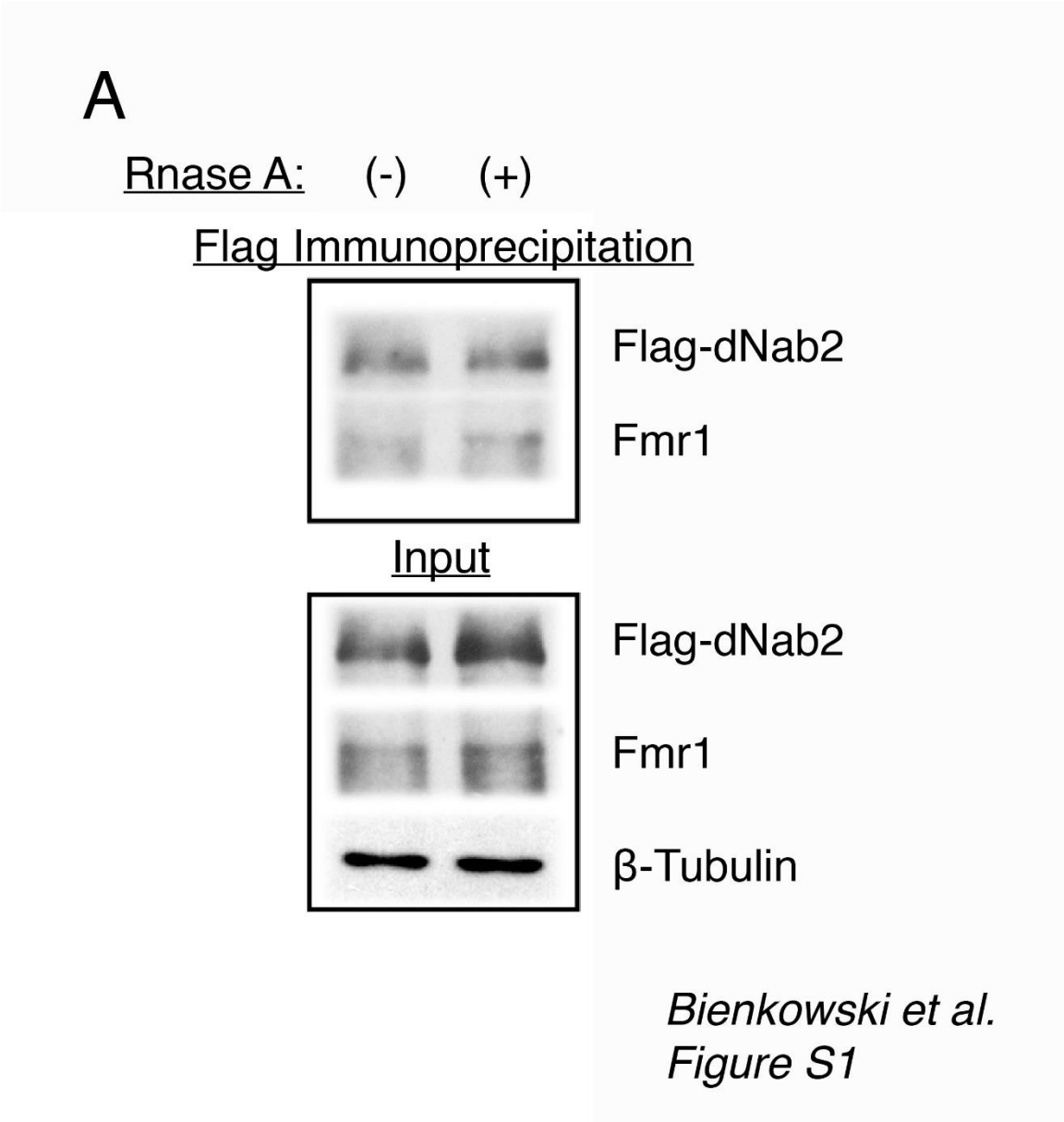

Figure 3—S1: dNab2 and dFMRP co-precipitate in the presence of RNAse A.

Western blot analysis of anti-Flag immunoprecipitates (top panel) and input (bottom panel) from adult heads expressing Flag-tagged dNab2 in neurons (*C155/+;Flag-dNab2/+*). Prior to immunoprecipitation, lysates were split into two aliquots, RNase (+) and (-). The RNase (+) aliquot was treated with RNase A at a final concentration of 50 μg/ml, and the RNase (-) aliquot was mock-treated. Samples were incubated for 30 minutes at 37ºC. The membrane was probed with anti-Flag, anti dFMRP, and anti β-tubulin (loading control). Note that both the magnitude of dFMRP signal that co-precipitates with Flag-dNab2 is unchanged upon incubation with RNase A.

Table 3—S1

Table S1: GMR>dNab2 overexpression screen

Bloomington #	Allele	Modification (E or S)
	Pabp2^{EP2264}	S++
--	*UAS-puc*	S++
1507	*stau^{1}*	S++
22407	*robo2^{ey206209}*	S++
31788	*paip2^{epG4716}*	S +
58708	*UAS-Timp*	S
16659	*Trf4-2^{EY05585}*	S
11295	*spen^{3350}*	S
25789	*sif^{TRiP}- P{TRiP.JF01795}attP2*	S
9126	*sif^{ES11}*	S
32418	*Rps6^{Trip}*	S
19858	*Rm62^{EY06795}*	S
28669	*Rbp9^{TRIP}*	S
25775	*Rbp9[delta1]*	S
14276	*Pur-α^{KG05743}*	S
36127	*Pabp IR*	S
11624	*mub^{4093}*	S
14915	*mRpS29^{KG07362}*	S
10654	*hoip^{K07104}*	S
18062	*Hel25E^{e02545}*	S
6930	*Fmr1^{D50M}*	S
6929	*Fmr1^{D113M}*	S
11720	*eIF-4E^{7238}*	S
15364	*EF1alpha ^{ey010605}*	S
32067	*Dcr-1[Q1147X]*	S
11531	*cpo^{1432}*	S
29401	*CaMKII^{TRiP}-P{TRiP.JF03336}attP2*	S
10063	*bel^{NEO30}*	S
21645	*Atx2^{DG08112}*	S
11388	*ago1^{04845}*	S
33615	*Akt^{TRIP}*	lethal: no interaction (Akt TRiP is lethal alone)
--	*UAS-Fmr1.Z§*	lethal
17023	*qkr58E-2^{EP2103}*	E+++
--	*Pabp2^{55}*	E+++
8161	*hrg^{10}*	E+++
--	*UAS Pabp-flag*	E++
5930	*smg^{1}*	E++

34809	*Rrp6*^{TRIP}	E++
34796	*gawky*^{TRIP}	E++
7125	*UAS-lark-3HA 23A§*	E
--	*UAS-fne.C 4-10B§*	E
38391	*Pabp2*^{6}	E
1676	*fz*^{1}	E
28784	*fne*^{IR}	E
17117	*Dscam4*$^{[EP3362]}$	E
12863	*Zn72D*^{BG02677}	-
28534	*wnt5*^{TRIP}	-
6651	*Wnt4*^{C1}	-
16467	*wisp*^{KG05287}	-
4613	*wisp*$^{12-3147}$	-
2980	*Wg*$^{l-17}$	-
2978	*Wg* ^{1}	-
17408	*vig*^{EY07816}	-
8477	*UAS-Src64B*	-
--	*UAS-pde1c*	-
--	*UAS-bsk*^{DN}	-
--	*UAS-AvrA*	-
32490	*twin*^{TRiP}*-P{TRiP.HMS00493}attP2*	-
32901	*twin*^{TRiP}*- P{TRiP.HMS00690}attP2*	-
15863	*twin*^{EY02330}	-
15237	*tud*^{KG10175}	-
14097	*tsu*^{KG04415}	-
6597	*tsu*^{EP567}	-
14737	*tsr*^{N121}	-
27732	*trio*^{TRiP}*-P{TRiP.JF02815}attP2*	-
14718	*tra2*^{KG08361}	-
29517	*Tis11*^{TRIP}	-
-	*Tis11*^{EY09433}	-
--	*Tis11*^{EY09107}	-
-	*Tis11*^{BG00309}	-
14737	*TBPH*^{KG08578}	-
20801	*TBPH* ^{EY10530}	-
40875	*tau*^{TRIP}	-
6967	*stau*^{192}	-
41776	*stan*^{e59}	-
24071	*Src64B*^{MB03494}	-
7379	*Src64B [Pi/Pid]*	-
12133	*sqd*^{J6E3}	-
8735	*spen*^{3}	-

11177	*snRNP-U1-70K*^{2107}	-
17211	*Slbp*^{EP1045}	-
4095	*sgg*^{1}	-
12904	*SC35*^{KG02986}	-
23660	*sbr*^{Magellan}	-
94	*sbr*^{1}	-
32552	*S6k*$^{l-1}$	-
9404	*rut*^{1}	-
16981	*Rrp42*^{EY}	-
(harvard collection	*Rrp42*^{c02320}	-
8755	*robo*^{1}	-
20644	*Rm62*^{EY10915}	-
--	*Rm62*^{DG12402}	-
11520	*Rm62*^{1086}	-
--	*Rm62 (excision L3)*	-
31167	*RhoGAP93B*^{TRIP}	-
32417	*RhoGAP71E*^{TRIP}	-
7326	*Rho1*^{72F}	-
27	*Rd*^{1}	-
25778	*Rbp9*^{P2690}	-
6674	*rac1*$^{[J11]}$	-
6677	*rac1,rac2*	-
15086	*qkr58E-3*^{EY02038}	-
14653	*qkr58E-2*^{KG07766}	-
6782	*pum*^{BEM}	-
3260	*pum*^{13}	-
3332	*pum*^{13}	-
16420	*pUf68*^{EY07952}	-
9756	*Ptpmeg[1]*	-
23562	*ps*^{MB04043}	-
10236	*ps*^{10615}	-
28728	*pde1c*^{TRIP}	-
--	*park*^{25}	-
4759	*pan*^{2}	-
10970	*pAbp*^{K10109}	-
20684	*pAbp*^{EY11561}	-
17261	*pAbp*^{EP310}	-
--	*orb*^{EY08547}	-
--	*orb*^{dec}	-
27050	*orb2*^{TRiP}*-P{TRiP.JF02376}attP2*	-
12812	*orb2*^{BG02373}	-
18809	*Nxt1*^{f04855}	-

21033	*Nxt1*^{DG05102}	-
3285	*nos*^{L7}	-
125	*nonA*^{4B18}	-
5947	*msn*^{172}	-
5945	*msn*^{102}	-
4160	*msi*^{1}	-
7318	*mbl*^{E27}	-
8516	*mael*^{R20}	-
13015	*mael*^{KG03309}	-
16006	*mael*^{EY08554}	-
--	*lark*^{EY23084}	-
--	*lark*^{EY00297}	-
--	*lark*^{DG23107}	-
8250	*InR.R418P*	-
8252	*InR.K1409A*	-
8263	*InR .A1325D*	-
17294	*Imp*^{EP760}	-
41590	*Ime4*^{TRIP}	-
8160	*hrg*^{p1}	-
8162	*hrg*^{1}	-
6822	*Hrb98DE*^{ZCL0558}	-
14414	*Hrb87F*^{KG02089}	-
11204	*Hrb27C*^{2647}	-
12151	*how*^{J5B5}	-
9564	*homer*^{R102}	-
--	*GluRIIA*^{Sp16}	-
--	*GluRIIA*^{AD9}	-
34898	*gbb*^{TRIP}	-
8805	*futsch*^{N94}	-
8794	*futsch*^{K68}	-
28990	*fasII*^{RNAi}	-
--	*fasII*^{EB112}	-
--	*fasII*^{e7}	-
12240	*elav[G0319] arg[G0319] w[67c23]/FM7c*	-
10506	*eIF-4a*^{K01501}	-
11034	*Ef1α48D*^{1275}	-
--	*EF1beta*^{ep} *(#271921)*	-
16341	*EF1beta*^{ep}	-
22419	*EF1alpha100E* ^{ey20719}	-
7363	*drl*^{exc21}	-
2065	*dpp*$^{(s11)}$	-

2070	*dpp*$^{(d12)}$	-
12855	*Dp1*^{BG02288}	-
--	*Dp1*^{BG0145B}	-
6020	*dnc*^{1}	-
12164	*dco*^{J3B9}	-
38294	*CyFip*^{TRIP}	-
--	*Clp*^{G2556}	-
--	*CenG1A*^{EY01217}	-
--	*CCR4*^{0115}	-
201401	*CCR4/twin*^{8115}	-
22797	*bru-2*^{MB00431}	-
27190	*bru-2*^{G5819}	-
18300	*bru-2*^{f00171}	-
22296	*bru-2*^{EY18918}	-
--	*bl*^{KG02524}	-
--	*bl*^{EY09813}	-
4553	*BicD*^{r5}	-
11778	*bel*^{CAP1}	-
4024	*bel*^{6}	-
25933	*babo*^{TRIP}*-y1 v1; P{TRiP.JF01953}attP2*	-
4968	*aub*^{QC42}	-
14001	*aub*^{KG05389}	-
8517	*aub*^{HN}	-
11688	*Atx2*^{06490}	-
16608	*AGO2*^{EY04479}	-
12712	*Adar*^{BG02235}	-
18459	*abs*^{f01698}	-
21172	*abs*^{EY015915}	-
11504	*abs*^{00620}	-
8565	*Abl*^{2}	-
8653	*paip2-HA*	-
29517	*TBPH* ^{TRIP}	-
18987	*PBac{WH}Dcr-2*^{f06544}*/CyO*	-
10970	*Pabp* $^{[K10109]}$	-
--	*fne*$^{[KO26]}$	-
33657	*drosha*^{TRIP}	-
28269	*ago3*^{t2}	-
36512	*AGO2*^{454}*/TM3, Sb1*	-

Table 3—S1: **GMR>dNab2 rough eye screen results.**

dNab2 was overexpressed in the developing eye by driving the *dNab2* ^{EP3716} allele with the *GMR-Gal4* driver *(GMR>dNab2)*. *GMR>dNab2* driven overexpression causes a "rough" eye phenotype in adults that was screened against 200 candidate alleles for dominant modification. Of these, 14 alleles enhanced and 30 suppressed *GMR>dNab2* rough eyes. Fly stocks that were obtained from the Bloomington Stock center have the corresponding Bloomington Stock number listed (Column 1). The genotype of each fly tested for dominant modification of the rough eye phenotype is described (Column 2). Observed modification of the rough eye phenotype was recorded and is listed in Column 3. The degree of suppression or enhancement observed was classified according to the following scale- E: smaller, rougher eyes; E+: smaller, rougher eyes with increased pigment loss; E++: smaller, rougher eyes with necrosis; E+++: necrosis and greatly reduced viability; S: increased eye size, some rescue of ommatidia organization; S+: increased eye size, rescue of ommatidia organization, and rescue of pigment loss; S++: nearly indistinguishable from the eyes of flies expressing *GMR-Gal4* alone.

Chapter 4

ZC3H14 in neuronal development and synapse formation

***Nota bene*:**

This chapter consists of preliminary data collected and quantified by Julia Omotade in the laboratory of James Q. Zheng. The text was written by Jennifer Rha.

4.1 Introduction

In vitro analysis of neuronal development is an important tool to study neurodevelopmental deficit disorders such as fragile X syndrome (168). Neuronal development is a complex, multistep process that was well characterized by Dotti *et al.* in 1988 using rat hippocampal neurons *in vitro* (169). As depicted in **Figure 4—1**, within the first day of culturing, neurons form lamellopodia that develop into axons and dendrites by the third day. Dendrites expand and branch extensively during the first two weeks of culture. By the beginning of the third week, dendrites grow filopodia—extensions that can by 21 DIV (days *in vitro*) mature into spines that communicate with axon terminals across the synapse.

Synaptogenesis itself is complex. As illustrated in **Figure 4—2**, filopodia are the extensions sent out from the dendrite to explore the environment (170). Once filopodia makes contact with a presynaptic bouton, it morphologically transforms into a mushroom-like dendritic spine. Without this synaptic contact, the filopodium will withdraw and disappear. *In vivo*, dendritic spines form stable synapses from postnatal day 60 and onwards (171). In cultured neurons, stable dendritic spines form from 21 DIV and onwards (172). The tips of these spines are the major excitatory synapses of the central nervous system (173).

To investigate the role ZC3H14 plays in neuronal development and synapse formation, we analyzed wildtype and *Zc3h14* mutant hippocampal neurons grown *in vitro*.

4.2 Results

4.2.1 Young ZC3H14-deficient hippocampal neurons develop fewer and shorter neurites in culture.

Comparison of young (6 DIV) wildtype and *Zc3h14* mutant hippocampal neurons reveal that mutant neurons mature more slowly than wildtype neurons. The average neurite length of wildtype neurons is 1134 µm, whereas mutant neurite length is about half the length at 506 µm. Mutant neurons also extend half as many neurites (2.65 neurites/neuron) than do wildtype neurites (5.00 neurites/neuron). These results indicate that *Zc3h14* mutant neurons have a delayed growth during early neuronal development.

4.2.2 ZC3H14 localizes to dendritic spines in mature cultured hippocampal neurons.

In contrast to the axonal ZC3H14 enrichment seen in young primary neurons, ZC3H14 localizes to dendrites and axons as well as to the nucleus in mature neurons (data not shown). **Figure 4—3** shows colocalization of ZC3H14 and PSD-95, a well characterized post synaptic density marker, in a wildtype dendritic shaft. This data shows that ZC3H14 localizes to excitatory dendritic spines.

4.2.3 Loss of ZC3H14 causes abnormal spine morphology and density.

Neurons from wildtype and mutant hippocampi were cultured for 21 DIV to investigate synapse formation. As illustrated in a representative image in **Figure 4—4**, *Zc3h14* mutant neurons had fewer dendritic protrusions per 50 µm (wildtype 51; mutant 21) and an increase in the number of immature filopodia per 50 µm (wildtype 5; mutant 11) and a decrease in the number of mature spines per 50 µm (wildtype 46; mutant 10). These results indicate that ZC3H14 is important for normal spine morphology and density.

4.2.4 Loss of ZC3H14 causes increase in number of dendritic shaft synapses. As shown in **Figure 4—5**, *Zc3h14* mutant neurons grown 21 DIV show an increased shaft synapses when compared to dendrites of wildtype neurons.

4.3 Discussion

These data indicate that ZC3H14 is important for early neuronal development. Loss of ZC3H14 delays maturation of hippocampal neurons at 6 DIV, evidenced by fewer and shorter neurites. Further analysis is necessary to see whether mutant axons are shorter in length and whether there are fewer dendrites and/or shorter dendrites. As shown in Chapter 2, ZC3H14 is enriched in axons at this stage. These data together suggest that ZC3H14 may play a role in the establishment of polarity, axon sprouting, or axon guidance during this early stage of development. The absence of ZC3H14 may cause neurons to be developmentally delayed.

Analysis of wildtype primary hippocampal neurons cultured 21 DIV reveal a shift in the localization of ZC3H14, from axonal enrichment in young neurons to the dendritic shaft and spines of mature neurons. ZC3H14 may play differential roles during neuronal development versus synaptogenesis and synaptic maintenance or plasticity. The localization of ZC3H14 to excitatory spines poises ZC3H14 to play a role in post-synaptic processing of synaptic events. This data together with proteomic analysis of ZC3H14-deficient hippocampi showing unilateral increases in proteins important for synaptic function and signal transduction suggest that ZC3H14 plays an important role at the synapse.

Furthermore, imaging of ZC3H14-deficient dendrites reveal synaptic spine dysmorphology, characterized by an overall decrease in dendritic protrusions, an increase

in immature filopodia, and a decrease in mature mushroom-shaped spines. Loss of ZC3H14 also causes an increase in the formation of shaft synapses, which are believed to be either precursors for spine synapses (174, 175) or a completely independent type of synapse (176) nevertheless important for behavioral learning (177, 178). Of note, protein synthesis machinery (polyribosomes) is found in both spineous and shaft synapses, implying that both types of synapses have the ability to participate in activity-dependent local protein synthesis (179).

In conclusion, in vitro analysis of ZC3H14-deficient hippocampal neurons reveal a delay in neuronal maturation during early development and abnormal synaptogenesis or synaptic maintenance. These processes mediated by a loss of ZC3H14 may contribute to the pathogenesis of cognitive dysfunction observed in both ZC3H14-deficient mice and patients.

4.4 Figures

Figure 4—1

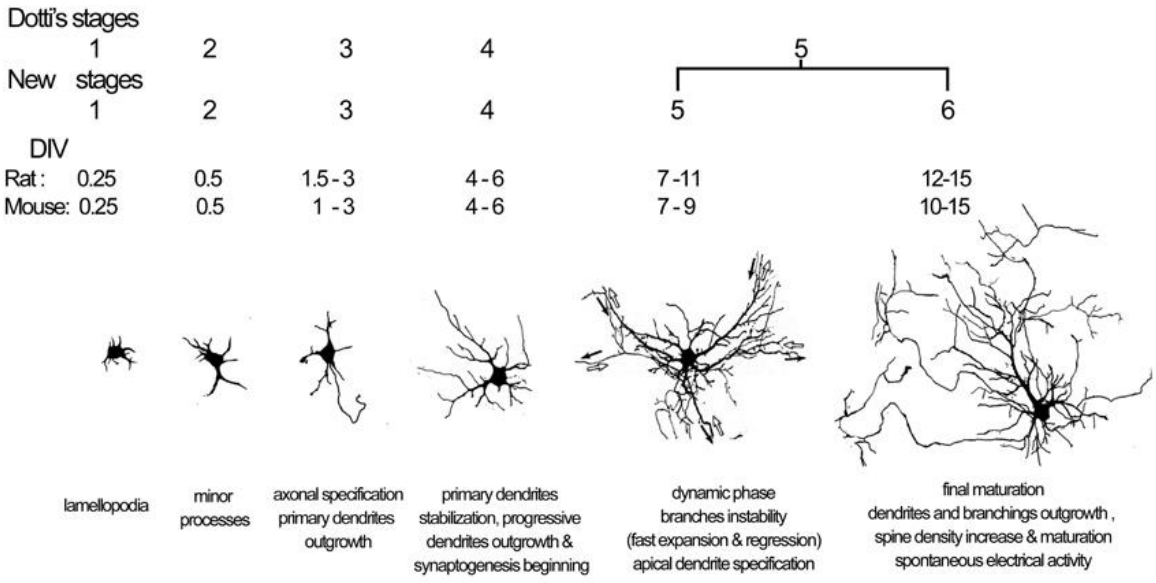

Figure 4—1. Model of *in vitro* neuron staging.

Axons specification occurs between 1-3 DIV (days *in vitro*). By 6 DIV dendrites stabilize. Final maturation of neurons occur after 15 DIV. This figure was modified from Baj *et al.* (2014) (180).

Figure 4—2

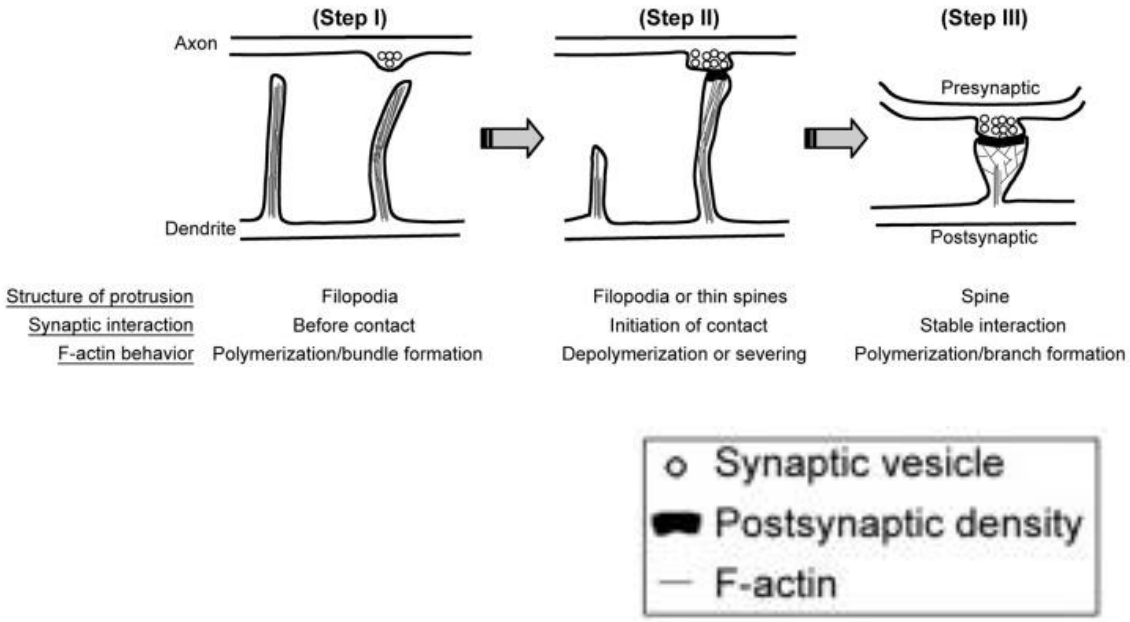
(Step I)
(Step II)
(Step III)
Axon
Dendrite
Presynaptic
Postsynaptic
Structure of protrusion
Synaptic interaction
F-actin behavior
Filopodia
Before contact
Polymerization/bundle formation
Filopodia or thin spines
Initiation of contact
Depolymerization or severing
Spine
Stable interaction
Polymerization/branch formation
Synaptic vesicle
Postsynaptic density
F-actin

Figure 4—2. Steps in filopodial maturation into spines.

In step I, dendrites send out thin filopodia to investigate the environment. Step II illustrates that if there is no contact with an axon or if no stimulatory signals are received, the filopodium will withdraw and disappear, while a filopodium that receives stimulatory input and finds an axon, it will mature into (Step III) a mushroom-shaped spine with a shortened neck and enlarged head. This figure is modified from Hsueh (2012) (170).

Figure 4—3

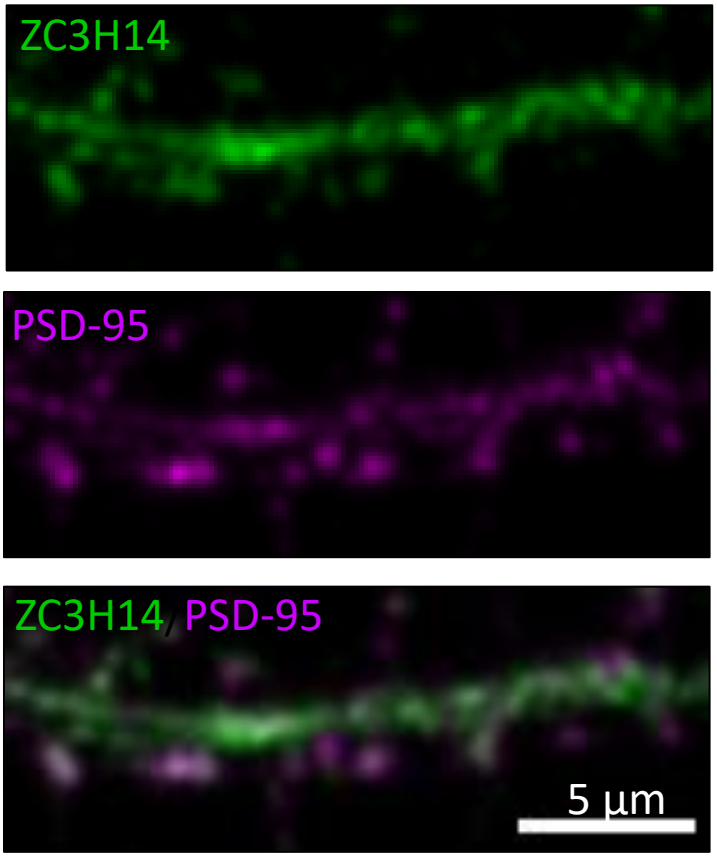

Figure 4—3. ZC3H14 colocalizes with PSD-95 in mature primary hippocampal neurons grown 21 DIV.

Top panel is ZC3H14, middle panel is PSD-95, and bottom panel is merged for ZC3H14 and PSD-95. Scale bar, 5 μm.

Figure 4—4

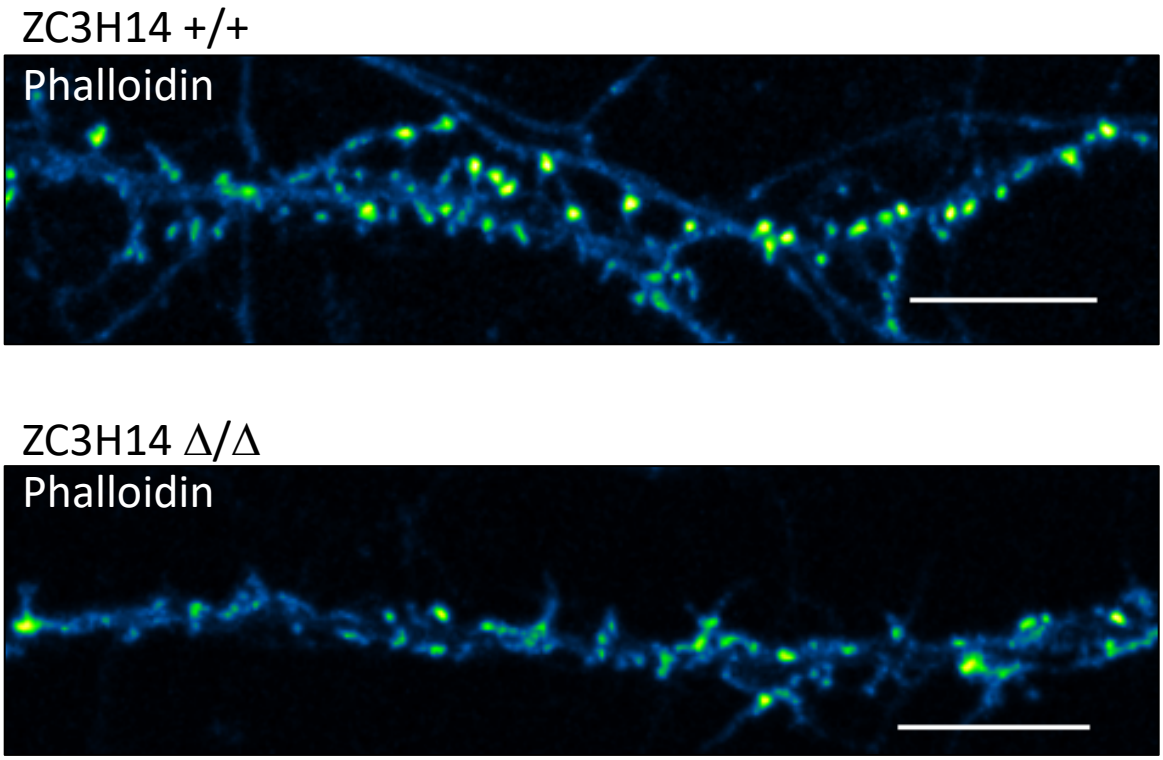

Figure 4—4. Loss of ZC3H14 causes spine dysmorphology and decrease in spine density.

Staining for F-actin using Phalloidin antibody to reveal cellular architecture in wildtype (*top*) and mutant (*bottom*) dendrites of primary hippocampal neuron grown 21 DIV. Artificial colors of image reveal intensity of staining. Green corresponds to areas of high pixel intensity (enrichment of F-actin). Scale bar, 10μm.

Figure 4—5

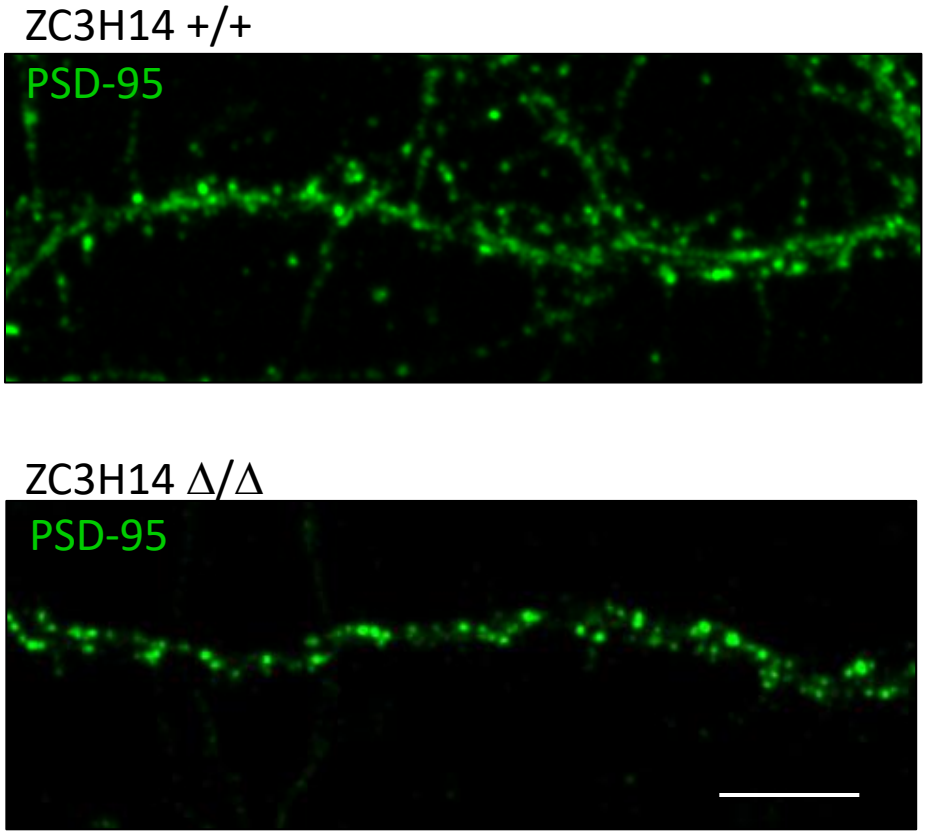

Figure 4—5. Loss of ZC3H14 causes an increase in shaft synapses.

PSD-95 staining of wildtype (*top*) and mutant (*bottom*) dendritic shaft of primary hippocampal neurons grown 21 DIV. Scale bar, 10μm.

Chapter 5

Discussion:
Brief summary, what we've learned, more questions, and future directions

5.1 Learning about learning and memory

> Learning and memory are two of the most magical capabilities of our mind. Learning is the biological process of acquiring new knowledge about the world, and memory is the process of retaining and reconstructing that knowledge over time. Most of our knowledge of the world and most of our skills are not innate but learned. Thus, we are who we are in large part because of what we have learned and what we remember and forget (181).
>
> –Eric R. Kandel

We learn, and we remember. Two of the most fascinating functions of the brain are how it processes and retains information. At the molecular level, RNA mechanisms provide the versatility to mediate steps necessary for learning and memory. Local translation of targeted mRNA transcripts provides neurons the flexibility to finely tune synaptic strength in response to incoming signals from the extracellular environment. Major disruptions of this carefully choreographed system often lead to disease manifestations. Indeed, development of intellectual disability in patients who fail to produce an RNA-binding protein is informative of the importance of the protein in learning and memory. Thus, we have recently initiated collaborative studies of one such RNA-binding protein, ZC3H14, to help us better understand how the brain works as well as perhaps how the patients develop intellectual disability.

In this dissertation, we generate and characterize the first *in vivo* mouse model to study the function of the polyadenosine RNA-binding protein, ZC3H14, which is lost in

an inherited form of nonsyndromic intellectual disability. We demonstrate that like in the patients and in the fly model organism (32), ZC3H14 in mice has a conserved function that is crucial for normal cognition. Thus, what we learn from the mouse model organism may translate into what is potentially occurring in the patients. Furthermore, developing a *Zc3h14* knockout mouse provides a useful and critical experimental control for investigating the function of ZC3H14, which will help us better understand how the brain works.

5.2 Discussion of answers to questions posed at the beginning of our investigation

1) Is ZC3H14 essential in mice?

ZC3H14 is not essential in mice. We have generated a *Zc3h14* conditional knockout mouse that has the first common exon (exon 13) of all four isoforms flanked by *loxP* sites. After mating the conditional knockout mice with a Cre-positive mouse (*EIIa-Cre*) that expresses Cre in oocytes and in pre-implantation embryos. Cre-recombinase excises any genetic material between the flanking *loxP* sites, which in our conditional knockout mouse creates a frameshift mutation that results in three premature stop codons in the transcript, which is expected to undergo nonsense mediated decay. After mating our Cre-positive and *Zc3h14* conditional knockout mice for several generations, we obtained the first *Zc3h14 exon 13* knockout mice, which were viable and fertile and matured to adulthood, which shows that *Zc3h14* is not essential in mice.

Analysis of Mendelian ratios of heterozygous matings show that this mutation of *Zc3h14* does confer a decrease in survivability, especially for male mice. Our colony had a statistically significant fewer homozygous knockout mice by postnatal day 8 (for finger

clipping identification in accordance with IACUC protocol). No decrease in survivability of mice beyond day 8 was observed. Thus, we believe that many of these mice died *in utero* and contributed to the decrease in homozygous ZC3H14 offspring. Additionally, litter size of mutant mice were slightly smaller, and fewer males than females were born from mutant pairings. In summary, though ZC3H14 is not essential for viability, the loss of ZC3H14 does confer a decreased survivability *in utero*.

The caveat to this answer is that a small amount of a truncated ZC3H14 still exists in the mutant mice, as revealed by specific analysis of the new band by mass spectrometry analysis (see chapter 2). Importantly, mass spectrometry did not detect any C-terminal peptides where the zinc fingers are located, though zinc fingers from wildtype samples were readily detected. Thus, this truncated ZC3H14 does not have the RNA-binding zinc finger domain, which is essential for growth (23) and essential for RNA binding in yeast (25). Notably, preliminary RNA-IP experiments comparing wildtype and mutant brain lysates suggest that the mutant ZC3H14 is unable to bind to RNA that wildtype ZC3H14 is able to bind.

2) Is ZC3H14 important for learning and memory in mice?

ZC3H14 is important for learning and memory in mice. Results from the Water Radial Arm Maze (WRAM) reveals that mutant mice have difficulty remembering which lane they had entered within the past two minutes (deficit in working memory). Though not statistically significant, mutant mice also trend toward limitations in learning efficiency, as they take a slightly longer time to find the escape platforms to complete the maze.

While generating the ZC3H14 knockout mouse allows us to study the function of ZC3H14 in complex behaviors such as learning and memory that is not possible to observe in *in vitro* models such as cell culture, there are some disadvantages to this approach. We have disrupted ZC3H14 *de novo* in every cell type and throughout development. It is therefore difficult to determine whether any phenotypic changes we see are due to loss of ZC3H14 directly (e.g. ZC3H14 is necessary in hippocampal neurons for learning and memory) or indirectly (e.g. loss of ZC3H14 causes changes in neural circuitry during development or a deficit in a brain region outside the hippocampus). On the other hand, the brain has had the opportunity to compensate for the loss of ZC3H14 during development, and phenotypes caused by disruption of ZC3H14 may be attenuated.

To address this issue, we could use Cre-recombinase that is tissue-specific or inducible, such as with tamoxifen-inducible Cre. Doing so will disrupt ZC3H14 acutely, giving the brain little opportunity to initiate compensatory measures and providing insight into ZC3H14 function that is analogous to knockdown in cultured cells. Furthermore, we would have the opportunity to compare brain function and behavior within the same individual mouse with and then without ZC3H14, which would eliminate variability from one mouse to another.

With a better understanding of what the loss of ZC3H14 does inside the hippocampus and other brain structures important for learning and memory, we arrive closer to the exact mechanisms of brain dysfunction. Then we can ask informed questions about whether the effects are partially or completely reversible or at least able to be attenuated for treatment purposes.

3) Is ZC3H14 important for development of normal overall morphology of the brain?

Loss of ZC3H14 causes enlarged lateral ventricles in adults (and in newborns at P0, data not shown). Besides this initial characterization, we do not know why ventricles are enlarged. This enlargement may be due to increased cerebral spinal fluid, weakened ependymal epithelial cells that line the ventricles, a malformed hippocampus, malformed cerebral cortex, and/or apoptosis of cells in the brain structures close to the periphery of the ventricles. The three-dimensional quality of the brain makes it difficult to determine changes in the shapes of brain structures without costly histological analyses of the whole brain and/or MRI studies. However, the weights of the whole brain and hippocampus are not different in mutant adult or developing mice. It appears that besides the lateral ventricular enlargement, no other brain structures are grossly malformed.

4) Is ZC3H14 necessary for the proper control of poly(A) tail length in a brain structure critical for learning and memory such as the hippocampus?

Loss of ZC3H14 leads to increased poly(A) tail length of bulk RNA in the hippocampus. This result is expected, as poly(A) tail length control by ZC3H14 orthologues is a conserved role shown extensively in other model organisms (24, 32, 35).

Because this role is evolutionarily conserved, we believe other brain structures like the cerebral cortex and other tissues outside the brain would show a similar phenotype of lengthened poly(A) tails. Nonetheless, it is possible this role is only conserved in the brain or maybe even only in the hippocampus, suggesting a potential reason why patients develop a brain-specific phenotype despite the ubiquitous expression

of ZC3H14. Indeed, our unpublished analysis of immortalized patient fibroblasts does not reveal an increase in poly(A) tail length. Therefore, future analysis of the cerebral cortex as well as other tissues like the kidney, lung, heart, stomach, or muscle will be important.

The mechanism by which the various ZC3H14 orthologues control poly(A) tail length is not yet known. The following model provides some mechanistic theories (**Figure 5—1**). ZC3H14 could bind to the poly(A) tail and sterically hinder binding of or compete off a) polyA binding protein (e.g. PABPN1 or PABPC1) which stabilizes the tail (50) or b) polyA polymerase (PAP) which elongates the tail (50). Alternatively, ZC3H14 could bind to the poly(A) tail and recruit poly(A)-specific ribonuclease (PARN) or another exonuclease to chew up the tail. In the yeast model organism, Nab2 was shown to interact with an RNA exosome subunit, Rrp6, in an RNA-dependent mechanism (182). Note that theoretically, regulation of polyadenylation by ZC3H14 can occur in the cytoplasm or the nucleus. ZC3H14-mediated regulation of polyadenylation in the cytoplasm would afford neurons greater flexibility in fine-tuning the lifespan and translational status of mRNA targets, especially in response to local extracellular signals.

The bulk PAT assay provides a view of the poly(A) tail length of all RNA isolated from the cell. ZC3H14 may regulate the tail of all RNA, subclasses of RNA, or specific transcripts. ZC3H14 may have a larger effect determining poly(A) tail length of specific transcripts, the magnitude of which could be masked by this global analysis. In the future, it will be important to test the poly(A) tail length of specific RNA candidates.

Whether ZC3H14 regulates the poly(A) tail length of general or specific RNA, the tail length can theoretically affect the fate of specific RNA. For example, quality control mechanisms that destroy aberrantly polyadenylated RNA before export from the

nucleus may have a certain degree of leniency for a subset of special RNA that are essential or crucial for the function of the cell. While others are retained, these special RNA would escape into the cytoplasm with an aberrantly lengthened poly(A) tail in *Zc3h14* mutant neurons, producing transcript-specific altered regulation based on ZC3H14-mediated changes in tail length. Another possible scenario in which changes in global poly(A) tail length may produce transcript-specific effects is if translation of a certain set of transcripts depends on tail length while translation occurs indiscriminately, regardless of tail length, in other transcripts. In neurons for example, transcripts containing the CPE (cytoplasmic polyadenylation element) binds to CPE-binding protein (CPEB), which promotes polyadenylation induced translation (115).

5) What is the localization of ZC3H14 in cultured murine primary neurons?

ZC3H14 is enriched in the nucleus as well as in the developing axon of primary hippocampal and cortical (data not shown) cultures at 5-6 days in vitro. ZC3H14 is thus poised as a potentially crucial protein to regulate mRNA (e.g., delivery of transcripts to the growth cone) involved in axonal specification, development, pathfinding, and growth. In addition to the unique localization of ZC3H14 in axons, three pieces of evidence suggest that ZC3H14 is critical for early neuronal development.

First, without ZC3H14, primary hippocampal neurons at 5-6 DIV mature more slowly than wildtype neurons. The evidence to support this statement is that *Zc3h14* mutant neurons develop half as many neurites (wildtype 5 neurites/cell, mutant 2.65 neurites/cell) that are also half the length (wildtype 1134 µm, mutant 506 µm) when compared to wildtype neurons.

As discussed in Chapter 4, culturing young neurons to 5-6 DIV (days *in vitro*) allows us to follow the path of neurites to the soma and easily differentiate dendrites from axons. We can also allow neurons to grow to 21 DIV, at which point neurons have formed long branching axons, a highly arborized dendritic tree, and several mature synapses that have spontaneous electrical activity (169, 180, 183), which suggests synaptic connectivity. Though at this stage, it is virtually impossible with the currently available techniques to follow axons back to their individual somas, we can obtain important synaptic information on more matured neurons. Preliminary evidence suggests that ZC3H14 may change its distribution throughout the neuron in these later stages. Primary hippocampal neurons cultured for 21 DIV show ZC3H14 enrichment in the nucleus with weak and equal dendritic and axonal staining (data not shown). First, this data in addition to the ZC3H14-negative staining of *Zc3h14* knockout primary cultures, suggest that the ZC3H14 axonal enrichment at 5-6 DIV is specific rather than merely background staining. Furthermore, this data is consistent with a role for ZC3H14 early on during axonal development and that at 21 DIV ZC3H14 may play a different role in both axons and dendrites. Preliminary evidence shown in Chapter 4 shows that ZC3H14 localizes to the dendritic spines of excitatory synapses. Loss of ZC3H14 causes abnormal spine morphology and density as well as an increase in shaft synapses. These data are consistent with a role for ZC3H14 in the maturation of neurons and the formation and maintenance of synapses.

Studies in flies also suggest that the ZC3H14 orthologue, dNab2, plays an important role in axon growth. The mushroom bodies are the hippocampal equivalent in flies and are required for learning and memory (91). Each mushroom body is composed

of bundled axons that grow in a stereotypical pattern (91). The axons of *Drosophila* dNab2 mutant mushroom bodies develop abnormal projections, evidenced overgrowth across the brain midline and failure to branch along developmentally sterotyped paths (34). To catch ZC3H14 in action, it may be necessary to continue to study the function of ZC3H14 in developing, not yet mature mice.

The caveat to culturing neurons is the lack of three-dimensional architecture, native synapses, and supportive glia. Future studies should investigate axonal paths in the hippocampus using histological sections of the developing mouse brain. Mossy fibers are axons that take a characteristic path, projecting from the dentate gyrus to the Cornu Ammonis area 3 (CA3) in the hippocampus (184). Mossy fibers stain positive for calbindin, a calcium-binding protein that is enriched in axons (185). The critical period of mossy fiber development is P0-P21, and by P12 growth appears to slow (186). Thus, we can investigate the mossy fibers in the hippocampus in young wildtype and mutant mice by staining for calbindin to assess potential differences in the paths of axonal growth *in vivo*. Additionally, experiments are currently underway to investigate axon projections of individual neurons using a GFP reporter mouse mated to the *Zc3h14* mutant mice and imaging using confocal and two-photon microscopy.

6) Does ZC3H14 play a role in translation?

Though we do not have any direct data, accumulating evidence suggests that ZC3H14 could play a role in regulating local translation. 1) In flies, dNab2 represses translation of CaMKII 3'UTR and aids dFMRP in repression of Futsch translation, 2) murine ZC3H14 associates with polyribosomes, 3) when compared to wildtype, the hippocampi of

ZC3H14 mutant mice show a unilateral increase in neuronal proteins that cluster into GO-term pathways important for brain function, whereas most proteins that decreased in expression fail to cluster into any biological pathway, 4) mRNA-sequencing shows there is no change in steady-state level of mRNA in wildtype versus mutant hippocampi, which suggests that a) ZC3H14 is not involved in transcription or degradation of mRNA, or b) regulation by ZC3H14 does not alter the sum total of any resulting changes in transcription and degradation of mRNA.

These data in addition to data that shows ZC3H14 controls poly(A) tail length would suggest the following model: ZC3H14 binds to target mRNA to limit tail length and inhibit unbridled translational. Upon the loss of ZC3H14, poly(A) tail length increases, allowing increased translational initiation and/or recycling of ribosomes to increase overall protein expression. A follow-up experiment to test this model is to assess the tail length of candidate mRNA that has shown increased protein levels by mass spectrometry analysis (e.g. Camk2a). We would expect hyperadenlyation of candidate mRNA and no change in tail length of mRNA that did not have increased protein expression. The up-regulation of neuron-specific proteins suggests ZC3H14 needs to have transcript-specificity at some point in its regulation. How ZC3H14 moderates tail length or translation in a transcript-specific manner will be discussed in the next section (question 7).

7) What about specific RNA targets of ZC3H14?

A candidate mRNA target for ZC3H14 is Camk2a.

Camk2a (Ca^{2+}/calmodulin-dependent protein kinase IIa) is a kinase that is activated in response to the arrival of a presynaptic stimulus and is responsible for initiating a cascade of events that can result in a stronger synapse (187). Camk2a is an important mediator of learning and memory (187). Camk2a mutant mice have impaired long-term potentiation and impaired long-term memory (188). As discussed in Chapter 3, in flies dNab2 was shown to inhibit translation of the *Drosophila* CaMKII 3'UTR. In the *Zc3h14* mutant mice, Camk2a protein levels are elevated as determined by mass spectrometry analysis of hippocampi. Recent research also reveals that neurons modulate the poly(A) tail length of Camk2a mRNA to regulate its translation, localization, and stability dependent on synaptic stimulation (15, 189). Considering that ZC3H14 regulates poly(A) tail length, Camk2a is a prime target to study whether its poly(A) tail length is increased in *Zc3h14* mutant mice and whether it is detectable by RNA-IP.

As discussed in detail in Chapter 1, a number of lines of evidence suggest ZC3H14 regulate specific mRNA targets. As a protein initially isolated in budding yeast as a polyadenosine RNA-binding protein that affects bulk poly(A) tail length, one would expect that ZC3H14 has no specific transcript but binds any mRNA with a poly(A) tail. While that may be true, it is still possible that ZC3H14 has specific targets, perhaps in addition to general targets.

Figure 5—2 illustrates three possible non-mutually exclusive ways ZC3H14 could bind to target mRNA. First, **(A)** ZC3H14 binds to all mRNA with a poly(A) tail but regulate only specific mRNA. In other words, ZC3H14 itself may not bind with sequence specificity, but the specificity of its role is afforded by its binding to other RNA-binding proteins that do have binding specificity. Alternatively, **(B)** ZC3H14 may bind to a

specific sequence that is enriched with adenosines, such as the sequence shown in studies with the *C. thermophilum* ZC3H14 orthologue, AAXAAXXA or AAXAXXAA, where X is an unknown nucleic acid (41). Furthermore, these sequences may belong to transcripts with important neural function, conferring ZC3H14 the ability to regulate them specifically.

Yet another alternative mechanism for ZC3H14 specificity is that **(C)** ZC3H14 could bind to a stretch of adenosines located in the 3'UTR, which also places it in the vicinity of the poly(A) tail to serve a regulatory function. Camk2a has a stretch of adenosines in their 3'UTRs that are conserved across species: Camk2a in fly (9 A's), mouse (10 A's), human (11 A's). These stretches of adenosines are relatively unique and not found very often in the 3'UTRs of the mouse transcriptome. A run of 9 A's is present in 7% of the transcriptome's 3'UTRs. (10 A's in 4.7%, 11 A's in 3.2%, 12 A's in 2.3%, and 13 A's in 1.7%.) This analysis is consistent with a previously published analysis of the 3'UTRs of the human transcriptome, which reported that a stretch of ≥ 12 A's appeared in 1.7% of transcripts (190).

Going forward, finding mRNA targets of ZC3H14 will be helpful for mechanistic investigations of how ZC3H14 functions.

5.3 Concluding remarks

The field of neurobiology is interdisciplinary and requires a multi-level approach. It combines the behavioral methods of psychology with the methods of anatomy, electrophysiology, cellular biology, biochemistry, and genetics (5). Each methodology requires specialized training and knowledge. In an effort to take a comprehensive

approach to the initial characterization of the *Zc3h14* mutant mouse, we have combined our efforts to produce a highly collaborative work. The findings of this study provide a basis for better understanding the role ZC3H14 plays in mouse neuronal development, brain morphology, and cognition. **Figure 5—3** presents a model along with some of the evidence gathered by this dissertational work that could explain the pathogenesis of intellectual disability in ZC3H14-deficient patients. Indeed, this investigation has merely scratched the surface and raises many questions.

In addition to the ones mentioned in the previous paragraphs, some outstanding questions in the study of ZC3H14 are: Is Camk2a mRNA a target of ZC3H14? What are other RNA targets of ZC3H14, and how exactly does ZC3H14 regulate those targets? Are there RNA consensus motifs to which ZC3H14 preferentially binds? How does ZC3H14 regulate poly(A) tail length, and does ZC3H14 regulate the tail length of the majority of RNA or specific RNA? What are the protein binding partners of ZC3H14? Does ZC3H14 play a direct role in translation of RNA? Do the different isoforms of ZC3H14, especially the truncated fourth isoform, play unique roles in general or in various tissues? Are the isoforms differentially regulated through post-translational modifications?

Questions range from determining molecular mechanism of RNA regulation to understanding tissue-specific functional roles of ZC3H14 in the pathogenesis of intellectual disability. With the continuing and concerted efforts of collaborative investigators across various model organisms and the development of new mutant models to study ZC3H14, we are optimistic that we will more fully be able to understand the function of this important polyadenosine RNA-binding protein in biology and disease.

5.4 Figures

Figure 5—1

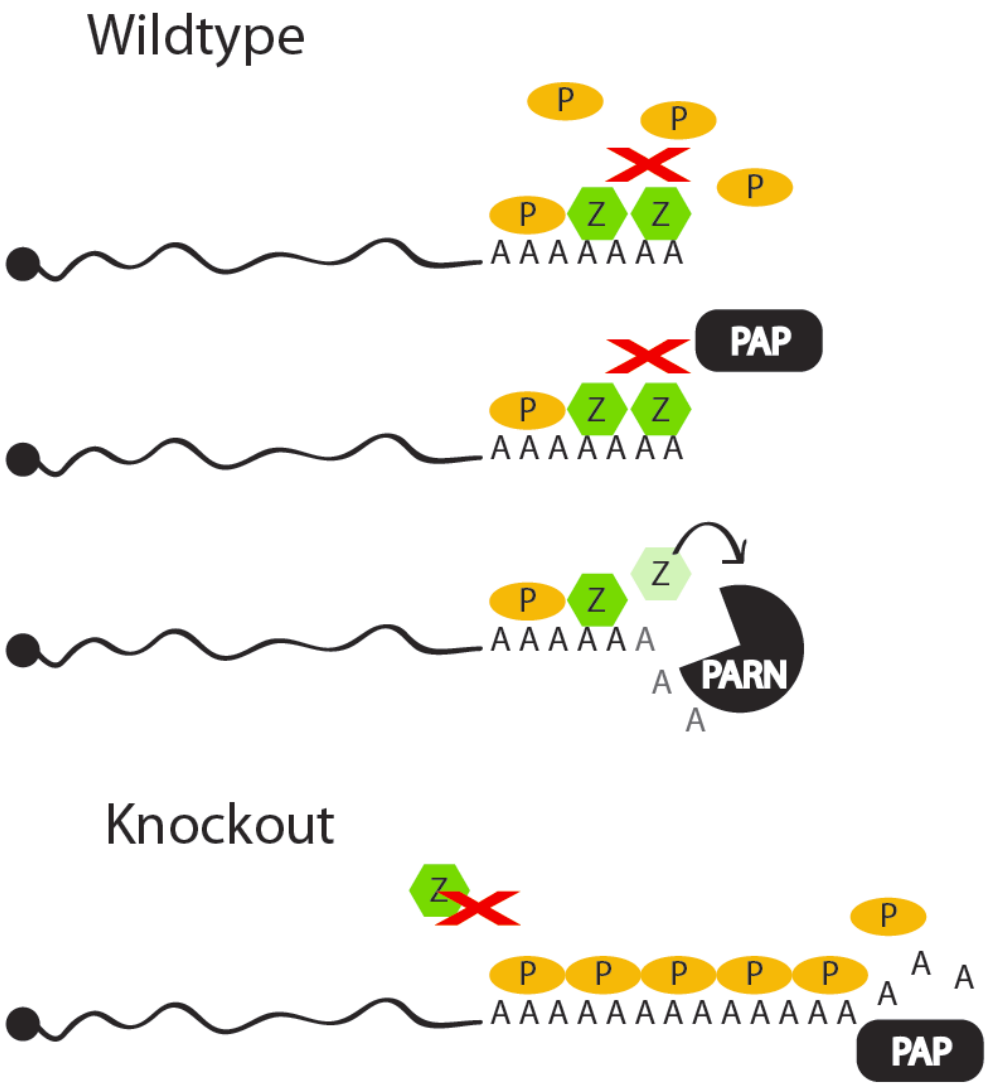

Figure 5—1. Models for ZC3H14 poly(A) tail length regulation.

In wildtype cells, ZC3H14 (Z) competes off or blocks pro-elongating factors like PABPC1 or PABPN1 (P) and PAP (polyA polymerase). ZC3H14 may also recruite deadenylating factors like PARN (polyA-specific ribonuclease). In mutant cells without ZC3H14, poly(A) tail length is elongated due to binding of poly(A) tail stabilizing factors (PABPN1/PABPC1) or elongation factors (PAP).

Figure 5—2

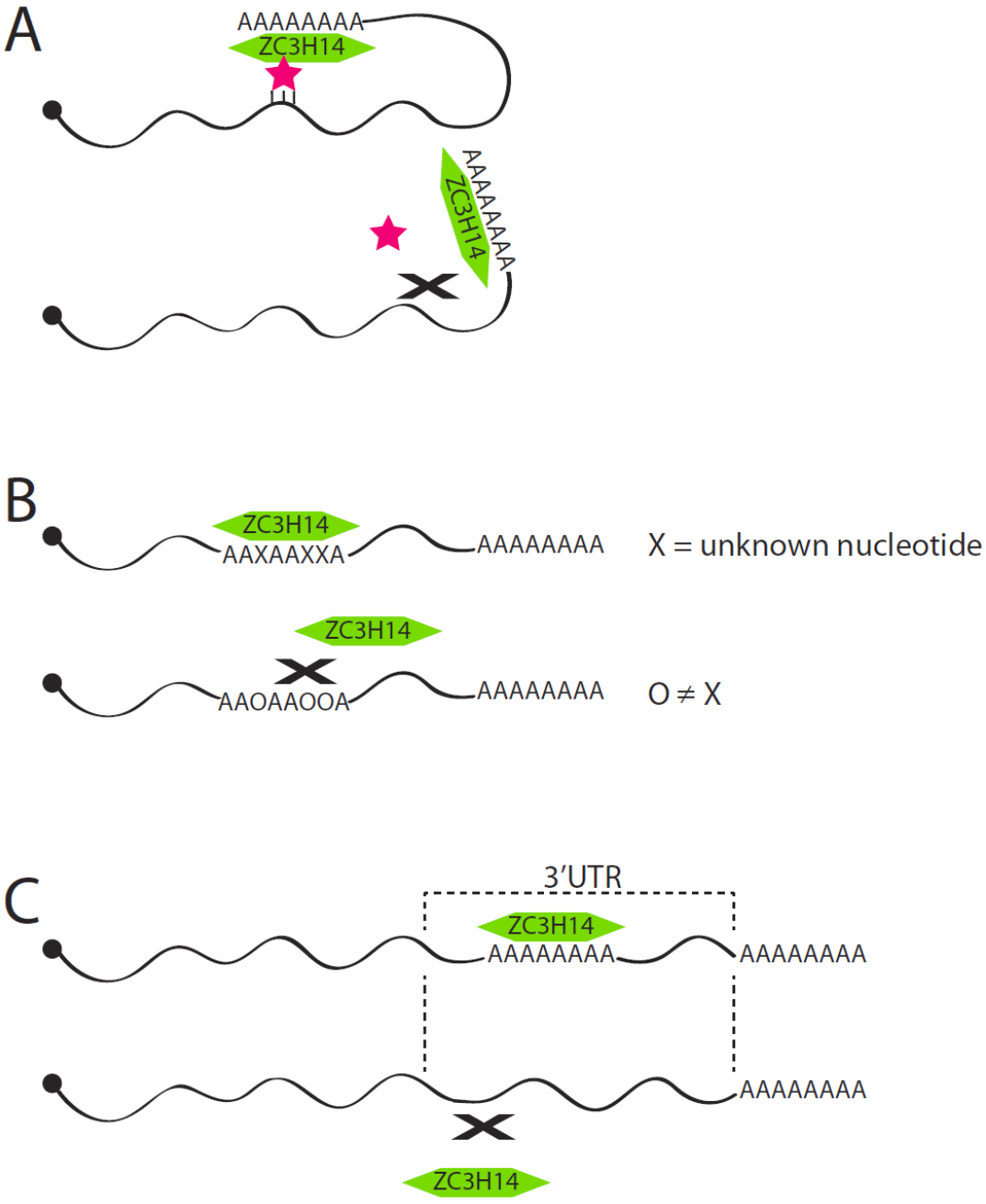
A
AAAAAAAA
ZC3H14
AAAAAAAA
ZC3H14
B
ZC3H14
AAXAAXXA
AAAAAAAA
X = unknown nucleotide
ZC3H14
AAOAAOOA
AAAAAAAA
O ≠ X
C
3'UTR
ZC3H14
AAAAAAAA
AAAAAAAA
AAAAAAAA
ZC3H14

Figure 5—2. Models for ZC3H14 target mRNA binding specificity.

(A) ZC3H14 binds all mRNA, but specificity of regulation is afforded by an associated protein (indicated by pink star) that has binding specificity itself. mRNA that do not have the binding motif of the associated protein will not be regulated. (B) ZC3H14 has a specific binding motif that is enriched with As. Parts of the motif are currently unknown (indicated by Xs). Those transcripts that lack the specific sequence motif will not bind ZC3H14. (C) ZC3H14 binds to the stretches of As located in the 3'UTR of specific transcripts.

Figure 5—3

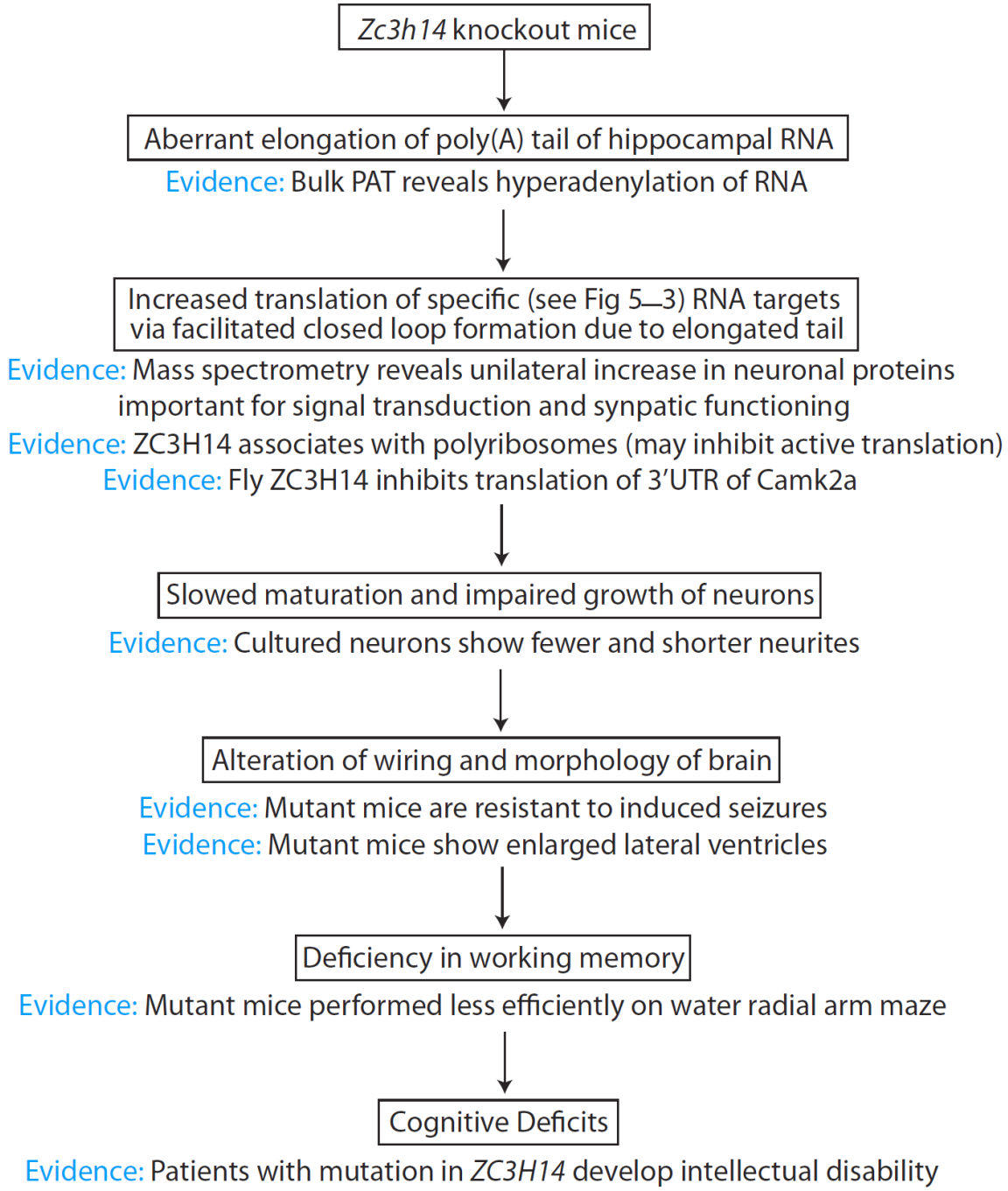
Zc3h14 knockout mice
Aberrant elongation of poly(A) tail of hippocampal RNA
Evidence: Bulk PAT reveals hyperadenylation of RNA
Increased translation of specific (see Fig 5—3) RNA targets via facilitated closed loop formation due to elongated tail
Evidence: Mass spectrometry reveals unilateral increase in neuronal proteins important for signal transduction and synpatic functioning
Evidence: ZC3H14 associates with polyribosomes (may inhibit active translation)
Evidence: Fly ZC3H14 inhibits translation of 3'UTR of Camk2a
Slowed maturation and impaired growth of neurons
Evidence: Cultured neurons show fewer and shorter neurites
Alteration of wiring and morphology of brain
Evidence: Mutant mice are resistant to induced seizures
Evidence: Mutant mice show enlarged lateral ventricles
Deficiency in working memory
Evidence: Mutant mice performed less efficiently on water radial arm maze
Cognitive Deficits
Evidence: Patients with mutation in *ZC3H14* develop intellectual disability

Figure 5—3. Model for pathogenesis of intellectual disability in ZC3H14 deficiency. Proposed model for pathogenesis along with lines of evidence presented in this dissertational work.

Chapter 6

Materials and Methods

6.1 Materials and Methods: Chapter 2

Generation of *Zc3h14*$^{\Delta/\Delta}$ mouse. Mouse embryonic stem cells (clone EPD0366_5_F01, ES cell strain C57BL/6N, Parental Cell Line JM8A3.N1) were obtained from Knockout Mouse Project Repository (UC Davis, Davis, CA). This clone flanks with *loxP* sites exon 13, the first common exon among all four *Zc3h14* isoforms (a, b, c, d) (see Fig. 1 A and B). *In vitro* Flp-*FRT* recombination to eliminate the *LacZ*/*neomycin* cassette and subsequent blastocyst injections were performed by the Emory Mouse Transgenic and Gene Targetting Core. We generated heterozygously floxed *Zc3h14* exon 13 mice (*Zc3h14*$^{F/+}$) by mating adult male chimeras to C57BL/6N wildtype female mice (The Jackson Laboratory). Offspring generated from this mating were then mated to generate homozygously floxed mutant mice (*Zc3h14*$^{F/F}$). *EIIa-Cre* mice (purchased from The Jackson Laboratory, Stock #003724, mixed C57BL/6J and C57BL/6N genetic background) which express Cre-recombinase active at the zygotic stage (69), were mated to homozygously floxed *Zc3h14* exon 13 (*Zc3h14*$^{F/F}$) mice for 3-4 generations to generate a germline-transmissible *Zc3h14* allele lacking exon 13 (*Zc3h14*$^{\Delta/\Delta}$). These mice with confirmed proper recombination were mated to wildtype C57BL/6 mice (purchased from The Jackson Laboratory) to breed out the *EIIa-Cre* allele. *EIIa-Cre*-negative, *Zc3h14*$^{\Delta/+}$ were mated to generate *Zc3h14*$^{\Delta/\Delta}$ mutant homozygous mice for at least four generations.

Control *Zc3h14*$^{+/+}$ were maintained in the colony as control counterparts from the heterozygous *Zc3h14*$^{\Delta/+}$ breeders. Generations F4-F8 of *Zc3h14*$^{+/+}$ (and *Zc3h14*$^{\Delta/\Delta}$) homozygous pairings were used for experiments, and homozygous off-spring were routinely cross-bred to minimize genetic drift between *Zc3h14*$^{+/+}$ and *Zc3h14*$^{\Delta/\Delta}$ mice.

All procedures involving mice were done in accordance with the NIH guidelines for use and care of live animals and were approved by the Emory University Institutional Animal Care and Use Committee.

Genotyping. Mice were screened for the conditional floxed allele, Cre-mediated recombination, and the Cre-recombinase gene by PCR of genomic DNA isolated from toe clippings using a standard DNA isolation protocol (191). Tissue from toe clippings was lysed in 50 µl of standard lysis buffer supplemented with Proteinase K overnight at 55°C. Samples were centrifuged for 5 min at full speed to sediment cellular debris. Genomic DNA was precipitated using ice-cold 100% ethanol, washed two times in 75% ethanol, and allowed to air dry before being resuspended in 30 µl of water. Template DNA was amplified by standard PCR per the Qiagen *Taq DNA Polymerase* PCR kit manufacturing protocol (Qiagen 201205). The following primers were used to genotype mice at the *Zc3h14* locus (as illustrated in Fig. 1 B and C): Fwd (5'-GTTGGCTCATCTTCTGTA AAGC-3') and RevI (5'- GGTAAGGAAAACTAATCCACATCTAG-3') for the conditional floxed allele (generating a product of either 885 bp for control, 994 bp for floxed, or 230 bp for recombined alleles) or RevII (5'-GCCACACTCAGGTCAGTC ATCTCG-3') for the direct detection of exon 13 (generating a product of either 469 bp for control or 625 bp for floxed, or no product for the recombined allele which excises exon 13). For detection of the Cre-recombinase gene, generic Cre-recombinase primers were used: Fwd-Cre (5'-GCGGTCTGGCAGTAAAAACTATC-3') and Rev-Cre (5'GTGAAACAGCATTGCTGTCACTT-3').

Immunoblotting. Mouse brain tissue samples were lysed in RIPA-2 buffer (50 mM Tris–HCl, pH 8.0, 150 mM NaCl, 1% IGEPAL or NP-40, 0.5% deoxycholic acid, 0.1% SDS) containing protease inhibitors (Complete Mini; Roche) and centrifuged at 9,200 x g for 10 min at 4°C. The pellet was discarded, and the supernatant was subjected to SDS-PAGE and immunoblotting. An equal amount of protein from each sample was loaded onto 10% SDS-polyacrylamide gels and transferred to a 0.2 μm nitrocellulose membrane (Bio-Rad Laboratories) (192). After blocking non-specific binding, the membranes were incubated with the primary antibodies. Primary antibodies used were as follows: anti-ZC3H14 (rabbit polyclonal antibody generated against the N-terminal PWI-like domain) (30), EIF5 (Santa Cruz sc-282), α-Tubulin (Sigma T9026), Histone H3 (Abcam ab1791), THOC1 (kind gift from Dr. Robin Reed, Harvard University, Boston, MA), S6 Ribosomal Protein (5G10) (Cell Signaling 2217), followed by incubation with the appropriate horseradish peroxidase (HRP)-conjugated secondary IgG antibody (Jackson ImmunoResearch).

Real-time PCR analysis of *Zc3h14* splice variant d mRNA. To obtain RNA from mouse tissue, brain was lysed using QIAzol, according to the guidelines of the manufacturer (Qiagen). cDNA was synthesized from RNA isolated from mouse whole brain using M-MLV Reverse Transcriptase kit (Invitrogen 28025), GoTaq DNA Polymerase (Promega M3001), and Recombinant RNasin Ribonuclease Inhibitor (Promega N2511). Briefly, 5 ng of cDNA was subjected to PCR amplification using SYBR Green PCR Master Mix (Applied Biosystems) and *Zc3h14* splice variant d-specific primers: Fwd (5'GGTTGAGAAAGGAACTCAACAGAGGC-3') (junction of alternative exon 1 and exon 10) and Rev (5'-TCATCTCGGCTTGACTCATCTCCA-3') (junction of exons 10

and 13). PCR amplification was performed with an Applied Biosystems, StepOnePlus Real-Time PCR System. The 18S rRNA was used to normalize mRNA. Relative quantitation of mRNA expression level was determined using the relative standard curve method as previously described (193) and according to the instructions of the manufacturer (Applied Biosystems).

ZC3H14 immunoprecipitation for mass spectrometry analysis. Brain tissue was homogenized in IP buffer (50 mM Tris-HCl, pH 7.4, 100 mM NaCl, 32 mM NaF, 0.5% NP-40 in DEPC-treated water) containing protease inhibitors (Complete Mini; Roche; 1 tablet/10 mL of IP buffer). Cells were sonicated on ice 5 times at 0.5% output for 10 sec, passed through a 27-gauge syringe 5 times, and placed back on ice for 20 minutes with occasional vortexing. Lysates were spun at 15,600 x g for 10 minutes at 4°C and protein concentrations were determined with a standard BCA assay. Protein G magnetic beads (DYNA beads, Invitrogen) were rinsed and resuspended in IP buffer and incubated with pre-immune rabbit serum or an equal volume of N-terminal ZC3H14 antibody for 1 hour at room temperature. Bead/antibody and bead/pre-immune samples were rinsed in IP buffer and added to clarified cell lysates. Ten percent of the sample was then removed and reserved for input analysis, and the remainder of the sample was incubated overnight at 4°C while tumbling end over end. Beads were then magnetized to collect bound and unbound species separately. The beads were washed 5 times with ice-cold IP buffer. ZC3H14 protein complexes were eluted with reducing sample buffer (RSB): 250 mM Tris HCL, 500 mM DTT, 10% SDS, 0.5% bromophenol blue, 50% glycerol. Upon submission to the Emory Proteomics Core for mass spectrometry analysis, the samples were further

reduced with DTT and alkylated with Iodoacetamide (IAA), and then subjected to sequential in-solution digestion with LysC (1:100 enzyme-to-protein ratio) for 4 hrs and with trypsin (1:100 enzyme-to-protein ratio) overnight. After desalting and sample cleanup with Water's Sep-Pak, the samples were submitted for analysis on the Orbitrap Fusion Mass Spectrometer (Thermo Scientific).

Determination of bulk poly(A) tail length. Bulk poly(A) tails were analyzed using a standard poly(A) tail length assay (194) as described previously (195). Total RNA was isolated from hippocampi of P0 *Zc3h14*$^{+/+}$ and *Zc3h14*$^{\Delta/\Delta}$ mice using a RNeasy mini kit (Qiagen 74104). Total RNA was 3'end labeled with [^{32}P]pCp using T4 RNA ligase and digested with a cocktail of RNAse A/T1. The resulting tracts of poly(A) RNA were resolved by gel electrophoresis and imaged by film or PhosphorImager. Three biological replicates were performed for each mouse genotype analyzed. Using ImageJ software, densitometry analysis of each experiment was performed in order to obtain profile curves for each sample that was analyzed, as described previously (35). Profiles of the relative signal intensity at a given location on the gel were plotted in Microsoft Excel and a moving average (period = 25) calculated.

Immunohistochemical analysis of brain morphology. Whole brains were fixed overnight in 4% PFA, processed for routine embedding in paraffin, and cut 9 μm in thickness onto glass slides. Slides were dewaxed in xylene and rehydrated through graded ethanol washes. Haematoxylin and eosin staining was performed using standard procedures.

Images were visualized on an Olympus BX51 microscope using a 2X magnification objective and captured using DP Controller (Olympus) software. Genotype of brain images was blinded, and the quantification of ventricular area was performed using ImageJ.

Water radial arm maze (WRAM). The WRAM apparatus was used as previously described (80). A radial maze, 2 m in diameter with 8 arms of equal width and length (10 cm wide and 60 cm long) at 45-degree angles surrounding an open center section, was filled with water at approximately 21ºC (see Fig. 5A). The water was made opaque by mixing in water-soluble, non-toxic paint of the same color (black) as the maze and the platforms. The water was filled to a level 0.5-1.0 cm above the top of all four total submerged platforms, placed one each at the far end of half of the arms. A specific orientation of platforms, constant for each mouse throughout the testing period, was placed in the arena with the following criteria: the “start” arm always contained no platform and no more than 2 adjacent arms contained platforms.

Ten *Zc3h14*$^{+/+}$ and nine *Zc3h14*$^{\Delta/\Delta}$ male adult (5 month old) mice were tested. At the start of each trial, a mouse was placed inside a clean, dry, empty cage heated with a lamp to approximately 40ºC. Once the platforms were placed in the correct orientation, the mouse was gently placed in the water at the far end of the "start" arm, and the timer was started. A blinded researcher monitored the progress of the mouse by recording both the sequence of arms the mouse entered and the time in seconds the mouse took to locate a platform, with a maximum trial length of 120 seconds before the trial was aborted and the mouse was gently guided to the nearest platform. When a mouse reached a platform, it was allowed to remain there for 15 seconds, allowing time for it to identify any visual cues

placed on the walls to aid in spatial memory. The mouse was then returned to the heated and dry cage for a period of 30 seconds as a reward for successfully completing the trial. The platform on which the mouse was seated was removed, and the next trial commenced in the same manner. Four trials were performed per mouse, per day, until each mouse had located all 4 platforms. Testing was conducted for 9 consecutive days.

We used the following criteria to analyze WRAM data. To plot *total latency*, time required to reach the platforms were recorded for each mouse and summed across the four trials per day. After groups were unblinded, these latencies were calculated across the 9-day testing period. To plot *overall total errors*, each entry into an arm that did not result in locating a platform was summed across the four trials for each mouse per day. These errors were then sorted into 3 types: I) errors in which the first time on a given trial a mouse enters any arm that contained a platform on a previous trial on the same day (shows good working and spatial memory but poor procedural memory); II) errors in which the first time on a given trial a mouse enters any arm that never contained a platform or else enters an arm with a platform but does not successfully locate the platform (shows poor spatial memory); III) errors in which a mouse makes a repeated entry into any arm for which it has previously registered a type I or type II error on the same trial (shows poor working memory). To plot *working memory errors*, groups were then unblinded, and type III errors were summed for the four trials per day across the 9-day testing period, at which point a steady-state minimum was achieved, indicating sufficient performance. Sufficient performance on the WRAM requires that a group make an average of no more than approximately 1.0 type III error per subject per day by the conclusion of testing in order to demonstrate learning.

Optokinetic tracking (OKT). To assess visual function, we measured visual acuity and contrast sensitivity using optokinetic tracking behavior (OptoMotry, Cerebral Mechanics, Inc., Lethbridge, Alberta, Canada) (117-119). Four *Zc3h14*$^{+/+}$ and four *Zc3h14*$^{\Delta/\Delta}$ mice were placed on a platform in the center of a virtual optomotor drum consisting of four computer monitors. Spatial frequency thresholds were determined by varying the spatial frequency at 100% contrast. Contrast sensitivity thresholds were determined by varying contrast at peak contrast sensitivity (0.064 cycles/degree). Positive responses were noted as reflexive head-tracking in the direction of the moving gratings. Both eyes were tested by using clockwise and counter-clockwise rotations (82). The values from the left and right eyes were averaged for analysis of differences between groups at 6 weeks of age using a two-way repeated ANOVA with Holm-Sidak post-hoc.

Wire-hang assay. Testing was performed with 1- x 1-cm mesh hardware fixed to a 19- x 19-cm frame. Nine *Zc3h14*$^{+/+}$ and 14 *Zc3h14*$^{\Delta/\Delta}$ male adult mice were placed on the wire mesh, which was slowly inverted 27.5 cm over a soft, thick heating pad (unheated), lined with paper towels. Latency to fall was recorded in seconds as previously described (196). The test was performed three trials a day for three days for each mouse. The maximum latency to fall for each day was averaged together for the three days for each mouse.

Rotarod. A four-lane motorized rotarod (Rotamex-5 Controller, Columbus Instruments, Columbus, OH) was used according to manufacturer's instructions and as previously described (196). Each rod was 3.0 cm in diameter and 9.5 cm long. The fall height from rod center was 44.5 cm to the base. Scanning infrared beam sensors monitored animals'

absence from rod to detect time to fall. The acceleration interval (1.0 sec), acceleration step (0.1 RPM), and maximum speed (50.0 RPM) was the same for each mouse and for all testing days. Prior to testing, mice were trained on a rotarod (AccuRotor Rota Rod RR4/M, AccuScan Instruments, Columbus, OH) that had a constant speed of 4.2 RPM.

Nine *Zc3h14*$^{+/+}$ and 10 *Zc3h14*$^{\Delta/\Delta}$ male adult mice were allowed to acclimate to the room for 15 min. All mice were oriented on the rod to walk forward to maintain balance. To avoid falling, mice were required to move forward in a coordinated manner. Training occurred over 3 days. Four mice at a time were trained for 10 min on the rotarod at constant speed, replacing mice back on the rod when subjects had fallen from the rotarod. After training on the third day, the mice started the 3-day testing phase. Each day of testing consisted of 3 trials, with at least 15 min of rest in between trials, for a total of 9 trials. Latency to fall was averaged for the three trials within a particular day and analyzed using the two-tailed Student's *t*-test with the Bonferroni correction for repeated measures. *P* values of 0.05 or less were taken as statistically significant. The genotype of the mice were blinded until all latency times were recorded.

Open field. Open field was performed as previously described (197). Briefly, the mice were acclimated to the testing room for two hours prior to initiating the task. Twelve *Zc3h14*$^{+/+}$ and twelve *Zc3h14*$^{\Delta/\Delta}$ male adult mice (3-4 months) were examined. Each mouse was placed into the center of an opaque Plexiglas box (60 x 60 x 60 cm) and given 10 minutes to explore the apparatus. The center zone was defined as the region 15 cm from each side of the box. The time spent in the center, number of entries into the center, total

distance traveled, and average speed were recorded and scored with AnyMaze video tracking software (Stoelting Co. IL) by a user blinded to genotype.

Novel cage. Twelve *Zc3h14*$^{+/+}$ and twelve *Zc3h14*$^{\Delta/\Delta}$ male adult mice (3-4 months) were examined. Each mouse was placed into an uncovered cage with corncob bedding for 10 minutes. General mobility and exploratory actions such as rearing, digging, and grooming were scored.

Light-dark box. Twelve *Zc3h14*$^{+/+}$ and twelve *Zc3h14*$^{\Delta/\Delta}$ male adult mice (3-4 months) were examined. The apparatus comprised a Plexiglas box (30 x 14 x 14.5 cm) was divided into a light (20 x 14 x 14.5 cm) and dark side (10 x 14 x 14.5 cm). The walls of the dark side were blackened to reduce external illumination. A hole in the divider between the two sides enabled movement of the mouse between the two sections. Each mouse was placed into the light side and given 10 minutes to explore freely. Latencies to first enter the dark side, the number of transitions between each side, and total time spent in each side was recorded for each mouse.

Seizure induction. Seizures were induced using the 6-Hz psychomotor seizure model and the chemiconvulsant flurothyl. The 6-Hz seizure induction was conducted as previously described (84, 198). Briefly, 30 minutes prior to seizure induction, a topical anesthetic (0.5% tetracaine hydrochloride) was applied to the cornea. Each mouse was manually restrained during corneal stimulation (6 Hz, 0.2-ms pulse, 3s) using a constant current device (ECT Unit 57800; Ugo Basile, Comerio Italy). Behavioral seizures were scored on

a modified Racine Scale (RS): RS0, no abnormal behavior; RS1, staring; RS2, forelimb clonus or paw waving; RS3, rearing and falling. Female and male *Zc3h14*$^{+/+}$ and *Zc3h14*$^{\Delta/\Delta}$ mice (*N* = 22-24/genotype/sex) were tested at current intensities of 13 mA or 15 mA, respectively. Comparisons of seizure severity and occurrence between *Zc3h14*$^{+/+}$ and *Zc3h14*$^{\Delta/\Delta}$ mice were analyzed using an unpaired non-parametric *t*-test followed by the Mann-Whitney *post hoc* analyses.

For flurothyl seizure induction**,** female and male *Zc3h14*$^{+/+}$ and *Zc3h14*$^{\Delta/\Delta}$ mice (*N* = 11-12/genotype/sex) were exposed to flurothyl as previously described (85, 199, 200). Briefly, each mouse was placed into a clear acrylic glass chamber and flurothyl (2,2,2-trifluroethylether; Sigma-Aldrich) was introduced at a rate of 20 µL/minute. Latencies to the first myoclonic jerk (MJ) and generalized tonic-clonic seizure (GTCS) were recorded and analyzed using an unpaired *t*-test.

Mass spectrometry analysis of *Zc3h14*$^{+/+}$ and *Zc3h14*$^{\Delta/\Delta}$ hippocampi. Samples submitted for mass spectrometry analysis consisted of eight hippocampi from four *Zc3h14*$^{+/+}$ and eight hippocampi from four *Zc3h14*$^{\Delta/\Delta}$ mice at P0. Each tissue piece was uniformly homogenized in 300 µL of urea lysis buffer (8 M urea, 100 mM $NaHPO_4$, pH 8.5), including 3 µL (100x stock) HALT protease and phosphatase inhibitor cocktail (Pierce). All homogenization was performed using a Bullet Blender (Next Advance) according to manufacturer protocols. Briefly, each tissue piece was added to Urea lysis buffer in a 1.5 mL Rino tube (Next Advance) harboring 750 mg stainless steel beads (0.9-2 mm in diameter) and blended twice for 5 minute intervals in the cold room (4°C). Protein supernatants were transferred to 1.5 mL Eppendorf tubes and sonicated (Sonic

Dismembrator, Fisher Scientific) 3 times for 5 s with 15 s intervals of rest at 30% amplitude to disrupt nucleic acids and subsequently vortexed. Protein concentration was determined by the bicinchoninic acid (BCA) method, and samples were frozen in aliquots at −80°C. Protein homogenates (100 µg) were diluted with 50 mM NH_4HCO_3 to a final concentration of less than 2 M urea and then treated with 1 mM dithiothreitol (DTT) at 25°C for 30 minutes, followed by 5 mM iodoacetimide (IAA) at 25°C for 30 minutes in the dark. Protein was digested with 1:100 (w/w) lysyl endopeptidase (Wako) at 25°C for 2 hours and further digested overnight with 1:50 (w/w) trypsin (Promega) at 25°C. Resulting peptides were desalted with a Sep-Pak C18 column (Waters) and dried under vacuum.

For LC-MS/MS analysis, hippocampal derived peptides were resuspended in peptide 100 µL of loading buffer (0.1% formic acid, 0.03% trifluoroacetic acid, 1% acetonitrile). Peptide mixtures (2 µL) were separated on a self-packed C18 (1.9 µm Dr. Maisch, Germany) fused silica column (25 cm x 75 µM internal diameter (ID); New Objective, Woburn, MA) by a Dionex Ultimate 3000 RSLCNano and monitored on a Fusion mass spectrometer (ThermoFisher Scientific , San Jose, CA). Elution was performed over a 120 minute gradient at a rate of 400 nL/min with buffer B ranging from 3% to 80% (buffer A: 0.1% formic acid in water, buffer B: 0.1 % formic in acetonitrile). The mass spectrometer cycle was programmed to collect at the top speed for 3 second cycles. The MS scans (400-1600 m/z range, 200,000 AGC, 50 ms maximum ion time) were collected at a resolution of 120,000 at m/z 200 in profile mode and the HCD MS/MS spectra (0.7 m/z isolation width, 30% collision energy, 10,000 AGC target, 35 ms maximum ion time) were detected in the ion trap. Dynamic exclusion was set to exclude

previous sequenced precursor ions for 20 seconds within a 10 ppm window. Precursor ions with +1, and +8 or higher charge states were excluded from sequencing.

MaxQuant for label-free quantification. Raw data files were analyzed using MaxQuant v1.5.2.8 with Thermo Foundation 2.0 for RAW file reading capability. The search engine Andromeda was used to build and search a concatenated target-decoy IPI/Uniprot mouse reference (downloaded at Aug 14, 2015) supplement with eGFP protein sequence. Protein Methionine oxidation (+15.9949 Da) and protein N-terminal acetylation (+42.0106 Da) were variable modifications (up to 5 allowed per peptide); cysteine was assigned a fixed carbamidomethyl modification (+57.0215 Da). Only fully tryptic peptides were considered with up to 2 miscleavages in the database search. A precursor mass tolerance of ±10 ppm was applied prior to mass accuracy calibration and ±4.5 ppm after internal MaxQuant calibration. Other search settings included a maximum peptide mass of 6,000 Da, a minimum peptide length of 6 residues, 0.6 Da Tolerance for iron trap HCD MS/MS scans. The false discovery rate (FDR) for peptide spectral matches, proteins, and site decoy fraction were all set to 1%. The label free quantitation (LFQ) algorithm in MaxQuant (201, 202) was used for protein quantitation. LFQ intensity of each protein for each mouse was averaged from two hippocampi (left and right). No more than two missing values were considered per group ($Zc3h14^{\Delta/\Delta}$ or $Zc3h14^{+/+}$). Differentially expressed proteins were found by calculating Student's t-test p values and fold difference $|\log2(Zc3h14^{\Delta/\Delta}/Zc3h14^{+/+})| \geq 0.32$ ($\geq \pm 1.25$ fold change). Volcano plots were plotted with ggplot2 packages in R.

GO enrichment and network. Functional enrichment of the modules was determined using the GO-Elite (v1.2.5) package (203). The set of total proteins identified

and quantified (n = 4,161) was used as the background. Input lists included proteins either significantly decreased (n = 50) or increased (n = 63) in *Zc3h14*$^{\Delta/\Delta}$ mice. Z-score determines overrepresentation of ontologies in a module and permutation P-value was used to assess the significance of the Z-score. For these down regulated proteins in *Zc3h14*$^{\Delta/\Delta}$ mice, Z-score cut off of 1.96, p value cut off of 0.05 with a minimum of 3 proteins per category were used as filters in pruning the ontologies. For these up regulated proteins in *Zc3h14*$^{\Delta/\Delta}$ mice, Z-score cut off of 2.58, P value cut off of 0.01 with a minimum of 5 proteins per category were used as filters in pruning the ontologies. Horizontal bar graph was plotted in R. The networks were constructed using the igraph package in R (204).

Statistical analysis. Data were analyzed using R, GraphPad Prism 6.0, or Microsoft Excel. R, Prism, or Microsoft Excel was also used to generate graphs, column and row means and standard error of the means (SEMs), and statistical analyses (two-way ANOVA, *t*-tests, and post-hoc analysis) to compare between genotypes. P values are > 0.05, unless otherwise noted. P values < 0.05 were considered statistically significant. Error bars indicate SEM unless otherwise noted.

6.2 Materials and Methods: Chapter 3

Drosophila stocks and genetics. All crosses and stocks were maintained in standard conditions at 27^{o} C. The *dNab2^{ex3}* loss of function mutant, *dNab2^{pex41}* precise excision isogenic control, and UAS-*Flag-dNab2* stocks were described previously (32, 35). The following Gal4 drivers were utilized to drive expression of UAS transgenes: *GMR-Gal4* (expresses in the eye cells behind the morphogenic furrow, BL#1350), *C155-Gal4* (pan-neuronal expression, BL#458), *OK107-Gal4* (expresses in all lobes of the mushroom body, BL#854), and *GH146-Gal4* (expresses in antennal lobe projection neurons). The following alleles and transgenic stocks were also used in this study: *dfmr1$^{\Delta 50}$* (BL#6930), *dfmr1$^{\Delta 113M}$* (BL#6929), *UAS-CD8-GFP* (205), *UAS-eYFP-CAMKII 3' UTR*(152), *UAS-dNab2^{IR}* (obtained from the Vienna *Drosophila* Research Center), and *dfmr1^{IR}* (BL#35200). The *UAS-dfmr1* transgenic stock was a gift from Thomas A. Jongens. The *eYFP-CaMKII* reporters (152) were a gift from Dr. Sam Kunes.

Brain dissection and immunohistochemistry. Brain dissections were performed as previously described (34). Briefly, brains were dissected from adult flies in PBT (1x PBS, 0.1% Triton X-100) and immediately transferred to PBS at 4^{o} C. Brains were fixed in 4% paraformaldehyde at room temperature and then washed 3 times in 1x PBS. Subsequently, brains were permeablized in 0.3% PBS-T (1xPBS, 0.3% Triton X-100), incubated in blocking solution (0.1% PBS-T, 5% normal goat serum) for 1 hour, followed by an overnight incubation in blocking solution and primary antibodies. After a series of 5x washes in PBT, brains were incubated in blocking solution for 1 hour and then incubated for 3 hours in blocking solution plus secondary antibodies. The brains were then washed 5x in PBT and mounted in Vectashiel (Vector Labs). The FasII antibody clone 1D4

hybridoma used to label the mushroom bodies at a 1:20 dilution was obtained from the Developmental Studies Hybridoma Bank (DSHB).

Primary culture of *Drosophila* brain neurons and immunohistochemistry. Brains were dissected from pupae 24 hours after puparium formation (APF), disassociated with the Liberase enzyme blend (following the manufacturer's instructions), and plated on #1.5 35mm glass coverslips coated with Laminin and Concanavalin A. Plated neurons were incubated in Schenider's Medium, 10% FBS and 0.05 mg/mL insulin for three days at 27^{o} C. Cells were washed 3x with Rinaldi's Saline before fixing in 4% paraformaldehyde. Fixed cells were dehydrated with an ethanol gradient and stored in 70% ethanol prior to antibody staining. Primary antibodies were incubated for 1 hour at room temperature, and secondary antibodies were incubated for 40 minutes. The polyclonal dNab2 antibody has been described previously (32), was pre-absorbed with fixed *Drosophila* embryos and used at a final concentration of 1:1000. Anti-dFMRP monoclonal antibody 6A15 was used at a 1:400. Anti-HRP FITC (Jackson ImmunoResearch Laboratories, Inc.) was used at a concentration of 1:500.

Microscopy and image processing. Drosophila eye images were collected with a Leica DFC500 charge-coupled device digital camera. All other images were collected with the Zeiss LSM 510 confocal microscope. Whole brain images were captured with a 20x objective, and cultured neurons were captured at 63x. Image Processing: Maximum intensity projections of brain images were obtained by combining serial optical sections with the Zeiss Zen software suite. Images of primary *Drosophila* brain neurons were processed with the Gaussian Blur filter, then background removed using the subtract function in Fiji.

Immunoprecipitation: Immunoprecipitation *Drosophila* neuronal tissue was adapted from Yang et al. (144). Briefly, heads from 5 day old adult flies were isolated and lysed in 400 µl of Nuclear Lysis Buffer: 50mM Tris HCl, pH 8.1, 10 mM EDTA, 150mM NaCl,1%SDS. Heads were incubated on ice for 20 minutes, then mixed with 800 µl of IP Dilution buffer: 50mM Tris HCl, pH 8.1, 10 mM EDTA, 50mM NaCl. The diluted homogenate were cleared by centrifugation at 12,000 RPMs for 10 minutes. FLAG-dNab2 lysates were then immunoprecipitated using anti-FLAG-M2 affinity agarose beads (Sigma) for 3 hours at 4^{o} C. After a series of 5 washes with IP Dilution Buffer, beads were eluted at 65^{o} C for 30 minutes with Elution buffer: 50 mM Tris HCl, pH 7.0, 10 mM EDTA, 1.3% SDS. All buffers were treated with RNaseIN and complete protease inhibitor tablets immediately before use.

Nucleocytoplasmic fractionation of *Drosophila* tissue. Five flies of each genotype were homogenized in 250 µl of cold nuclear isolation buffer (10 mM Tris•Cl, pH 7.4, 10 mM NaCl, 3 mM MgCl2, 0.5% (v/v) NP-40, 1 x complete protease inhibitor cocktail). The homogenate was transferred to a fresh tube and incubated on ice for 5 minutes followed by centrifugation for 5 minutes at 500xg. The supernatant was collected as the cytosolic fraction and the pellet contained nuclei. Pelleted nuclei were washed once by gently resuspending in nuclear isolation buffer, collected by centrifugation for 5 minutes at 500xg and lysed by sonication in 250 µl of nuclear isolation buffer.

Western Blot Analysis. 25 µl of immunoprecipitates were mixed with 5 µl of 6x laemmli sample buffer and boiled for 5 min. Equal amounts of protein were loaded onto a 5% SDS-PAGE gel, then transferred to a PVDF membrane (Immuno-Blot, Bio-Rad). The membrane was subsequently blocked with 5% NFDM, 1x TBS-T and probed with primary antibodies.

To detect FLAG-tagged proteins, membranes were incubated the M2 antibody (Sigma-Aldrich) at a concentration of 1:1000. The anti-dFMR1 monoclonal antibody 6A15 was obtained from Abcam and used at a 1:1500 dilution. The anti-Lamin antibody was used at a concentration of 1:2000 and was obtained from the DSHB.

Primary hippocampal culture. Hippocampi were dissected and cultured from postnatal day 1 *Zc3h14*$^{+/+}$ control and *Zc3h14*$^{\Delta/\Delta}$ mutant mice and repeated using at least three independent litters for each genotype. Neuronal isolation and culture were performed as previously described (206, 207). Briefly, dissociated neurons were plated on poly-L-lysine coated coverslips (1.0 mg/ml). Neurons were attached to the substrate in minimal essential medium with FBS (10%) for 3 h, inverted onto dishes containing astroglia previously isolated from the appropriate corresponding control *Zc3h14*$^{+/+}$ or mutant *Zc3h14*$^{\Delta/\Delta}$ pups, and grown in defined Neurobasal Medium (Invitrogen, Eugene, OR) with Glutamax (Invitrogen) and B-27 supplements (Invitrogen). Neurons were cultured for 5 days *in vitro* and fixed with 4% PFA in 1× PBS at room temperature for 15 min.

Immunofluorescence staining of mouse primary hippocampal neurons. Anti-ZC3H14 (1:500 (30)), Map2 (1:500; Sigma-Aldrich M 1406), Tau (1:500; Millipore MAB3420), β-Tubulin E7a (1:2000; Developmental Studies Hybridoma Bank, University of Iowa) antibodies were incubated overnight at 4°C. Fluorescein (FITC)- and Texas Red-conjugated secondary antibodies (1:500; Jackson ImmunoResearch 711-096-152 and 111-076-047, respectively) were incubated for 1 h at room temperature. Fluorescent images were visualized using a 63X oil objective on a Leica TCS SP8 MP multiphoton confocal microscope. Images were captured using LAS-AF (Leica) software.

Nucleocytoplasmic fractionation of mouse tissue. Brains were collected from control and *Zc3h14*$^{\Delta/\Delta}$ mice and homogenized in CLB buffer (10 mM HEPES, 10 mM NaCl, 1 mM KH2PO4, 5 mM NaHCO3, 5 mM EDTA, 1 mM CaCl2, 0.5 mM MgCl2). 10% of the sample was removed as the whole cell fraction and resuspended in RIPA-2 (150 mM NaCl, 1% IgePal or NP-40, 0.5% sodium deoxycholate, 0.1% SDS, 50 mM Tris pH 8.0). Cytoplasmic and nuclear fractions were then isolated as previously described (208). All fractions were sonicated on ice 5 times at 0.5% output for 10 seconds and then centrifuged at 13,000 x RPM for 10 minutes at 4°C. The pellet was then discarded, and the supernatant was subjected to SDS-PAGE and immunoblotting as described above.

Polyribosome fractionation. Analysis was performed as previously described (209, 210). Briefly, age P13 mice were sacrificed by isoflurane anesthesia and decapitation. The brain was removed and placed in ice-cold, freshly prepared dissection buffer (10 mM HEPES, pH 7.3, 150 mM KCl, 5 mM $MgCl_2$, 100 ug/ml cycloheximide). Each cortex was dissected and manually homogenized with 12 strokes in 1 ml of lysis buffer (10 mM HEPES, pH 7.3, 150 mM KCl, 5 mM $MgCl_2$, 100 ug/ml cycloheximide, 1 tablet of Complete EDTA-free protease inhibitor cocktail (Roche), 100 U/ml SUPERase-In (RNase inhibitor, Life technologies)). For EDTA treated samples, lysis buffer included 0.030 M EDTA. The homogenate was spun at 2000 x g for 10 min at 4°C. The supernatant (S1) was transferred to new Eppendorf tubes. Igepal was added to S1 for a final concentration of 1% IgePal and mixed by inverting 8 times, followed by incubation on ice for 5 min and centrifugation at 20,000 x g for 10 min at 4°C. The resulting supernatant (S2) was loaded onto a 15-45% wt/wt linear density gradient of sucrose in 10 mM HEPES, pH 7.3, 150 mM KCl, 5 mM $MgCl_2$, 100 ug/ml cycloheximide, 100 U/ml SUPERase-In. Gradients were centrifuged at

38,000 x RPM for 2 hr at 4°C in a Beckman SW41 rotor and fractionated into 10 x 1.1-ml fractions with continuous monitoring at OD_{254}. Fractions were processed for immunoblotting using standard techniques, without need for further concentration of samples.

6.3 Materials and Methods: Chapter 4

Quantification. The average neurite length and the total neurite number were quantified in wildtype and *Zc3h14* mutant DIV6 neurons. The number of actin-based protrusions on the dendrite were quantified and are expressed as the total number of protrusions per 50 µm of the dendritic shaft. The relative abundance of dendritic spines versus dendritic filopodia were quantified.

Chapter 7

References

1. Squire LR (1987) *Memory and Brain* (Oxford University Press, New York) 1 Ed p 336.
2. Squire LR & Dede AJ (2015) Conscious and unconscious memory systems. *Cold Spring Harb Perspect Biol* 7(3):a021667.
3. Owen AM, Milner B, Petrides M, & Evans AC (1996) A specific role for the right parahippocampal gyrus in the retrieval of object-location: a positron emission tomography study. *J Cogn Neurosci* 8(6):588-602.
4. Dossani RH, Missios S, & Nanda A (2015) The Legacy of Henry Molaison (1926-2008) and the Impact of His Bilateral Mesial Temporal Lobe Surgery on the Study of Human Memory. *World Neurosurg* 84(4):1127-1135.
5. Rudy JW (2014) *The Neurobiology of Learning and Memory* (Sinauer, Sunderland, MA) Second Ed.
6. Riedel GP, Bettina (2004) *From Messengers to Molecules: Memories Are Made of These* (Landes Bioscience and Kluwer Academic Plenum) p 614.
7. Condeelis J & Singer RH (2005) How and why does beta-actin mRNA target? *Biol. Cell* 97(1):97-110.
8. Ben-Ari Y*, et al.* (2010) The life of an mRNA in space and time. *J. Cell Sci.* 123(Pt 10):1761-1774.
9. Zhang HL*, et al.* (2001) Neurotrophin-induced transport of a beta-actin mRNP complex increases beta-actin levels and stimulates growth cone motility. *Neuron* 31(2):261-275.
10. Kislauskis EH, Zhu X, & Singer RH (1997) beta-Actin messenger RNA localization and protein synthesis augment cell motility. *J. Cell Biol.* 136(6):1263-1270.
11. Soucek S, Corbett AH, & Fasken MB (2012) The long and the short of it: the role of the zinc finger polyadenosine RNA binding protein, Nab2, in control of poly(A) tail length. *Biochim Biophys Acta* 1819(6):546-554.
12. Lenzken SC, Achsel T, Carri MT, & Barabino SM (2014) Neuronal RNA-binding proteins in health and disease. *Wiley Interdiscip Rev RNA* 5(4):565-576.
13. Xing L & Bassell GJ (2013) mRNA localization: an orchestration of assembly, traffic and synthesis. *Traffic* 14(1):2-14.
14. Di Giammartino DC, Nishida K, & Manley JL (2011) Mechanisms and consequences of alternative polyadenylation. *Mol. Cell* 43(6):853-866.
15. Weill L, Belloc E, Bava FA, & Mendez R (2012) Translational control by changes in poly(A) tail length: recycling mRNAs. *Nat Struct Mol Biol* 19(6):577-585.
16. Zhang X, Virtanen A, & Kleiman FE (2010) To polyadenylate or to deadenylate: that is the question. *Cell Cycle* 9(22):4437-4449.
17. Shonesy BC, Jalan-Sakrikar N, Cavener VS, & Colbran RJ (2014) CaMKII: a molecular substrate for synaptic plasticity and memory. *Prog Mol Biol Transl Sci* 122:61-87.
18. Wu L*, et al.* (1998) CPEB-mediated cytoplasmic polyadenylation and the regulation of experience-dependent translation of alpha-CaMKII mRNA at synapses. *Neuron* 21(5):1129-1139.
19. Besse F & Ephrussi A (2008) Translational control of localized mRNAs: restricting protein synthesis in space and time. *Nat. Rev. Mol. Cell Biol.* 9(12):971-980.
20. Mendez R & Richter JD (2001) Translational control by CPEB: a means to the end. *Nat. Rev. Mol. Cell Biol.* 2(7):521-529.
21. D'Ambrogio A, Nagaoka K, & Richter JD (2013) Translational control of cell growth and malignancy by the CPEBs. *Nat. Rev. Cancer* 13(4):283-290.
22. Udagawa T*, et al.* (2012) Bidirectional control of mRNA translation and synaptic plasticity by the cytoplasmic polyadenylation complex. *Mol. Cell* 47(2):253-266.

23. Anderson JT, Wilson SM, Datar KV, & Swanson MS (1993) NAB2: a yeast nuclear polyadenylated RNA-binding protein essential for cell viability. *Mol Cell Biol* 13(5):2730-2741.
24. Hector RE*, et al.* (2002) Dual requirement for yeast hnRNP Nab2p in mRNA poly(A) tail length control and nuclear export. *EMBO J* 21(7):1800-1810.
25. Marfatia KA, Crafton EB, Green DM, & Corbett AH (2003) Domain Analysis of the Saccharomyces cerevisiae Heterogeneous Nuclear Ribonucleoprotein, Nab2p. *Journal of Biological Chemistry* 278(9):6731-6740.
26. Dheur S, Nykamp KR, Viphakone N, Swanson MS, & Minvielle-Sebastia L (2005) Yeast mRNA Poly(A) tail length control can be reconstituted in vitro in the absence of Pab1p-dependent Poly(A) nuclease activity. *J. Biol. Chem.* 280(26):24532-24538.
27. Kelly SM*, et al.* (2010) Recognition of Polyadenosine RNA by the Zinc Finger Domain of Nuclear Poly(A) RNA-binding Protein 2 (Nab2) Is Required for Correct mRNA 3'-End Formation*. *Journal of Biological Chemistry* 285(34):26022-26032.
28. Lee DC & Aitchison JD (1999) Kap104p-mediated nuclear import. Nuclear localization signals in mRNA-binding proteins and the role of Ran and Rna. *J Biol Chem* 274(41):29031-29037.
29. Green DM*, et al.* (2002) Nab2p Is Required for Poly(A) RNA Export in Saccharomyces cerevisiae and Is Regulated by Arginine Methylation via Hmt1p. *Journal of Biological Chemistry* 277(10):7752-7760.
30. Leung SW*, et al.* (2009) Splice variants of the human ZC3H14 gene generate multiple isoforms of a zinc finger polyadenosine RNA binding protein. *Gene* 439(1-2):71-78.
31. Kelly SM*, et al.* (2007) Recognition of polyadenosine RNA by zinc finger proteins. *Proceedings of the National Academy of Sciences* 104(30):12306-12311.
32. Pak C*, et al.* (2011) Mutation of the conserved polyadenosine RNA binding protein, ZC3H14/dNab2, impairs neural function in Drosophila and humans. *Proc Natl Acad Sci U S A* 108(30):12390-12395.
33. Najmabadi H*, et al.* (2011) Deep sequencing reveals 50 novel genes for recessive cognitive disorders. *Nature* 478(7367):57-63.
34. Kelly SM*, et al.* (2015) The Drosophila ortholog of the Zc3h14 RNA binding protein acts within neurons to pattern axon projection in the developing brain. *Dev Neurobiol*.
35. Kelly SM*, et al.* (2014) A conserved role for the zinc finger polyadenosine RNA binding protein, ZC3H14, in control of poly(A) tail length. *RNA* 20(5):681-688.
36. Kelly S*, et al.* (2012) New kid on the ID block: neural functions of the Nab2/ZC3H14 class of Cys_3His tandem zinc-finger polyadenosine RNA binding proteins. *RNA Biol* 9(5):555-562.
37. Kraemer BC*, et al.* (2003) Neurodegeneration and defective neurotransmission in a Caenorhabditis elegans model of tauopathy. *Proc Natl Acad Sci U S A* 100(17):9980-9985.
38. Guthrie CR, Schellenberg GD, & Kraemer BC (2009) SUT-2 potentiates tau-induced neurotoxicity in Caenorhabditis elegans. *Hum Mol Genet* 18(10):1825-1838.
39. Brockmann C*, et al.* (2012) Structural basis for polyadenosine-RNA binding by Nab2 Zn fingers and its function in mRNA nuclear export. *Structure* 20(6):1007-1018.
40. Kuhlmann SI, Valkov E, & Stewart M (2014) Structural basis for the molecular recognition of polyadenosine RNA by Nab2 Zn fingers. *Nucleic Acids Res* 42(1):672-680.
41. Grant RP*, et al.* (2008) Structure of the N-terminal Mlp1-binding domain of the Saccharomyces cerevisiae mRNA-binding protein, Nab2. *J Mol Biol* 376(4):1048-1059.

42. Blencowe BJ & Ouzounis CA (1999) The PWI motif: a new protein domain in splicing factors. *Trends Biochem. Sci.* 24(5):179-180.
43. Szymczyna BR*, et al.* (2003) Structure and function of the PWI motif: a novel nucleic acid-binding domain that facilitates pre-mRNA processing. *Genes Dev.* 17(4):461-475.
44. Aitchison JD, Blobel G, & Rout MP (1996) Kap104p: a karyopherin involved in the nuclear transport of messenger RNA binding proteins. *Science* 274(5287):624-627.
45. Truant R, Fridell RA, Benson RE, Bogerd H, & Cullen BR (1998) Identification and functional characterization of a novel nuclear localization signal present in the yeast Nab2 poly(A)+ RNA binding protein. *Mol Cell Biol* 18(3):1449-1458.
46. Hu J & Gao S (2014) Mutant of RNA Binding Protein Zc3h14 Causes Cell Growth Delay/Arrest through Inducing Multinucleation and DNA Damage. *JSM Biochemistry & Molecular Biology* 2(1).
47. Chekanova JA & Belostotsky DA (2003) Evidence that poly(A) binding protein has an evolutionarily conserved function in facilitating mRNA biogenesis and export. *RNA* 9(12):1476-1490.
48. Viphakone N, Voisinet-Hakil F, & Minvielle-Sebastia L (2008) Molecular dissection of mRNA poly(A) tail length control in yeast. *Nucleic Acids Res.* 36(7):2418-2433.
49. Fasken MB & Corbett AH (2005) Process or perish: quality control in mRNA biogenesis. *Nat. Struct. Mol. Biol.* 12(6):482-488.
50. Eckmann CR, Rammelt C, & Wahle E (2011) Control of poly(A) tail length. *Wiley Interdiscip Rev RNA* 2(3):348-361.
51. Iglesias N*, et al.* (2010) Ubiquitin-mediated mRNP dynamics and surveillance prior to budding yeast mRNA export. *Genes Dev.* 24(17):1927-1938.
52. Batisse J, Batisse C, Budd A, Bottcher B, & Hurt E (2009) Purification of nuclear poly(A)-binding protein Nab2 reveals association with the yeast transcriptome and a messenger ribonucleoprotein core structure. *J. Biol. Chem.* 284(50):34911-34917.
53. Gonzalez-Aguilera C*, et al.* (2011) Nab2 functions in the metabolism of RNA driven by polymerases II and III. *Mol Biol Cell* 22(15):2729-2740.
54. Reuter LM, Meinel DM, & Sträßer K (2015) The poly(A)-binding protein Nab2 functions in RNA polymerase III transcription. *Genes Dev* 29(14):1565-1575.
55. Kim Guisbert K, Duncan K, Li H, & Guthrie C (2005) Functional specificity of shuttling hnRNPs revealed by genome-wide analysis of their RNA binding profiles. *RNA* 11(4):383-393.
56. Ward AJ & Cooper TA (2010) The pathobiology of splicing. *J. Pathol.* 220(2):152-163.
57. van den Bogaart G, Meinema AC, Krasnikov V, Veenhoff LM, & Poolman B (2009) Nuclear transport factor directs localization of protein synthesis during mitosis. *Nat Cell Biol* 11(3):350-356.
58. Bassell GJ & Warren ST (2008) Fragile X Syndrome: Loss of Local mRNA Regulation Alters Synaptic Development and Function. *Neuron* 60(2):201-214.
59. Kojima S, Shingle DL, & Green CB (2011) Post-transcriptional control of circadian rhythms. *J. Cell Sci.* 124(Pt 3):311-320.
60. Moore MJ (2005) From birth to death: the complex lives of eukaryotic mRNAs. *Science* 309(5740):1514-1518.
61. Shyu AB, Wilkinson MF, & van Hoof A (2008) Messenger RNA regulation: to translate or to degrade. *EMBO J.* 27(3):471-481.
62. Neelamraju Y, Hashemikhabir S, & Janga SC (2015) The human RBPome: From genes and proteins to human disease. *J Proteomics* 127(Pt A):61-70.

63. Lukong KE, Chang KW, Khandjian EW, & Richard S (2008) RNA-binding proteins in human genetic disease. *Trends Genet* 24(8):416-425.
64. Dredge BK, Polydorides AD, & Darnell RB (2001) The splice of life: alternative splicing and neurological disease. *Nat Rev Neurosci* 2(1):43-50.
65. Squire LR & Kandel ER (2000) *Memory: from mind to molecules* (Scientific American Library, New York) pp xi, 235 p.
66. Santoro MR, Bray SM, & Warren ST (2012) Molecular mechanisms of fragile X syndrome: a twenty-year perspective. *Annu Rev Pathol* 7:219-245.
67. Guthrie CR, Greenup L, Leverenz JB, & Kraemer BC (2011) MSUT2 is a determinant of susceptibility to tau neurotoxicity. *Hum Mol Genet* 20(10):1989-1999.
68. Duncan K, Umen JG, & Guthrie C (2000) A putative ubiquitin ligase required for efficient mRNA export differentially affects hnRNP transport. *Curr Biol* 10(12):687-696.
69. Lakso M*, et al.* (1996) Efficient in vivo manipulation of mouse genomic sequences at the zygote stage. *Proc Natl Acad Sci U S A* 93(12):5860-5865.
70. Dooley TP, Miranda M, Jones NC, & DePamphilis ML (1989) Transactivation of the adenovirus EIIa promoter in the absence of adenovirus E1A protein is restricted to mouse oocytes and preimplantation embryos. *Development* 107(4):945-956.
71. Abdeen SK*, et al.* (2013) Conditional inactivation of the mouse Wwox tumor suppressor gene recapitulates the null phenotype. *J Cell Physiol* 228(7):1377-1382.
72. Gerber EE*, et al.* (2013) Integrin-modulating therapy prevents fibrosis and autoimmunity in mouse models of scleroderma. *Nature* 503(7474):126-130.
73. Wang Y*, et al.* (2010) Cosmc is an essential chaperone for correct protein O-glycosylation. *Proc Natl Acad Sci U S A* 107(20):9228-9233.
74. Cao Y*, et al.* (2012) Regulators of G protein signaling RGS7 and RGS11 determine the onset of the light response in ON bipolar neurons. *Proc Natl Acad Sci U S A* 109(20):7905-7910.
75. Chandra D*, et al.* (2006) GABAA receptor alpha 4 subunits mediate extrasynaptic inhibition in thalamus and dentate gyrus and the action of gaboxadol. *Proc Natl Acad Sci U S A* 103(41):15230-15235.
76. Bergo MO*, et al.* (2002) Zmpste24 deficiency in mice causes spontaneous bone fractures, muscle weakness, and a prelamin A processing defect. *Proc Natl Acad Sci U S A* 99(20):13049-13054.
77. Higashi Y*, et al.* (2002) Generation of the floxed allele of the SIP1 (Smad-interacting protein 1) gene for Cre-mediated conditional knockout in the mouse. *Genesis* 32(2):82-84.
78. Vorhees CV & Williams MT (2014) Assessing spatial learning and memory in rodents. *ILAR J* 55(2):310-332.
79. Bunge SA, Ochsner KN, Desmond JE, Glover GH, & Gabrieli JD (2001) Prefrontal regions involved in keeping information in and out of mind. *Brain* 124(Pt 10):2074-2086.
80. Penley SC, Gaudet CM, & Threlkeld SW (2013) Use of an eight-arm radial water maze to assess working and reference memory following neonatal brain injury. *J Vis Exp* (82):50940.
81. Morris RG, Garrud P, Rawlins JN, & O'Keefe J (1982) Place navigation impaired in rats with hippocampal lesions. *Nature* 297(5868):681-683.
82. Douglas RM*, et al.* (2005) Independent visual threshold measurements in the two eyes of freely moving rats and mice using a virtual-reality optokinetic system. *Vis Neurosci* 22(5):677-684.

83. Robinson SJ (2012) Childhood epilepsy and autism spectrum disorders: psychiatric problems, phenotypic expression, and anticonvulsants. *Neuropsychol Rev* 22(3):271-279.
84. Barton ME, Klein BD, Wolf HH, & White HS (2001) Pharmacological characterization of the 6 Hz psychomotor seizure model of partial epilepsy. *Epilepsy Res* 47(3):217-227.
85. Prichahd JW, Gallagher, B.B., and Glaser, G.H. (1969) Experimental seizure-threshold testing with flurothyl. *The Journal of pharmacology and experimental therapeutics* 166(1):170-178.
86. Cox J*, et al.* (2014) Accurate proteome-wide label-free quantification by delayed normalization and maximal peptide ratio extraction, termed MaxLFQ. *Mol Cell Proteomics* 13(9):2513-2526.
87. Kreitz C, Furley P, Memmert D, & Simons DJ (2015) Working-memory performance is related to spatial breadth of attention. *Psychol Res* 79(6):1034-1041.
88. Rummel J & Boywitt CD (2014) Controlling the stream of thought: working memory capacity predicts adjustment of mind-wandering to situational demands. *Psychon Bull Rev* 21(5):1309-1315.
89. Kail RV, Lervag A, & Hulme C (2015) Longitudinal evidence linking processing speed to the development of reasoning. *Dev Sci*.
90. Nagel IE*, et al.* (2008) Human aging magnifies genetic effects on executive functioning and working memory. *Front Hum Neurosci* 2:1.
91. Heisenberg M (2003) Mushroom body memoir: from maps to models. *Nat Rev Neurosci* 4(4):266-275.
92. Michel CI, Kraft R, & Restifo LL (2004) Defective neuronal development in the mushroom bodies of Drosophila fragile X mental retardation 1 mutants. *J Neurosci* 24(25):5798-5809.
93. Correa-Cerro LS*, et al.* (2006) Development and characterization of a hypomorphic Smith-Lemli-Opitz syndrome mouse model and efficacy of simvastatin therapy. *Hum Mol Genet* 15(6):839-851.
94. Ishihara K*, et al.* (2010) Enlarged brain ventricles and impaired neurogenesis in the Ts1Cje and Ts2Cje mouse models of Down syndrome. *Cereb Cortex* 20(5):1131-1143.
95. White NS, Alkire MT, & Haier RJ (2003) A voxel-based morphometric study of nondemented adults with Down Syndrome. *Neuroimage* 20(1):393-403.
96. Pearlson GD*, et al.* (1998) MRI brain changes in subjects with Down syndrome with and without dementia. *Dev Med Child Neurol* 40(5):326-334.
97. Driscoll I*, et al.* (2009) Longitudinal pattern of regional brain volume change differentiates normal aging from MCI. *Neurology* 72(22):1906-1913.
98. Zhou H, Mangelsdorf M, Liu J, Zhu L, & Wu JY (2014) RNA-binding proteins in neurological diseases. *Sci China Life Sci* 57(4):432-444.
99. Kapeli K & Yeo GW (2012) Genome-wide approaches to dissect the roles of RNA binding proteins in translational control: implications for neurological diseases. *Front Neurosci* 6:144.
100. Paronetto MP & Sette C (2010) Role of RNA-binding proteins in mammalian spermatogenesis. *Int J Androl* 33(1):2-12.
101. Venables JP & Eperon I (1999) The roles of RNA-binding proteins in spermatogenesis and male infertility. *Curr Opin Genet Dev* 9(3):346-354.
102. Cheng CY*, et al.* (2015) ENU mutagenesis identifies mice modeling Warburg Micro Syndrome with sensory axon degeneration caused by a deletion in Rab18. *Exp Neurol* 267:143-151.

103. Bakker NE, Wolffenbuttel KP, Looijenga LH, & Hokken-Koelega AC (2015) Testes in infants with Prader-Willi syndrome: human chorionic gonadotropin treatment, surgery and histology. *J Urol* 193(1):291-298.
104. Sammour ZM*, et al.* (2014) Congenital genitourinary abnormalities in children with Williams-Beuren syndrome. *J Pediatr Urol* 10(5):804-809.
105. Yi T*, et al.* (2014) LGR4/GPR48 inactivation leads to aniridia-genitourinary anomalies-mental retardation syndrome defects. *J Biol Chem* 289(13):8767-8780.
106. Cabezas DA*, et al.* (2000) A new X linked mental retardation (XLMR) syndrome with short stature, small testes, muscle wasting, and tremor localises to Xq24-q25. *J Med Genet* 37(9):663-668.
107. Siffroi JP*, et al.* (2001) Expression of the TAR RNA binding protein in human testis. *Mol Hum Reprod* 7(3):219-225.
108. Kimura M, Ishida K, Kashiwabara S, & Baba T (2009) Characterization of two cytoplasmic poly(A)-binding proteins, PABPC1 and PABPC2, in mouse spermatogenic cells. *Biol Reprod* 80(3):545-554.
109. Sutherland JM, Siddall NA, Hime GR, & McLaughlin EA (2015) RNA binding proteins in spermatogenesis: an in depth focus on the Musashi family. *Asian J Androl* 17(4):529-536.
110. Curinha A, Oliveira Braz S, Pereira-Castro I, Cruz A, & Moreira A (2014) Implications of polyadenylation in health and disease. *Nucleus* 5(6):508-519.
111. Darnell JC & Richter JD (2012) Cytoplasmic RNA-binding proteins and the control of complex brain function. *Cold Spring Harb Perspect Biol* 4(8):a012344.
112. Liu-Yesucevitz L*, et al.* (2011) Local RNA Translation at the Synapse and in Disease. *The Journal of Neuroscience* 31(45):16086-16093.
113. Richter JD, Bassell GJ, & Klann E (2015) Dysregulation and restoration of translational homeostasis in fragile X syndrome. *Nat Rev Neurosci* 16(10):595-605.
114. Udagawa T*, et al.* (2013) Genetic and acute CPEB1 depletion ameliorate fragile X pathophysiology. *Nat Med* 19(11):1473-1477.
115. Richter JD (2007) CPEB: a life in translation. *Trends in Biochemical Sciences* 32(6):279-285.
116. Cheever A, Blackwell E, & Ceman S (2010) Fragile X protein family member FXR1P is regulated by microRNAs. *RNA* 16(8):1530-1539.
117. Prusky GT, Alam NM, Beekman S, & Douglas RM (2004) Rapid quantification of adult and developing mouse spatial vision using a virtual optomotor system. *Invest Ophthalmol Vis Sci* 45(12):4611-4616.
118. Aung MH, Kim MK, Olson DE, Thule PM, & Pardue MT (2013) Early visual deficits in streptozotocin-induced diabetic long evans rats. *Invest Ophthalmol Vis Sci* 54(2):1370-1377.
119. Aung MH*, et al.* (2014) Dopamine deficiency contributes to early visual dysfunction in a rodent model of type 1 diabetes. *J Neurosci* 34(3):726-736.
120. Castello A, Fischer B, Hentze MW, & Preiss T (2013) RNA-binding proteins in Mendelian disease. *Trends Genet.* 29(5):318-327.
121. Lu B & Vogel H (2009) Drosophila models of neurodegenerative diseases. *Annu Rev Pathol* 4:315-342.
122. Leung SW*, et al.* (2009) Splice variants of the human ZC3H14 gene generate multiple isoforms of a zinc finger polyadenosine RNA binding protein. *Gene* 439(1-2):71-78.

123. Kelly SM*, et al.* (2010) Recognition of polyadenosine RNA by the zinc finger domain of nuclear poly(A) RNA-binding protein 2 (Nab2) is required for correct mRNA 3'-end formation. *The Journal of biological chemistry* 285(34):26022-26032.
124. Antar LN, Afroz R, Dictenberg JB, Carroll RC, & Bassell GJ (2004) Metabotropic glutamate receptor activation regulates fragile x mental retardation protein and FMR1 mRNA localization differentially in dendrites and at synapses. *J. Neurosci.* 24(11):2648-2655.
125. Penagarikano O, Mulle JG, & Warren ST (2007) The pathophysiology of fragile x syndrome. *Annu Rev Genomics Hum Genet* 8:109-129.
126. Antar LN, Li C, Zhang H, Carroll RC, & Bassell GJ (2006) Local functions for FMRP in axon growth cone motility and activity-dependent regulation of filopodia and spine synapses. *Mol. Cell. Neurosci.* 32(1-2):37-48.
127. Li C, Bassell GJ, & Sasaki Y (2009) Fragile X Mental Retardation Protein is Involved in Protein Synthesis-Dependent Collapse of Growth Cones Induced by Semaphorin-3A. *Front Neural Circuits* 3:11.
128. Christie SB, Akins MR, Schwob JE, & Fallon JR (2009) The FXG: a presynaptic fragile X granule expressed in a subset of developing brain circuits. *J. Neurosci.* 29(5):1514-1524.
129. Akins MR, Leblanc HF, Stackpole EE, Chyung E, & Fallon JR (2012) Systematic mapping of fragile X granules in the mouse brain reveals a potential role for presynaptic FMRP in sensorimotor functions. *J. Comp. Neurol.* 520(16):3687-3706.
130. Rorth P (1996) A modular misexpression screen in Drosophila detecting tissue-specific phenotypes. *Proc Natl Acad Sci U S A* 93(22):12418-12422.
131. Siller SS & Broadie K (2011) Neural circuit architecture defects in a Drosophila model of Fragile X syndrome are alleviated by minocycline treatment and genetic removal of matrix metalloproteinase. *Dis Model Mech* 4(5):673-685.
132. Barbee SA*, et al.* (2006) Staufen- and FMRP-containing neuronal RNPs are structurally and functionally related to somatic P bodies. *Neuron* 52(6):997-1009.
133. Cziko AM*, et al.* (2009) Genetic modifiers of dFMR1 encode RNA granule components in Drosophila. *Genetics* 182(4):1051-1060.
134. Sudhakaran IP*, et al.* (2014) FMRP and Ataxin-2 function together in long-term olfactory habituation and neuronal translational control. *Proc Natl Acad Sci U S A* 111(1):E99-E108.
135. Jin P*, et al.* (2004) Biochemical and genetic interaction between the fragile X mental retardation protein and the microRNA pathway. *Nat. Neurosci.* 7(2):113-117.
136. Wan L, Dockendorff TC, Jongens TA, & Dreyfuss G (2000) Characterization of dFMR1, a Drosophila melanogaster homolog of the fragile X mental retardation protein. *Mol Cell Biol* 20(22):8536-8547.
137. Zarnescu DC*, et al.* (2005) Fragile X protein functions with lgl and the par complex in flies and mice. *Dev. Cell* 8(1):43-52.
138. Kelly S*, et al.* (2012) New kid on the ID block: neural functions of the Nab2/ZC3H14 class of Cys(3)His tandem zinc-finger polyadenosine RNA binding proteins. *RNA biology* 9(5):555-562.
139. Santos AR, Kanellopoulos AK, & Bagni C (2014) Learning and behavioral deficits associated with the absence of the fragile X mental retardation protein: what a fly and mouse model can teach us. *Learn Mem* 21(10):543-555.
140. Feng Y*, et al.* (1997) Fragile X mental retardation protein: nucleocytoplasmic shuttling and association with somatodendritic ribosomes. *J. Neurosci.* 17(5):1539-1547.

141. Green DM*, et al.* (2002) Nab2p is required for poly(A) RNA export in Saccharomyces cerevisiae and is regulated by arginine methylation via Hmt1p. *The Journal of biological chemistry* 277(10):7752-7760.
142. Kim M, Bellini M, & Ceman S (2009) Fragile X mental retardation protein FMRP binds mRNAs in the nucleus. *Mol. Cell. Biol.* 29(1):214-228.
143. Aso Y*, et al.* (2009) The mushroom body of adult Drosophila characterized by GAL4 drivers. *J. Neurogenet.* 23(1-2):156-172.
144. Yang Z, Edenberg HJ, & Davis RL (2005) Isolation of mRNA from specific tissues of Drosophila by mRNA tagging. *Nucleic Acids Res.* 33(17):e148.
145. Morales J*, et al.* (2002) Drosophila fragile X protein, DFXR, regulates neuronal morphology and function in the brain. *Neuron* 34(6):961-972.
146. Rha J*, et al.* (2016) The RNA-binding protein, ZC3H14, is required for proper polyadenylation and brain function in mice. *Submitted*.
147. Zhang YQ*, et al.* (2001) Drosophila fragile X-related gene regulates the MAP1B homolog Futsch to control synaptic structure and function. *Cell* 107(5):591-603.
148. Darnell JC*, et al.* (2011) FMRP stalls ribosomal translocation on mRNAs linked to synaptic function and autism. *Cell* 146(2):247-261.
149. Lu R*, et al.* (2004) The fragile X protein controls microtubule-associated protein 1B translation and microtubule stability in brain neuron development. *Proc Natl Acad Sci U S A* 101(42):15201-15206.
150. Zalfa F*, et al.* (2003) The fragile X syndrome protein FMRP associates with BC1 RNA and regulates the translation of specific mRNAs at synapses. *Cell* 112(3):317-327.
151. Malik BR & Hodge JJ (2014) CASK and CaMKII function in Drosophila memory. *Front Neurosci* 8:178.
152. Ashraf SI, McLoon AL, Sclarsic SM, & Kunes S (2006) Synaptic protein synthesis associated with memory is regulated by the RISC pathway in Drosophila. *Cell* 124(1):191-205.
153. Stocker RF, Heimbeck G, Gendre N, & de Belle JS (1997) Neuroblast ablation in Drosophila P[GAL4] lines reveals origins of olfactory interneurons. *J. Neurobiol.* 32(5):443-456.
154. Komiyama T, Johnson WA, Luo L, & Jefferis GS (2003) From lineage to wiring specificity. POU domain transcription factors control precise connections of Drosophila olfactory projection neurons. *Cell* 112(2):157-167.
155. Ahmed KM, Fan M, Nantajit D, Cao N, & Li JJ (2008) Cyclin D1 in low-dose radiation-induced adaptive resistance. *Oncogene* 27(53):6738-6748.
156. Rondón AG, Jimeno S, & Aguilera A (2010) The interface between transcription and mRNP export: from THO to THSC/TREX-2. *Biochim Biophys Acta* 1799(8):533-538.
157. Piruat JI & Aguilera A (1998) A novel yeast gene, THO2, is involved in RNA pol II transcription and provides new evidence for transcriptional elongation-associated recombination. *EMBO J* 17(16):4859-4872.
158. Kosik KS & Finch EA (1987) MAP2 and tau segregate into dendritic and axonal domains after the elaboration of morphologically distinct neurites: an immunocytochemical study of cultured rat cerebrum. *J Neurosci* 7(10):3142-3153.
159. Togashi H*, et al.* (2006) Interneurite affinity is regulated by heterophilic nectin interactions in concert with the cadherin machinery. *J Cell Biol* 174(1):141-151.
160. Stefani G, Fraser CE, Darnell JC, & Darnell RB (2004) Fragile X Mental Retardation Protein Is Associated with Translating Polyribosomes in Neuronal Cells. *The Journal of Neuroscience* 24(33):7272-7276.

161. Roux PP*, et al.* (2007) RAS/ERK signaling promotes site-specific ribosomal protein S6 phosphorylation via RSK and stimulates cap-dependent translation. *J Biol Chem* 282(19):14056-14064.
162. Li Y, Lin L, & Jin P (2008) The microRNA pathway and fragile X mental retardation protein. *Biochim. Biophys. Acta* 1779(11):702-705.
163. Fabian MR*, et al.* (2009) Mammalian miRNA RISC recruits CAF1 and PABP to affect PABP-dependent deadenylation. *Mol Cell* 35(6):868-880.
164. Khan MR*, et al.* (2015) Amyloidogenic Oligomerization Transforms Drosophila Orb2 from a Translation Repressor to an Activator. *Cell* 163(6):1468-1483.
165. Bassell GJ & Warren ST (2008) Fragile X syndrome: loss of local mRNA regulation alters synaptic development and function. *Neuron* 60(2):201-214.
166. Stackpole EE, Akins MR, & Fallon JR (2014) N-myristoylation regulates the axonal distribution of the Fragile X-related protein FXR2P. *Mol. Cell. Neurosci.* 62:42-50.
167. Hu J & Gao S (2014) Mutant of RNA Binding Protein Zc3h14 Causes Cell Growth Delay/Arrest through Inducing Multinucleation and DNA Damage. *JSM Biochem Mol Biol* 2(1).
168. Jacobs S, Nathwani M, & Doering LC (2010) Fragile X astrocytes induce developmental delays in dendrite maturation and synaptic protein expression. *BMC Neurosci.* 11:132.
169. Dotti CG, Sullivan CA, & Banker GA (1988) The establishment of polarity by hippocampal neurons in culture. *J Neurosci* 8(4):1454-1468.
170. Hsueh YP (2012) Neuron-specific regulation on F-actin cytoskeletons: The role of CTTNBP2 in dendritic spinogenesis and maintenance. *Commun Integr Biol* 5(4):334-336.
171. Koleske AJ (2013) Molecular mechanisms of dendrite stability. *Nat. Rev. Neurosci.* 14(8):536-550.
172. Boyer C, Schikorski T, & Stevens CF (1998) Comparison of hippocampal dendritic spines in culture and in brain. *J. Neurosci.* 18(14):5294-5300.
173. Harris KM & Stevens JK (1989) Dendritic spines of CA 1 pyramidal cells in the rat hippocampus: serial electron microscopy with reference to their biophysical characteristics. *J. Neurosci.* 9(8):2982-2997.
174. Ethell IM & Pasquale EB (2005) Molecular mechanisms of dendritic spine development and remodeling. *Prog. Neurobiol.* 75(3):161-205.
175. Fiala JC, Feinberg M, Popov V, & Harris KM (1998) Synaptogenesis via dendritic filopodia in developing hippocampal area CA1. *J. Neurosci.* 18(21):8900-8911.
176. Aoto J*, et al.* (2007) Postsynaptic ephrinB3 promotes shaft glutamatergic synapse formation. *J. Neurosci.* 27(28):7508-7519.
177. Helmeke C, Ovtscharoff W, Jr., Poeggel G, & Braun K (2001) Juvenile emotional experience alters synaptic inputs on pyramidal neurons in the anterior cingulate cortex. *Cereb. Cortex* 11(8):717-727.
178. Nikolakopoulou AM, Davies HA, & Stewart MG (2006) Passive avoidance training decreases synapse density in the hippocampus of the domestic chick. *Eur. J. Neurosci.* 23(4):1054-1062.
179. Steward O & Falk PM (1986) Protein-synthetic machinery at postsynaptic sites during synaptogenesis: a quantitative study of the association between polyribosomes and developing synapses. *J. Neurosci.* 6(2):412-423.
180. Baj G, Patrizio A, Montalbano A, Sciancalepore M, & Tongiorgi E (2014) Developmental and maintenance defects in Rett syndrome neurons identified by a new mouse staging system in vitro. *Front Cell Neurosci* 8:18.

181. Kandel ER, Dudai Y, & Mayford MR (2014) The molecular and systems biology of memory. *Cell* 157(1):163-186.
182. Schmid M*, et al.* (2012) Rrp6p controls mRNA poly(A) tail length and its decoration with poly(A) binding proteins. *Mol. Cell* 47(2):267-280.
183. Caceres A, Ye B, & Dotti CG (2012) Neuronal polarity: demarcation, growth and commitment. *Curr. Opin. Cell Biol.* 24(4):547-553.
184. Nicoll RA & Schmitz D (2005) Synaptic plasticity at hippocampal mossy fibre synapses. *Nat. Rev. Neurosci.* 6(11):863-876.
185. Perrone-Bizzozero NI, Tanner DC, Mounce J, & Bolognani F (2011) Increased expression of axogenesis-related genes and mossy fibre length in dentate granule cells from adult HuD overexpressor mice. *ASN Neuro* 3(5):259-270.
186. Blaabjerg M & Zimmer J (2007) The dentate mossy fibers: structural organization, development and plasticity. *Prog. Brain Res.* 163:85-107.
187. Braun AP & Schulman H (1995) The multifunctional calcium/calmodulin-dependent protein kinase: from form to function. *Annu. Rev. Physiol.* 57:417-445.
188. Miller S*, et al.* (2002) Disruption of dendritic translation of CaMKIIalpha impairs stabilization of synaptic plasticity and memory consolidation. *Neuron* 36(3):507-519.
189. Huang YS, Jung MY, Sarkissian M, & Richter JD (2002) N-methyl-D-aspartate receptor signaling results in Aurora kinase-catalyzed CPEB phosphorylation and alpha CaMKII mRNA polyadenylation at synapses. *EMBO J.* 21(9):2139-2148.
190. Wigington CP, Williams KR, Meers MP, Bassell GJ, & Corbett AH (2014) Poly(A) RNA-binding proteins and polyadenosine RNA: new members and novel functions. *Wiley Interdiscip Rev RNA* 5(5):601-622.
191. Laird PW*, et al.* (1991) Simplified mammalian DNA isolation procedure. *Nucleic Acids Res* 19(15):4293.
192. Simionescu-Bankston A*, et al.* (2013) The N-BAR domain protein, Bin3, regulates Rac1- and Cdc42-dependent processes in myogenesis. *Dev Biol* 382(1):160-171.
193. Rankin EB*, et al.* (2005) Inactivation of the arylhydrocarbon receptor nuclear translocator (Arnt) suppresses von Hippel-Lindau disease-associated vascular tumors in mice. *Mol Cell Biol* 25(8):3163-3172.
194. Chekanova JA, Shaw RJ, & Belostotsky DA (2001) Analysis of an essential requirement for the poly(A) binding protein function using cross-species complementation. *Curr Biol* 11(15):1207-1214.
195. Apponi LH*, et al.* (2010) Loss of nuclear poly(A)-binding protein 1 causes defects in myogenesis and mRNA biogenesis. *Human Molecular Genetics* 19(6):1058-1065.
196. Crawley JN (2000) *What's Wrong With My Mouse: Behavioral Phenotyping of Transgenic and Knockout Mice* (John Wiley & Sons, Inc., New York) pp 52-55.
197. Makinson CD*, et al.* (2016) An Scn1a epilepsy mutation in Scn8a alters seizure susceptibility and behavior. *Experimental neurology* 275 Pt 1:46-58.
198. Gilchrist J*, et al.* (2014) Nav1.1 modulation by a novel triazole compound attenuates epileptic seizures in rodents. *ACS Chem Biol* 9(5):1204-1212.
199. Dutton SB*, et al.* (2011) Protective effect of the ketogenic diet in Scn1a mutant mice. *Epilepsia* 52(11):2050-2056.
200. Sawyer NT*, et al.* (2015) Scn1a dysfunction alters behavior but not the effect of stress on seizure response. *Genes, brain, and behavior*.
201. Cox J*, et al.* (2014) Accurate Proteome-wide Label-free Quantification by Delayed Normalization and Maximal Peptide Ratio Extraction, Termed MaxLFQ. *Molecular & Cellular Proteomics* 13(9):2513-2526.

202. Luber CA*, et al.* (2010) Quantitative proteomics reveals subset-specific viral recognition in dendritic cells. *Immunity* 32(2):279-289.
203. Zambon AC*, et al.* (2012) GO-Elite: a flexible solution for pathway and ontology over-representation. *Bioinformatics* 28(16):2209-2210.
204. Csardi G NT (2006) The igraph software package for complex network research. *InterJournal Complex Systems* 1695.
205. Lee T & Luo L (1999) Mosaic analysis with a repressible cell marker for studies of gene function in neuronal morphogenesis. *Neuron* 22(3):451-461.
206. Kaech S & Banker G (2006) Culturing hippocampal neurons. *Nature protocols* 1(5):2406-2415.
207. Beaudoin GM*, et al.* (2012) Culturing pyramidal neurons from the early postnatal mouse hippocampus and cortex. *Nature protocols* 7(9):1741-1754.
208. Guillemin I, Becker M, Ociepka K, Friauf E, & Nothwang HG (2005) A subcellular prefractionation protocol for minute amounts of mammalian cell cultures and tissue. *Proteomics* 5(1):35-45.
209. Myrick LK*, et al.* (2015) Independent role for presynaptic FMRP revealed by an FMR1 missense mutation associated with intellectual disability and seizures. *Proc Natl Acad Sci U S A* 112(4):949-956.
210. Zang JB*, et al.* (2009) A mouse model of the human Fragile X syndrome I304N mutation. *PLoS Genet* 5(12):e1000758.